Martina Weiß

Modelling of Global Change Impacts on Hydrology with focus on Europe and Africa

kassel university press

This work has been accepted by the faculty of Electrical Engineering and Computer Science of the University of Kassel as a thesis for acquiring the academic degree of Doktor der Ingenieurwissenschaften (Dr.-Ing.).

Supervisor: Prof. Dr. Joseph Alcamo (Universität Kassel)
Co-Supervisor: Prof. Dr. Lucas Menzel (Universität Heidelberg)

Defense day: 10th July 2009

Bibliographic information published by Deutsche Nationalbibliothek
The Deutsche Nationalbibliothek lists this publication in the Deutsche Nationalbibliografie; detailed bibliographic data is available in the Internet at http://dnb.d-nb.de.

Zugl.: Kassel, Univ., Diss. 2009
ISBN print: 978-3-89958-758-6
ISBN online: 978-3-89958-759-3
URN: http://nbn-resolving.de/urn:nbn:de:0002-7592

Printed in Germany

DANKSAGUNG

Mein Dank gilt Prof. Dr. Joseph Alcamo und Prof. Dr. Lucas Menzel für die Übernahme der Gutachten und die wissenschaftliche Begleitung während der Anfertigung der Arbeit.

Weiterhin danke ich Dr. Martina Flörke und Dr. Rüdiger Schaldach für wertvolle Ratschläge und konstruktive Zusammenarbeit sowie Achim Manche für technischen Support.

Außerdem herzlichen Dank an alle Kolleginnen und Kollegen am CESR für die angenehme Arbeitsatmosphäre und anregende Gespräche.

Nicht zuletzt gilt mein Dank meinen Eltern für ihre immerwährende Unterstützung.

ZUSAMMENFASSUNG

Die anthropogene Wassernutzung, und damit die Wasserentnahme aus dem hydrologischen Kreislauf, hat in den vergangenen Jahren deutlich zugenommen. Dies kann zurückgeführt werden auf Bevölkerungs- und Wirtschaftswachstum, Änderungen im Lebenswandel und einer Zunahme von Wasserversorgungssystemen in weiten Teilen der Welt. Ökosysteme sind dadurch zunehmend gefährdet, da eine nachhaltige Nutzung der knappen Ressource Wasser nicht gegeben ist. Wasserentnahmen zur Bewässerung spielen dabei eine große Rolle: Weltweit dienen durchschnittlich 70% aller Entnahmen der Bewässerung. Nur einige industrialisierte Länder konnten mithilfe technologischer Innovationen ihre Nutzungseffizienz erhöhen, wodurch der Pro-Kopf Bedarf sank. Allerdings sind auch industrialisierte Länder weiterhin der Bedrohung durch Extremereignisse, wie Überschwemmungen und Dürren ausgesetzt. Am schlimmsten betroffen sind jedoch industriell nicht entwickelte Regionen in semiariden Gebieten, die unter einer Vielzahl von wasserbedingten Problemen leiden, welche durch das oft vorherrschende hohe Bevölkerungswachstum verstärkt werden. Messdaten haben bereits gezeigt, dass Wasserressourcen empfindlich auf klimatische und globale Veränderungen reagieren, mit vielfältigen Auswirkungen auf die Gesellschaft und Ökosysteme.

Ziel dieser Arbeit ist es, den Einfluss des globalen Wandels auf den hydrologischen Kreislauf herauszuarbeiten. Dabei liegt der Schwerpunkt auf der Untersuchung von Dürren, Verdunstung und langjähriger Wasserverfügbarkeit, um insbesondere die Verflechtung von Klima, Landnutzung, Sozioökonomie und Wasserressourcen aufzudecken. Die Analysen werden mit Hilfe des WaterGAP Modells, einem dem derzeitigen aktuellen Stand der Forschung entsprechenden, globalen hydrologischen Modell durchgeführt. WaterGAP ermöglicht eine Gegenüberstellung derzeitiger und künftiger Wasserverfügbarkeit und Wassernutzung auf Einzugsgebietsebene. Weitere hydrologische Komponenten können auf Raster-Ebene mit einer Größe von 30 Bogenminuten berechnet werden.

Als Teil dieser Arbeit wird der im Modell implementierte semi-physikalische Verdunstungsansatz der potentiellen Evapotranspiration regionalisiert. In einem ersten Schritt werden vier verschiedene Verdunstungsformulierungen mit Hinblick auf ihre globale Anwendbarkeit verglichen. Dabei wird der strahlungsbasierte Ansatz nach Priestley Taylor aufgrund seines geringen Datenbedarfs bei vergleichbar guten Ergebnissen als am geeignetsten befunden. Dieser wird dann anhand von Evaporimeter-Messdaten (‚Class-A Pan') parametrisiert, wobei nun 12 Klimaklassen unterschieden werden, im Vergleich zu ehemals zwei. Zusätzlich wird ein neuer Ansatz zur Berechnung der Albedo eingeführt, da diese ganz entscheidend den Verdunstungsprozess beeinflusst. Im Gegensatz zu einer Parametrisierung nach Landnutzungsklassen erfolgt nun eine zeitlich abhängige Berechnung gemäß der Entwicklung des Blattflächenindex in Kombination mit einer Hintergrundalbedo aufgrund des Bodentyps. Die Entwicklung des Blattflächenindex wird hierzu ebenfalls modifiziert, so dass ein realistischer Jahresverlauf erzielt wird. Durch die verbesserte Simulation von potentieller Evapotranspiration verbessert sich auch die Abbildung des Abflusses im Modell.

Nach Identifikation der Eingangs beschriebenen Probleme, wie beispielsweise Extremereignisse oder hoher Bewässerungsbedarf, wurde für diese jeweils ein Regionsbezug hergestellt. Diese bilden im Kontext des globalen Wandels die weiteren Forschungsschwerpunkte der einzelnen Kapitel dieser Arbeit.

Beginnend mit einer Analyse von Extremereignissen wurde die Änderung des Wiederkehrintervalls der derzeitigen 100-jährlichen Dürre in den 2070ern für die gesamte Mittelmeerregion untersucht. Die Analyse stützte sich auf eine statistische Auswertung der Jahreshöchstwerte des ‚Defizitvolumens', d.h. der Menge Wasser, die im Vergleich zum mittleren Monatswert fehlt. Dabei berücksichtigte die Modellierung des künftigen Abflusses Änderungen im Klima und in der anthropogenen Wassernutzung, die wiederum selbst vom künftigen Klima sowie sozioökonomischen Faktoren abhängt.

Randbedingungen für die 2070er wurden den A2 und B2 Szenarien des IPCC (‚Intergovernmental Panel on Climate Change') entnommen. Das A2 Szenario geht von starkem, aber regional orientiertem wirtschaftlichen Wachstum und fragmentiertem technologischen Wandel aus, wobei der Wohlstand des Einzelnen im Vordergrund steht. Im B2 Szenario hingegen stehen Umweltschutz und soziale Gleichheit im Mittelpunkt, aber auch hier findet die wirtschaftliche und soziale Entwicklung sowie umweltbezogene Nachhaltigkeit nur auf regionaler Ebene statt. Das ECHAM4 Klimamodell projiziert im Mittel die folgenden Klimaänderungen für die beiden Szenarien: Im B2 Szenario erhöht sich die Temperatur um ca. 4°C, im A2 Szenario um ca. 6°C in der betrachteten Region Südeuropa bis Nordafrika. Im A2 Szenario nimmt der Niederschlag um 10%-20% ab, während er im B2 Szenario außer im Sommer um 5% abnimmt. Für den Sommer wird eine leichte Zunahme des Niederschlags projiziert.

Die Simulationsergebnisse mit dem WaterGAP Modell zeigen eine Häufigkeitszunahme der derzeitigen alle 100 Jahre auftretenden Dürre auf bis zu alle 10 Jahre in den 2070ern für ein Gebiet das sich unter dem B2 Szenario von Nordspanien über Südfrankreich und Norditalien bis zur Schweiz erstreckt. Unter dem A2 Szenario umfasst dieses Gebiet weite Teile Südeuropas. Diese Häufigkeitsänderung ist unter dem B2 Szenario zu 69% statistisch signifikant und unter dem A2 Szenario zu 75%. Weiterhin wird gezeigt, dass Klimaänderungen das Wiederkehrintervall der 100 jährlichen Dürre stärker beeinflussen als die anthropogene Wassernutzung. Der Einfluss der anthropogenen Wassernutzung auf die Änderung des Wiederkehrintervalls ist zu 58% statistisch signifikant. Der zunehmende Wasserbedarf insbesondere im Haushaltssektor aufgrund von projiziertem Bevölkerungswachstum verstärkt die Wasserknappheit und damit die Dürrehäufigkeit in Afrika und dem nahen Osten. Projizierte steigende Wassernutzungseffizienz im Industriesektor, auf der anderen Seite, führt zu geringerem Wasserbedarf insbesondere in Mittel- und Osteuropa und damit zu einer geringfügig niedrigeren Dürrehäufigkeit.

Der zu Beginn beschriebene hohe Bewässerungsanteil in der anthropogenen Wassernutzung ist von zentraler Bedeutung in der nachfolgenden Studie zur Wassernutzung in der afrikanischen Agrarwirtschaft. Auch diese Analyse stützt sich auf die Nutzung von Szenarien. Dadurch kann erstmalig der Einfluss von Landnutzungsänderungen, Klimaänderungen und technologischem Wandel einzeln und in seinem Zusammenwirken auf die Wassernutzung analysiert werden. Zu diesem Zweck werden das LandSHIFT Modell, ein globales Landnutzungsmodell, und das hydrologische WaterGAP Modell gekoppelt. Des Weiteren wird erstmalig das Konzept des so genannten ‚blauen und grünen Wassers' auf kontinentaler Ebene angewandt, um eine umfassende Analyse der tatsächlichen Wassernutzung durchzuführen. Als blaues Wasser wird dabei das Wasser bezeichnet, welches für Bewässerungszwecke dem hydrologischen System entnommen wird. Grünes Wasser ist definiert als das Wasser, welches durch die Feldfrucht sowie den die Pflanze umgebenden Ackerboden verdunstet, d.h. die Summe aus Evaporation und Transpiration.

In diesem Modellexperiment werden die zwei Szenarien ‚Policy First' und ‚Security First' des ‚Global Environmental Outlook-4' (GEO-4) Report der UNEP verwendet, die eine mögliche Entwicklung für die 2050er Jahre beschreiben. Das ‚Policy First' Szenario beschreibt eine Welt, in der der Umweltschutz und der Wohlstand jedes Menschen gesetzlich geregelt sind. Starkes wirtschaftliches Wachstum wird durch gesteigerte internationale Kooperation erreicht. Im ‚Security First' Szenario

hingegen steht die regionale Sicherheit im Vordergrund, inklusive der Ressourcensicherheit. Weiterhin ist dieses Szenario gekennzeichnet durch eine geringe Ausbreitung von neuen Technologien und Informationen aufgrund niedriger internationaler Kooperation. Da für beide Szenarien ein ähnlicher Entwicklungspfad für Treibhausgase bis zum Jahr 2050 projiziert wird, ist auch die zu erwartende Entwicklung des Klimas bis Mitte des 21. Jahrhunderts ähnlich. Die Temperatur nimmt um ca. 2°C im kontinentalen Mittel zu, mit etwas höheren Zunahmen im Nordwesten und Süden Afrikas. Der Niederschlag nimmt um ca. 10% in weiten Teilen Afrikas zu, mit Ausnahme von kleinen Regionen im Westen, Süden und an der nördlichen Küste, für die eine Abnahme um ca. 15%-20% projiziert wird.

WaterGAP Ergebnisse zeigen für das Jahr 2000 (Mittelwert aus 1971-2000) einen Absolutwert der Evapotranspiration (grünes Wasser) von afrikanischem Regenfeldbau, d.h. Gebieten, die ohne zusätzliche Bewässerung auskommen, von 1,085km^3/Jahr. Die Wasserentnahmen zur Bewässerung (blaues Wasser) betragen ungefähr 180km^3/Jahr. Gemäß der Simulationsergebnisse mit dem LandSHIFT Modell wird zwischen dem Jahr 2000 und 2050 eine Fläche von circa 1.25 Mio. km² bis 1.56 Mio. km², je nach Szenario, zusätzlich in Ackerland umgewandelt. Im Jahr 2050 steigt die simulierte Evapotranspiration auf 1,870 bis 2,040 km^3/Jahr, während die Wasserentnahmen zur Bewässerung auf 194 bis 330 km^3/Jahr ansteigen. Diese Ergebnisse zeigen zum einen, dass der Evapotranspiration von landwirtschaftlichen Flächen eine viel größere Bedeutung zukommt als der absoluten Menge des Bewässerungswassers. Zum anderen deuten diese Ergebnisse aber auch auf das Potential hin, welches in der technologischen Entwicklung zu sehen ist. Diese sollte nicht nur auf blaues Wasser abzielen, sondern in Anbetracht seiner Menge insbesondere auch das grüne Wasser berücksichtigen. Dadurch könnten sich große Einsparmöglichkeiten ergeben, aufgrund derer mehr Wasser für die Unterstützung der Ökosysteme oder anderer Sektoren bleibt.

Abschließend wird eine neue Methode entwickelt, die es ermöglicht, die Sensitivität sowie die Schadensanfälligkeit gegenüber Klimaänderungen einer beliebigen Anzahl von Wassereinzugsgebieten systematisch zu analysieren und gegenüberzustellen. Wie hier am Beispiel von 18 Einzugsgebieten Europas gezeigt, werden ‚response surfaces' konstruiert, die die Antwort der Wasserverfügbarkeit auf simultane Änderungen der Temperatur (T) im Bereich [-1°C bis +6°C] und des Niederschlags (P) im Bereich [-40% bis +100%] widerspiegeln. Dabei wird durch Interpolation der Antwortpunkte jeder Kombination aus T und P eine kontinuierliche Fläche im 3D-Raum erzeugt. Anhand des Volumens unter der Fläche in Kombination mit der Verschiebung der Jahresganglinie wird die Sensitivität eines Einzugsgebiets gegenüber Klimaänderungen analysiert.

Es zeigt sich, dass die nordischen Einzugsgebiete, wie Lule, Glomma und Angermann, am sensitivsten reagieren, gefolgt von mitteleuropäischen Einzugsgebieten. Südeuropäische Einzugsgebiete, wie Tajo, Duero and Guadalquivir reagierten weniger sensitiv. Die hohe Sensitivität der nordischen Einzugsgebiete kann auf die Schneedominanz im Abflussregime zurückgeführt werden, wodurch diese Einzugsgebiete besonders stark auf Temperaturänderungen reagieren, da der Zeitpunkt der einsetzenden Schneeschmelze einen starken Einfluss auf das Abflussregime hat. Südeuropäische Einzugsgebiete reagieren dagegen weniger sensibel auf Klimaänderungen, weil die Verdunstung einen großen Teil der Wasserbilanz ausmacht. Niederschlagszunahmen, insbesondere bei zunehmender Temperatur, schlagen sich verhältnismäßig geringer im Abfluss nieder.

Anschließend wurde das Schadenspotential analysiert, indem Grenzwerte für diverse Indikatoren, wie Hochwasserabfluss, Niedrigwasserabfluss und Wasserstress, entwickelt wurden. Diese Grenzwerte werden in Form von Isolinien auf die zuvor konstruierte Antwortfläche der Wasserverfügbarkeit aufgetragen. Auf diese Weise kann abgelesen werden, bei welchen T und P Kombinationen der Grenzwert überschritten wird. Um für das Jahr 2100 (repräsentant für den Zeitraum 2071-2100) eine Abschätzung der Wasserverfügbarkeitssituation geben zu können, wurden die projizierten T und P

Änderungen von sechs verschiedenen regionalen Klimamodellen unter dem IPCC A1B Szenario ebenfalls aufgetragen. Somit konnte die Anzahl der Modelle bestimmt werden, die zu einer Überschreitung der Grenzwerte führen. Die sich ergebende Rangfolge der Einzugsgebiete sortiert nach dem höchsten Schadenspotential weicht von der in der Sensitivitätsanalyse festgestellten ab. Bei Weichsel, Tiber and Donau ist das Schadenspotential am höchsten, gefolgt von den südeuropäischen Einzugsgebieten, da dort sowohl die Grenzwerte für Hoch-, bzw. Niedrigwasserindikatoren sowie extremen Wasserstress überschritten werden.

SUMMARY

Water use has increased over recent decades due to population and economic growth, changes in lifestyle, and expanded water supply systems in most parts of the world, putting ecosystems and the sustainable use of water resources increasingly at risk. Irrigation water hereby plays a prominent role: on a global average, 70% of fresh water is withdrawn for irrigation purposes. Only some industrialised nations were able to increase their water use efficiency, mainly by means of technological innovations, leading to decreasing per-capita water use. But also industrialised countries remain hampered by extreme events, such as floods and droughts. And the poorest economies in semi-arid climates still remain hostage to water problems and suffer large-scale poverty and strong population growth. Observational records provide evidence that freshwater resources are vulnerable and have the potential to be strongly impacted by global change, with wide-ranging consequences for human societies and ecosystems.

In this thesis, the impact of global change on the hydrological system is analysed, with special focus on droughts, evapotranspiration and long term water availability. The superior aim is to reveal the linkage between climate, land use, socio-economy and water resources. Research is carried out by means of one of the current state-of-the-art integrated global hydrological models that enables the assessment of current and future water availability and water use at river basin level. Further hydrological components are simulated at the grid-cell level with a resolution of 30 arc minutes.

As part of this thesis, the implemented semi-physical approach to calculating evapotranspiration was regionalised. In order to do so, four different potential evapotranspiration equations were compared and evaluated with regards to their applicability on a global basis. The radiation based equation according to Priestley Taylor was found to be most appropriate for global applications due to its overall low input requirements and comparably good performance. It was then parameterized by use of Class A pan evaporation measurements, now dividing the globe into 12 climate classes from previously two. Additionally, a new approach of calculating albedo was implemented, now being a function of the leaf area development in combination with a background albedo based on soil type. For this purpose, the representation of the leaf area development was also modified to better represent vegetation phenology. The improved simulation of potential evapotranspiration lead to enhanced discharge simulations with the global model.

The aforementioned water resource problems, for example extreme events or increasing irrigation demand, were each associated with particular case-study regions that successively guided the research in this thesis. The different research topics are described in the following.

First, an analysis of extreme events was carried out, i.e. the change in return intervals of the current 100 year drought in the 2070s. For the first time, this analysis considered future climate conditions and future socio-economic effects on anthropogenic water uses for the whole Mediterranean region. The analysis was based on a statistical evaluation of the annual maximum series of deficit volumes resulting from a comparison of current to average hydrographs.

Future conditions were assumed according to the IPCC (‘Intergovernmental Panel on Climate Change’) A2 and B2 scenarios. The A2 scenario projects a strong, but regionally oriented economic growth and fragmented technological change with an emphasis on human wealth, while the IPCC B2

scenario accentuates the protection of the environment and social equity, but also relies on local solutions to economic, social, and environmental sustainability. The ECHAM4 climate model projects the following climate changes for the tow scenarios: an overall increase in temperature throughout the seasons of approximately 4°C in the B2 scenario and approximately 6 °C in the A2 scenario for the region South Europe – Northern Africa. Precipitation decreases by around 10% - 20% in all seasons for the A2 scenario and by about 5% in all seasons except for summer in the B2 scenario, where a slight increase is projected.

As a result, increasing drought frequencies for a belt that stretches from Northern Spain over Southern France towards Northern Italy and Switzerland were calculated for the IPCC B2 scenario for the 2070s and strong increases over most of Southern Europe for the IPCC A2 scenario. Current 100-year droughts would, under the conditions of the IPCC scenarios, return up to once per decade. These changes are statistically significant to 69% and 75%, respectively.

Model simulations imply that climate change has a comparably stronger impact on the change in drought frequency than anthropogenic water uses. But still, anthropogenic water uses can aggravate the situation because they further reduce stream flows. Increasing water uses in the domestic sector due to increasing population, for example, influence droughts in Africa and the Near East. On the other hand, industrial water use decreases in some central and eastern European countries, caused by more efficient technologies. Therefore, droughts return slightly less frequent, because more water remains in the hydrological system. Overall, the impact of anthropogenic water abstractions on drought frequencies is comparably low, with a statistically significance of 58%.

As described in the beginning, irrigation water use plays a prominent role in total anthropogenic water uses. The human appropriation of fresh water for agricultural purposes in Africa was therefore analyzed. Hereby, both ‘blue water’ and ‘green water’ was considered, i.e. the amount of water used for cropland irrigation versus evapotranspiration from cropland. In this study, the spatially explicit land-use change model LandSHIFT and the hydrology model WaterGAP were soft-linked in order to, for the first time, account for the combined effect of land-use change, climate change and technological change on water resources.

Model experiments were conducted for the two scenarios ‘Policy First’ and ‘Security First’ of the UNEP Global Environmental Outlook-4 Report (GEO-4) with a time horizon of 2050. In ‘Policy First’, strong policies are implemented to protect the environment and increase human well-being while promoting economic growth through a high level of international cooperation. ‘Security First’ focuses on regional security including that of resources, with a low diffusion of technology and information at a low level of international cooperation. For both scenarios, similar climate changes are projected. Temperature increase by, in average, 2°C. Precipitation increases by about 10% over most of the continent, except for mall areas of western and southern Africa and the coastline of northern Africa, where precipitation increases by approximately 15% to 20%.

For the year 2000, evapotranspiration from Africa’s rainfed cropland (green water flux) is estimated to 1,085km^3/year, while the abstraction of water for irrigation purposes from the renewable water resources (blue water flux) is estimated to approximately 180km^3/year. Based on model simulations, an additional area of approximately 1.25 mln km² to 1.56 mln km² of natural biomes is converted to cropland during 2000 and 2050, depending on the scenario considered. As a result for the year 2050, simulated evapotranspiration from rainfed cropland is substantially greater than in the year 2000, ranging from 1,870 to 2,040km^3/year, while irrigation abstraction increases up to 194 to 330km^3/year. These findings point out the significant role of water appropriated for rainfed crop production in the continental water cycle in contrast to the sum of water appropriated for irrigation. Further, the results un-

derline that it is worthwhile to not only improve the irrigation water efficiency, but also the efficiency of water used by rainfed crops, given its magnitude.

Thereafter, a systematic approach to assessing both the sensitivity and vulnerability of river basins to climate change was developed. For 18 European catchments, response surfaces of water availability were constructed by interpolating the resulting simulated water availability for each combination of temperature perturbations in the range of [-1°C to +6°C] and precipitation perturbations in the range of [-40% to +100%]. The resulting response surfaces were analysed with regards to the volume below the surface. This indicator in combination with resulting shifts in the flow regime was used for the sensitivity classification, thus considering both the impact on annual as well as monthly flows.

The most sensitive to climate change were the Nordic basins, e.g. Lule, Glomma and Angerman, followed by more central European basins, while southern European basins, e.g. Tagus, Douro and Guadalquivir were least sensitive. The high sensitivity of the Nordic basins can be explained by the fact that they are characterized by a mostly snow-dominated regime. Temperature increases directly affect the onset of high discharges due to snowmelt, and therefore the stability of the flow regime. Southern European basins are found to be least sensitive under the chosen indicators because evaporation makes up a major component in the water balance and increasing precipitation can be counterbalanced by increasing evaporation, especially under rising temperatures.

The vulnerability of river basins to climate change was assessed by developing thresholds for various indicators of high flow, low flow and water stress, relevant to the populations living in these basins. These thresholds were imposed onto the response surfaces as isolines, connecting all those points of the surface where water availability is equal to the threshold value. Results from six regional climate models (RCM) for 2100 under the IPCC A1B scenario were used to assess the number of RCM projections under which these thresholds were violated.

The vulnerability ranking is quite different from the sensitivity ranking and sees the southern European basins much higher ranked based on higher water stress levels they might be facing in the future. Comparably highest vulnerable in Europe are the Vistula and Tiber basins due to the fact that both the high or low flow threshold and water stress threshold are violated under all climate model simulations.

CONTENTS

CHAPTER 1

INTRODUCTION

1.1 Background

One of the most pressing environmental concerns at the beginning of the 21st century still is the assured availability of fresh water resources both now and in the future to satisfy anthropogenic requirements and sustain ecosystem services. With currently one-third of the population living in water-stressed regions (Alcamo et al. 2003b) and the global population expected to surpass nine billion from currently 6.8 billion within the next forty years (UN 2009), the pressure on water resources will increase due to increasing water demand.

Fulfilling this demand can only be achieved by improved management of existing resources, due to their finite character in many parts of the world. The most problematic regions are found in the semi-arid savanna and steppe regions, due to high evaporative demands and land degradation, as pointed out by Falkenmark and Lannerstad (2005). One of the greatest water related challenges is to achieve sustainable development particularly in sub-Saharan Africa, caused by the superimposition of water scarcity and land degradation with high population growth rates and poverty (Falkenmark and Rockström 2006).

Adding to these pressures is the uncertain impact of climate change. Some important factors determining the global climate are the level of solar irradiance at the troposphere, and radiative properties of atmosphere and soils surfaces. During the last century, the composition of the atmosphere has been severely affected by human activity, for example by increased emissions of aerosols and greenhouse gases. Anthropogenic induced land cover changes have further affected climate by e.g. modified energy exchanges due to changes in surface albedo (Sagan et al. 1979, O'Brien 1996), or changes in the effectiveness of ecosystems to act as carbon sinks and sources

(Lockwood 1983, Woodwell et al. 1983, Houghton 1999). These changes are likely to already have influenced temperature, precipitation, and the frequency of extreme events, such as droughts (IPCC 2007).

Droughts are natural hazards, temporarily affecting almost every region in the world. The temporary shortage of water, however, poses an even greater threat to nature, human well-being and the economy where it coincides with a structural imbalance between supply and demand. Although, for example, EU countries are abstracting on average only 21% of their renewable resources each year (Krinner et al. 1999), recent years have shown an extreme vulnerability of southern European countries, where periodic droughts caused major environmental, social and economic problems (Krinner et al. 1999).

In water resources management, as well as in the planning of climate change related mitigation and adaptation strategies in the water sector, scientific support is indispensable to build a common understanding of the nature of water resource systems and the potential for societal response. In order to develop sound climate-related policies to limit the total burden of, and residual impacts associated with climate change, integrated modelling tools are essential to analyse the current situation, examine expected changes and evaluate strategies for sustainable pathways. Based on the fact that political units are usually unrelated to river basin boundaries, and the urge to analyse large river basins, global scale hydrological modelling has become well established during the last decade (Döll et al. 2008).

In large-scale hydrological models, however, a tendency towards biased discharge simulations in arid[1] to semi-arid[2] regions of the globe is generally found (Fekete et al. 1999, Nijssen et al. 2001, Döll et al. 2003). One reason is the lack of high quality observations and longterm time series, which can be explained by a rather sparse population in most arid areas, limited economic resources and irregularity of hydrological extreme events, which has hindered the understanding of specific features of dryland responses (McMahon 1979, Pilgrim et al. 1988).

In these regions, water resources are scarce and under severe as well as increasing pressure due to growing per capita water use, high irrigation water demands, increasing volumes of industrial and domestic waste and over-exploitation of groundwater and fossil water. Ecosystems are most fragile, and sensitive to even small changes in prevailing conditions. They suffer from heat stress, frequent drought, and salinity (Solh et al. 2003). Rainfall patterns are inherently erratic. Rain falls mostly as heavy

[1] Arid regions are hereby defined as ecosystems that receive less than 250 mm of precipitation per year (IPCC 2001b)

[2] Semi-arid areas receive more than 250mm of precipitation and are characterized by scrubby vegetation with short, coarse grass

showers and is lost to runoff due to mostly sparse vegetation cover, crusted soils and reduced infiltration capacity (Morin and Benyamini 1977). A high rate of potential evapotranspiration further reduces directly available water.

The substantial progress in the development of national data networks and experimental research during the last years, that resulted in a number of small-scale studies (Hess 1998 for Nigeria, Ma and Fu 2003 for north China, Hübener et al. 2005 for Morocco, Krol and Bronstert 2007 for north-east Brazil), now offers the opportunity to incorporate distinctive hydrological processes of semi- arid and arid environments into global hydrological models. Considering further that semi-arid and arid regions make up 41% of the earth's surface and are inhabited by one-sixth of the world's population (Solh et al. 2003), the urge to improve their representation in global hydrological models becomes even more pressing.

1.2 Global modelling of water balance components

The assessment of the current water resources situation, including current anthropogenic interference and the analysis of global change impacts on the hydrological system, as carried out in this thesis, requires a modelling tool that incorporates major hydrological processes to simulate the continental water cycle under the various influences. There are a number of models that are suitable for a global simulation of water balance components, for example land surface modules that have lately been incorporated into general circulation models (e.g. Hagemann and Gates 2003), or dynamic vegetation models (Sitch et al. 2003, Gerten et al. 2004). These, however, mostly simulate specific components of the water balance, to the extend as required for other (vegetation/atmospheric) processes. For the purpose of this thesis, the choice of models was narrowed down to global water balance models, as with these, the focus lays on the simulation of all major hydrological processes at grid cell- and basin level.

Currently, there exist five well-known global hydrological models, which have already been applied on a global scale. These are the following models: WBM (Vörösmarty et al. 2000), Macro-PDM (Arnell 1999b, 2003), GWAVA (Meigh et al. 1999), WASMOD-M (Widén-Nilsson et al. 2007, Widén-Nilsson et al. 2009) and WaterGAP (Alcamo et al. 2003a, Döll et al. 2003). All models have a spatial resolution of 30 arc minutes and work with a (quasi-) daily time step using monthly climate input data. More or less, these models try to capture the same hydrological processes, partly by different semi-physical approaches. Great differences exist in routing routines and model tuning approaches.

The WaterGAP model is probably the most complex of the five models (Widén-Nilsson 2007). It is chosen for the purpose of this thesis, because it enables the inte-

grated modelling of water availability and water use, i.e. human impacts on the hydrological cycle in the form of water withdrawals in different water using sectors. The model is further well suited for scenario analysis because all drivers of the model can be adapted to scenario conditions. Kaspar (2004) has shown for selected parameters that the effect of climate change scenarios is stronger than parameter uncertainty within the model. In Chapter 2, the main functionalities of the WaterGAP model are further introduced.

1.3 Global change analysis

Global change is the term generally used to encompass a multitude of environmental, ecological and socio-economic changes that have been noticed, measured and studied on Earth, for example the study of climate change, species extinction, land use change, changes in the carbon cycle and hydrologic cycle, air quality, etc.

This thesis, in particular, seeks to analyze and compare hydrological processes under current conditions and in the light of global change, focusing explicitly on the combined effect of climate change, land use change and socio-economic changes, due to the following reasons.

The hydrological system has been shown to be strongly interrelated to the climate system, with change in one system inducing change in the other (Kundzewicz 2003). Over the last century, an increase in average global temperature of 0.6°C has already been observed (IPCC 2001c). The 1990s was very likely the warmest decade; temperature increase has reduced the global snow and ice cover since the late 1960s. More extreme and heavier precipitation events were observed in many areas. Observed impacts on global water resources show trends in annual, seasonal and extreme stream flows, and an increase in return intervals of floods and droughts in many regions (IPCC 2001a). A common expectation is strong changes in water cycle components caused by increased temperatures and a shift in rainfall and discharge regimes. The analysis of the current and future situation of water resources therefore has to consider possible impacts of climate change.

Land use changes are transforming the earth's surface at an accelerating pace (Meyer and B. L. Turner II 1992). There is an increased recognition that land use change is a major driver of climate change, through its interaction with ecosystems, biogeochemical cycles, biodiversity, and human activities. For example, land use change, especially deforestation, is considered to be responsible for about 25% of the anthropogenic carbon dioxide emissions (IPCC 2001c). Land degradation affects large parts of the developing world (Kishk 1990, Barbier 1997). Even more directly, land use change affects the water cycle by modifying interception, evapotranspiration, run-

off generation and runoff concentration. These impacts are still largely unknown, even more so under scenario conditions.

The amount of water needed for anthropogenic uses does not remain constant but changes over regions and time. The ability of societies to cope with climate change impacts is determined by their economic, political and institutional capabilities. Water use efficiency, i.e. the amount that must be expended to produce one unit of any good or service, depends for example on industrial processes and technological progress, which is strongly related to the economic conditions of a country. A requisite in that respect is whether the country is able to afford new technologies and invest into their development. On the other hand, water use efficiency also depends on social conditions. Among these are e.g. social tastes and preferences, public education, property rights, and public policy.

A central tool in combining these different components of global change are scenarios. Scenarios are defined as plausible descriptions about how the future might unfold (e.g. Alcamo 2008). They are based on coherent and consistent sets of assumptions on key driving forces and relationships and integrate quantitative models with qualitative assessments of social and political trends. Parson et al. (2007) introduce a simple linear causal chain extending from the socio-economic determinants of greenhouse-gas emissions to the impacts of climate change (Figure 1-1). Different scenario types can be distinguished based on where they fall along the causal chain and in which direction they are effective. These are emission scenarios, stating future paths of greenhouse-gas emissions and other climate perturbations, climate change scenarios, which are projections of the future climate, based on an internally consistent set of climatological relationships, and multivariate scenarios. The latter is used in this thesis, as it incorporates the previous two:

Assessing climate-change impacts requires not just considering climate in isolation, but other linked changes and stresses including both environmental and socio-economic trends. The factors that influence particular impacts and vulnerabilities are likely to be widely variable, and may include demographic, economic, technological, institutional, and cultural characteristics. Scenarios are generated in an exploratory manner in the context of attempting to assess specific local and regional impacts (Parson et al. 2007). They are based on coherent and consistent sets of assumptions on key driving forces and relationships. This qualitative description of driving forces is then translated during the scenario analysis into a quantitative description, on the one hand involving the close dialogue with experts, policy makers and stakeholders, on the other hand by model computations. With the key objective of exploring alternative future developments, the storylines are most often characterized by two opposite driving force pathways, e.g. globalization of markets versus regionalization (Alcamo 2008).

Multivariate scenarios, for example, have been developed as part of the following studies: *'IPCC TAR'* (IPCC 2001a), *'GEO4'* (UNEP 2007b), or *'MEA'* (Carpenter et al. 2005). These scenarios build the foundation for the global change analysis carried out in this thesis.

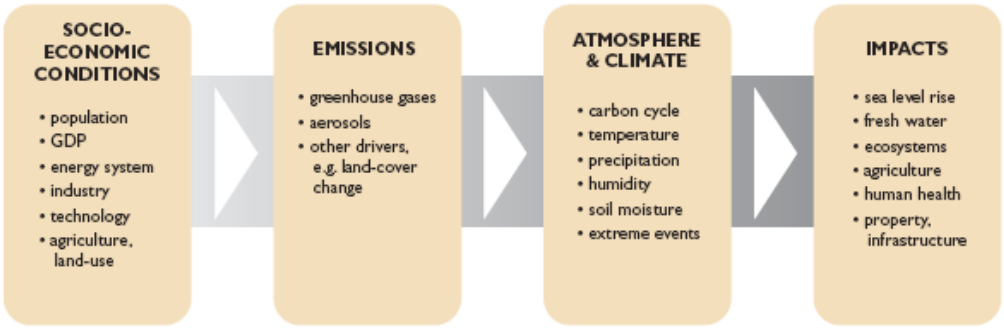

Figure 1-1. Simple linear causal chain for scenarios of anthropogenic climate change as given in Parson et al. (2007); Depending on the scenario analysis, the direction can also be reversed.

1.4 Objectives and structure of the thesis

The objective of this thesis is to integratively model the impact of global change on the hydrological system with respect to droughts, evapotranspiration and long term water availability, each in a specific case study region, i.e. the Mediterranean, Africa and Europe. In order to enhance the quality of model simulations of the global hydrological model WaterGAP in semi-arid to arid environments, the formulation of the potential evapotranspiration process is parameterized to better represent prevailing conditions in different climate classes. The overall aim is to gain new insights into hydrological processes under current and global change conditions as water resources can easily become a limiting factor for development of population, economic activity and ecosystems.

During the formulation of research needs in the previous sections, an association of identified problems with particular regions was carried out. Combining these with an impact analysis of global change, specific research questions were formulated that guide the research in this thesis towards revealing the linkage between climate, land use, socio-economy and water resources. The structure of this thesis is closely linked to the research required to answer these research questions and will be laid out below. All chapters are composed as stand-alone sections that are comprehensible in themselves. Before starting with the main research, an overview of the WaterGAP model is given in *Chapter 2*, where focal functionalities of the model are introduced. *Chapter 8* discusses the main findings and concludes by revisiting each of the research questions.

Additionally, an outlook is given on further research needs. The main research is described in *Chapters 3-7*. Each chapter is related to one of the following research questions, described in detail below:

What is the impact of climate change on droughts in the Mediterranean, and how is the impact affected by anthropogenic interference?

The impacts of climate change are expected to be most significant where they occur in the context of multiple stresses such as unequal access to resources, environmental degradation, poverty, and food insecurity. Droughts are a normal, recurrent feature of climate and occur in all climatic zones. A review of past drought events in Europe, however, shows a distinct vulnerability of the Mediterranean region as here, droughts coincide with an increased need for water for agriculture and life in an already water-scarce environment. The region disposes of 3% of the world's fresh water resources and 50% of the global 'water poor'[3] population (PNUE/PAM/PLAN BLEU 2004). Droughts are primarily caused by a temporal decrease in precipitation but anthropogenic water abstractions can aggravate the situation.

Chapter 3 therefore analyses the impact of climate change and socio-economic changes on future return intervals of the current 100 year hydrological drought in the Mediterranean. Hereby, the IPCC scenarios A2 and B2, as well as results from the global general circulation model ECHAM4 for the 2070s are considered.

What is the human appropriation of water for agriculture in Africa in the form of irrigation water compared to evapotranspiration? How is this appropriation affected by land cover change, climate change and technological change?

Whether technological innovation will enable adaptive capacity of societies and ecosystems to develop at a rate commensurate with climate change is a key question for all world regions. In Africa, however, this question is even more pressing because of high population growth rates and a low investment base. The level of vulnerability of the African population to climate change depends on their present day vulnerability, which is determined by their economic, political and institutional capabilities. Historical evidence shows that both natural and managed ecosystems in Africa face substantial adverse impacts from existing climate variability (Folland et al. 1990, Jones and

[3] Less than 1,000 m^3 water per capita and year (Falkenmark and Widstrand 1992)

Briffa 1992), the nature of which will almost certainly be altered by longterm climate change. Given the strong economic dependence of sub-Saharan Africa on rainfed agriculture, the question of how the various effects of land-use change, climate change and technological change might superimpose becomes even more pressing.

Hence, in *Chapter 4*, a comprehensive model-based analysis of water use for crop production on the African continent is presented. The analysis includes the components evapotranspiration from cropland ("green" water fluxes) and water used for cropland irrigation (crop-related fraction of "blue" water fluxes). Model experiments are conducted for two multivariate scenarios with a time horizon of 2050, taking into account the combined effect of land-use change, climate change and technological change.

How can the representation of evapotranspiration in global models be improved for semi-arid to arid environments? How can improvements of evapotranspiration processes be implemented in global models?

Evapotranspiration plays a significantly larger role in semi-arid catchments than in humid catchments (Schneider et al. 2007) and is a key component of the water balance. An improved representation of the evapotranspiration process might therefore be a key to enhance discharge simulations with a global model for these regions.

Chapter 5 compares the application of potential evapotranspiration equations based on Priestley Taylor, Kimberly Penman, Penman Monteith (FAO-56) and Hargreaves in a global hydrological model to demonstrate their difference, and assess their impact on the calculation of stream flows. In this chapter, recommendations are made which potential evapotranspiration equation is currently best suited for a global application given prevailing data constraints.

Chapter 6 parameterizes the α-coefficient of the Priestley Taylor potential evapotranspiration equation to enable an improved global application. Pan evaporation measurements are used, supplemented by α-values from existing small-scale studies. The parameterization is carried out within the boundaries of climate zones. The aim of this chapter is to improve discharge simulations with a global model by improving the representation of the potential evapotranspiration process.

What is a systematic method for characterizing the sensitivity of European river basin hydrology to climate change?

Last but not least, climate change is a global problem, which concerns industrialized countries as much as developing countries. The EU, for example, has defined an indicative long term global temperature target of not more than 2°C above pre-industrial levels (Sixth Environment Action Programme of the European Community 2002-2012 - 6th EAP[4]) which, according to recent findings[5], corresponds to a long term CO_2 stabilization level of 450ppm. The United Kingdom adopted a 60%, Germany a 40% reduction target of national emissions from 1990 levels to 2050. A country reaching its national environmental targets is also dependent on international environmental cooperation. Many river basins in the EU, for example, are trans-boundary resources and the EU Water Framework Directive[6] is a first step towards identifying surface waters at risk and managing water resources in a mutual effort. Europe exhibits a wide variety of typical annual stream flow distributions due to the diversity in regional climate and geo-physical conditions. In order to evaluate climate change impacts from a Pan-European perspective, a systematic approach is required that enables the comparison of the sensitivity to climate change of an arbitrary number of river basins.

In *Chapter 7* a new method is developed that enables a systematic, consistent and objective climate change sensitivity and vulnerability assessment of an optional number of river basins. This analysis introduces the response surface method to examine impacts of climate change on water availability, and rank 18 European river basins according to their sensitivity and vulnerability.

[4] http://ec.europa.eu/environment/newprg/intro.htm, accessed 01.05.09
[5] Results from the EU FP6 Ensembles Project, RT7 – Scenarios, http://www.feem-web.it/ensembles-rt7/, accessed 01.05.09
[6] http://ec.europa.eu/environment/water/water-framework/index_en.html, accessed 01.05.09

CHAPTER 2

THE WATERGAP MODEL

In the following, the WaterGAP Model is briefly introduced with the purpose of giving an overview of main functionalities of the model. Processes relevant to carry out analyses in question are described in more detail in the specific chapter.

With WaterGAP (see Figure 2-1), the continental water cycle is simulated on a spatial grid with a resolution of 30 arc minutes in a daily computation time step, taking into account precipitation (P), snowmelt, interception (E_c), evaporation (E_a), soil water, groundwater (R_g), base flow (Q_b) and runoff (R_s). Major hydrological processes are simplified by conceptual formulations. Based on climate input, actual evapotranspiration is derived from canopy and soil water balances. The level of crown moisture saturation determines the fraction of incoming precipitation that directly evaporates without reaching the soil, whereby the maximum canopy storage is calculated as a function of the leaf area index. The remainder accumulates actual soil moisture until saturation. The maximum soil water capacity results from the depth of the effective root zone, and specific water capacity of the particular soil. Excess water is routed to the adjacent grid-cell.

Water withdrawals and consumptions are computed with the water use modules for the domestic, industrial and agricultural sectors, as described below. The domestic sector includes municipal and household uses; the industrial sector is subdivided into electricity production and manufacturing facilities; the agricultural sector is subdivided into irrigation and livestock uses (Alcamo et al. 2005). The water uses are abstracted from the water availability in the respective grid cell. The remainder forms river discharge, which is routed through the respective river basin according to a global drainage direction map (Döll and Siebert 2002). WaterGAP simulations of river discharge are tested to measured discharges from the Global Runoff Data Centre (GRDC 2004) at currently 1235 stations world-wide.

2.1 Input data

Information on land surface characteristics such as the spatial distribution of vegetation, soil types, land use, groundwater and surface water bodies follows global data sets as published by FAO, USGS, and others (see Table 2-1). Climate input consists of the "CRU TS 2.1" gridded dataset for monthly precipitation, air temperature, cloud cover and frequency of wet days (Mitchell and Jones 2005).

Table 2-1. Static input maps used in WaterGAP.

Name	Content	Source
Global Lake and Wetland Database (GLWD)	location and size of lakes, reservoirs and wetlands worldwide	Lehner and Döll (2004)
FAO Soil Map of the World	digital soil map and derived soil properties	FAO (2003b)
DDM30	Drainage Direction Map and river network	Döll and Lehner (2002)
Glacier	World Glacier Inventory	NSIDC (2007)
Permafrost	Circum-Arctic Map of Permafrost and Ground-Ice Conditions	Brown et al. (1998)
LAI	Worldwide historical estimates of Leaf Area Index	Scurlock et al. (2001)
Soil water storage	soil water retention properties	Batjes (1996)
GLCC	Global Land Cover Characterization	USGS (2007)
GTOPO30	Global Digital Elevation	USGS (2006)

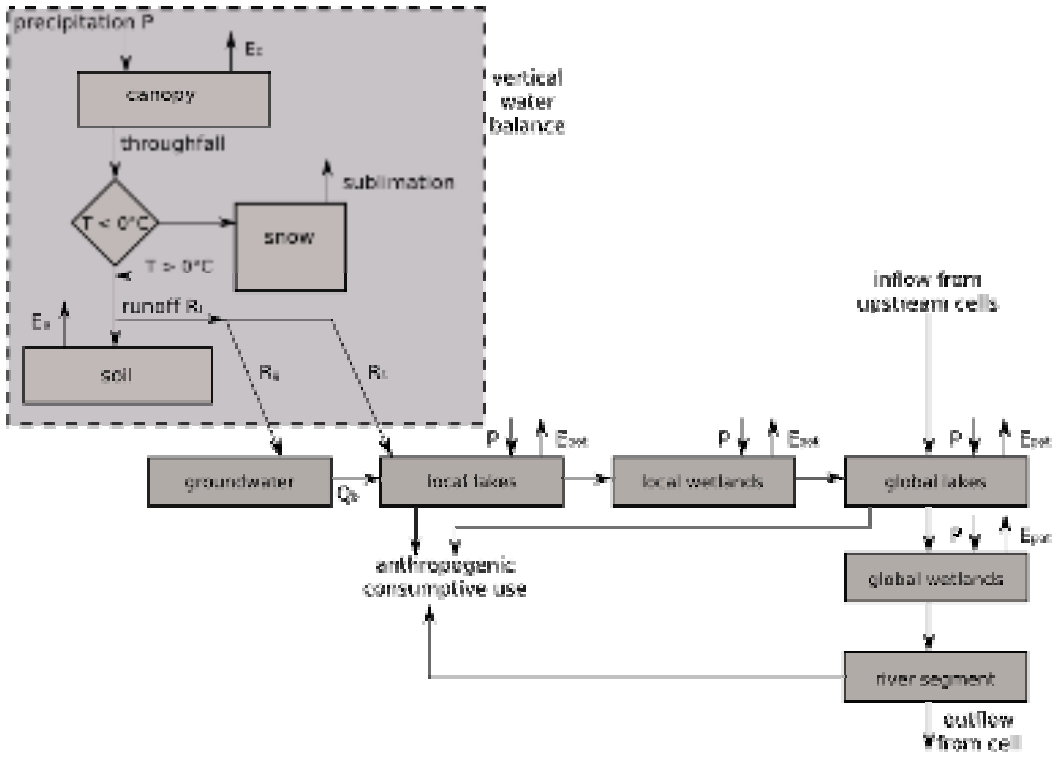

Figure 2-1. Conceptual structure of the WaterGAP Model.

2.2 Spatial and temporal aggregation

Climate input consists of time series of monthly values, which are model-internally disaggregated to daily values. The model then calculates water balances at a daily time step for a period of at least 30 years. Results of water availability are mostly given as long-term annual averages (e.g. the climate normal period 1961-1990, or lately also 1971-2000), in order to level out short-term fluctuations.

The spatial resolution of the WaterGAP model is 30 arc minutes, which is an arbitrary value, initially defined by the resolution of the input data. Meaningful assessments should be made at river basin level, because water from one grid-cell is theoretically accessible by its neighbouring cells. An assessment at country level is difficult, as many resources are trans-boundary resources, which can accessed by, and have to be shared among, all neighbouring states.

2.3 The water use modules

The water use modules cover the most important water use sectors to calculate water uses at the grid cell level. Globally, irrigation water withdrawals account for over 70% of total withdrawal but are more important in semi-arid and arid areas. In humid areas, water withdrawals are mainly composed by domestic and industrial requirements.

Based on data availability and with the prospect of modelling future water requirements, the basic concept consist of modelling water intensities per unit user/good and multiply these with absolute numbers per grid-cell.

Irrigation water uses are calculated as a function of climate (as described above), extent of irrigated area (Döll and Siebert 2000), cropping intensity and crop type with a 30 arc-minute grid cell resolution. Evapotranspiration is crop-specific and depends on the growing stage of the crop. Due to data constraints, the model currently distinguishes rice and non-rice crops. The irrigation requirements are determined in three steps: First cropping patterns and optimal growing seasons are determined based on soil suitability and climate, taking into account multi-cropping if applicable. Next, water consumption of irrigated crops (net irrigation requirement) is computed for each day of the growing season. Water withdrawals for irrigation (gross irrigation requirements) are computed by dividing plant water requirements by irrigation project efficiencies, which account for water distribution losses through seepage and evaporation (Döll and Siebert 2002, Alcamo et al. 2003). Project efficiencies were compiled from various sources, as described in Döll and Siebert (2002). Validation of the model with independent data shows a good agreement for modelled irrigation water demand (Döll and Siebert 2002).

Livestock water withdrawals equal consumptive uses. They are very small in comparison to irrigation water demand. Water uses are calculated by multiplying stock numbers per grid cell with stock-specific water demands. The model currently distinguishes 12 animal species: buffalos, dairy cattle, non-dairy cattle, camels, chicken, ducks, geese, goats, pigs, sheep, turkey, horses. Absolute stock numbers per grid cell have been derived based on literature research and scaled to meet national and subnational statistics (FAO).

Domestic and manufacturing sector: Water needs depend on structural and technologic conditions. The structure of water uses considers the combination of water using activities and habits within a sector. Technology directly affects the degree of water efficiency, which is usually higher in industrialized countries. The domestic sector includes household use, small business and other municipal water use. Water uses in the domestic sector take into account GDP (Gross Domestic Product) and population density. For the manufacturing sector, a function of GVA (Gross Value Added) and GDP is applied.

Electricity generation: Water use for electricity production mainly results from the need for cooling water. The amount of water required depends strongly on the cooling system and thermal power plant type. The model currently distinguishes four plant types and 3 cooling types. Water uses are allocated to the respective grid-cell based on the location of power plants.

CHAPTER 3

MODELLING FUTURE FREQUENCIES OF THE CURRENT 100 YEAR DROUGHT IN THE MEDITERRANEAN

Summary

This study examines the change in current 100-year hydrological drought frequencies in the Mediterranean in comparison to the 2070s as simulated by the global model WaterGAP. The analysis considers socio-economic and climate changes as indicated by the IPCC scenarios A2 and B2 and the global general circulation model ECHAM4. Under these conditions today's 100-year drought is estimated to occur 10 times more frequently in the future over a large part of the Northern Mediterranean while in North Africa, today's 100-year drought will occur less frequently. Water abstractions are shown to play a minor role in comparison to the impact of climate change, but can intensify the situation.

3.1 Introduction

The diversity and complexity of drought impacts and the low level of preparedness for future events is a point of global concern. Entries in the EM-DAT database (e.g. Guha-Sapir et al. 2004) show that total reported global economic losses due to droughts rank fourth in the list, following those reported for earthquakes, floods and windstorms. Two major droughts in Australia in the last twenty years have resulted in great financial losses, with the damage of the 1991-1995 drought amounting to an estimated $5 billion. Approximately 8 million of Ethiopia's 60 million people are at risk due to drought (UNICEF 2000). Large areas of Europe have been affected by droughts over the past 50 years (Estrela et al. 2001). Water shortages and poor harvests during the droughts of the early 1990s exposed an acute vulnerability of the Mediterranean region to climatic extremes. The latest drought of 2003 affected most of continental Europe. The ongoing debate about climate change and its potential effects on the fre-

quency and severity of extreme climatic events is adding further to the concerns of scientists and decision makers, because observed changes have shown that drought events are already on the rise (IPCC 2001b, Guha-Sapir et al. 2004).

3.2 Purpose of the study

This study will, explicitly for the Mediterranean Region, examine whether the upward trend of droughts (IPCC 2001b), as described above, is likely to continue in the future, examining drought frequency as the main indicator. It will investigate the impacts of global change, including climate and socio-economic changes on future hydrological drought frequencies using two of the IPCC global emission scenarios, A2 and B2 (IPCC 2000). These emission scenarios were constructed to explore future global developments of society and environment. Scenario A2 assumes a strong, but regionally oriented economic growth and fragmented technological change with an emphasis on human wealth, while B2 emphasizes the protection of the environment and social equity, but also relies on local solutions to economic, social, and environmental sustainability. Both scenarios represent a world in which the differences between developed and developing countries remain strong.

3.3 The WaterGAP Model

The analysis is based on the application of the integrated global water model WaterGAP (Water - Global Assessment and Prognosis). WaterGAP, developed at the Center for Environmental Systems Research at the University of Kassel, Germany, computes current and future water availability and water use. It consists of a global hydrology model to simulate the continental water cycle and a global water use model to simulate anthropogenic impacts on it (Alcamo et al. 2003a, Döll et al. 2003).

The hydrology model calculates daily water balances based on climate information on a 0.5° x 0.5° (geographical latitude and longitude) grid cell basis. For each grid cell, the daily vertical water balance is calculated to determine evapotranspiration, snow and groundwater storage, and surface runoff. With the water use model, water withdrawals for the different sectors household, industry (manufacturing and electricity production) and agriculture (livestock and irrigation) are calculated. Water withdrawals in the domestic and industrial sectors, for example, are calculated by relating changes in national income to changes in the amount of water used per person and per unit electricity generated. Structural changes are considered by taking into account an initially increasing water demand due to structural changes in the water use with increasing income (e.g. domestic appliances) followed by an eventual stabilization of water demands at high incomes. Technological change, on the other hand, effects wa-

ter use by improvements in water use efficiency (Alcamo et al. 2003b, a, Alcamo et al. 2007). The water use is subtracted from the surface runoff calculated in the hydrological model and discharges are computed for each grid cell. The cell discharge is routed through the respective river basin according to a global drainage direction map (Döll and Lehner 2002) to form river discharge. The model is calibrated and validated against measured discharges from the Global Runoff Data Center (GRDC 2004).

Current climatic conditions are represented by the climate normal period, 1961-1990, using CRU data (New et al. 2000). In order to derive future discharge values, WaterGAP is driven by climate change projections (temperature and precipitation) as calculated by the global climate Model ECHAM4 (Roeckner et al. 1996), and by a set of scenario assumptions for changes in human water use (IPCC 2000) that provide values for e.g. technological and structural changes, population growth rates, economic indicators, etc. Future conditions are represented by the time period 2061-2090, referred to as the 2070s.

Döll et al. (2003) showed that WaterGAP simulations are fairly robust for long-term average discharges and to be in reasonable limits for monthly high and low-flow statistics, especially for large river basins (> 20,000 km²). Lehner et al. (2006) further examined the suitability of WaterGAP to model low flow and droughts. They found a modelling efficiency (which is expressed as the degree of agreement between GRDC observed data with WaterGAP modelling results, where 0 means no agreement and 1 total agreement) of 0.88 for the 100-year drought deficit volume and a modelling efficiency of 0.79 for monthly Q_{90} (Nash-Sutcliffe coefficients) (Nash and Sutcliffe 1970). When looking at specific drought events, magnitude and timing, WaterGAP showed some significant errors and is therefore currently not capable of simulating single events. Relative changes, as well as large-scale low-flow regimes and general drought statistics, however, are captured well (Lehner et al. 2006). The model is used in this study to analyse long-term changes between now (1961-1990) and the future (2061-2090) and not to reproduce point events in exact timing and magnitude.

3.4 Droughts in general

The Mediterranean climate is characterized by mild wet winters and hot, dry summers. ECHAM4 shows an overall increase in temperature throughout the seasons of approximately 4 degrees Celsius in the B2 scenario and around 6 degrees Celsius in the A2 scenario for the region *South Europe – Northern Africa*. Precipitation decreases by around 10% - 20% in all seasons for the A2 scenario and by about 5% in all seasons except for summer in the B2 scenario, where a slight increase is projected. The question is what impact these climate changes will have on low flow conditions and drought frequencies.

Per definition, a drought marks a period of abnormally dry weather sufficiently prolonged so that the lack of water causes a serious hydrologic imbalance (such as crop damage, water supply shortage, etc.) in the affected area (McGraw-Hill 2003). It is hence the consequence of a natural reduction in the amount of precipitation received over an extended period of time, usually a season or more in length. Other climatic factors, e.g. high temperatures and winds or low relative humidity, can significantly aggravate the severity of the event. The effects of droughts often accumulate slowly over a considerable period of time and may linger for years after the termination of the event. Therefore, the onset and end of a drought are difficult to determine. Drought is a normal feature of climate and its recurrence is inevitable. It occurs in high, as well as low rainfall areas. Drought is a frequent and often catastrophic feature in semi-arid climates. It is less frequent and disruptive in humid regions and a less meaningful concept for deserts. However, there remains much disagreement within the scientific and policy community about its characteristics. This partly explains the lack of progress in drought management in many parts of the world (Wilhite 2000).

Drought severity is, on the one hand, dependent on duration, intensity and geographical extent of a specific drought episode. On the other hand it depends on anthropogenic and vegetation demands and can have far-reaching effects on society, economy and environment. Therefore, many disciplinary definitions of droughts exist (Wilhite 2000). Each discipline incorporates different physical, biological, or socioeconomic factors in its definition. For example *meteorological drought* is defined as an interval of time during which the actual moisture supply falls short of climatically specific moisture supply at a given place (Palmer 1965). *Agricultural drought* is defined as a period, in which soil moisture content is inadequate to meet evapotranspirative demands to initiate and sustain crop growth (WMO 1975). *Hydrologic drought* is associated with inadequate stream flow, reservoir and lake levels or groundwater recharge. Chronologically, hydrological droughts lag behind the occurrence of meteorological and agricultural droughts (Wilhite 2000). They can be of greater extent than the initial meteorological drought due to anthropogenic and other influences. This study will examine hydrological drought because it is the last in the chain and includes all other influences, e.g. of anthropogenic or climatic nature.

3.5 Drought analysis with WaterGAP

When analysing drought frequencies, a quantitative definition of the starting point and end point of a drought has to be set. A common method is the threshold level method, which has been applied in various studies (Stahl and Demuth 1999, Fleig et al. 2006, Lehner et al. 2006). The monthly discharge hydrograph is compared to a constant or seasonal threshold value. If the discharge falls below the threshold level, the drought event is defined to start and to last until the discharge curve intersects with the threshold line, i.e. exceeds the threshold value. The specific drought event is, besides its duration in time, further defined by its deficit volume, which is calculated as the area enclosed by the discharge curve and threshold line.

The explicit value of the threshold is of critical importance as it determines the onset and end of each event. If the value is too high, single events can no longer be distinguished but merge into one drought event. If the value is too low, too few droughts are computed and the statistical analysis of extreme values is no longer valid.

Common threshold values are, for example, the Q_{70} or Q_{90} (the flow that is exceeded in 70% or 90% percent of the time, respectively), as for example applied by Hisdal and Tallaksen (2000), Arnell (1999a), Gottschalk et al. (1997), and Chang and Stenson (1990). Tate and Freeman (2000) and Woo and Tarhule (1994) have, however, shown that the Q_{70} or Q_{90} thresholds are not applicable to intermittent streams where a value between Q_5 and Q_{20} is suggested. Consequently, the threshold would be basin dependent, which is a disadvantage in meso-scale studies.

As a compromise, Lehner et al. (2006) use the long-term mean discharge as a constant threshold value over time (red line in Figure 3-1). This value is rather high and the calculated drought events are characterized by a higher deficit volume and longer duration. Overall, a constant threshold will, by definition, lead to a computed drought in 90%, 70%, or 50% of the cases, depending on its quantitative value. Yet a drought is defined as a deviation from *normal*. Therefore, the definition of *normal* should be more strongly related to the regularly occurring variation of the discharge over time.

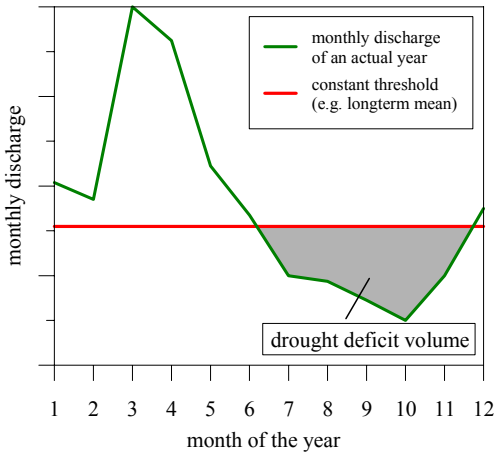

Figure 3-1. Drought deficit volume as calculated with a constant threshold.

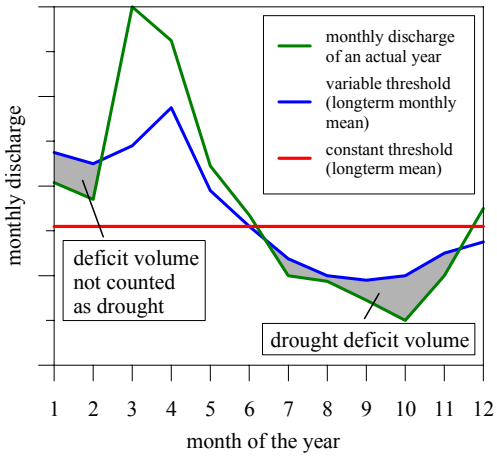

Figure 3-2. Drought deficit volume as calculated with a combination of constant threshold with a longterm monthly threshold.

Another possibility is, consequently, to apply a variable threshold following the seasonality of the hydrograph, e.g. the long-term monthly means (blue line in Figure 3-2). In this case a deficit volume might be calculated for periods when enough water is available in the river, e.g. if elevated discharges during spring due to snowmelt are for some reason lower than usual (grey area for the months January and February in Figure 3-2). Since a flow, which is reduced during a particular season, but not absolutely low, is commonly not considered a drought, a combined threshold is used in this study. A deficit volume (grey area in Figure 3-2) is calculated for each cell of a river basin as the difference between the long-term (1961-1990) monthly mean cell discharge (blue line in Figure 3-2) and the actual monthly cell discharge (green line in Figure 3-2) but only for that period of time when the hydrograph falls below the constant threshold of 90 percent of the long-term mean (red line in Figure 3-2). The same thresholds are applied to the discharge values under climate scenarios.

Many studies exist on the estimation of return periods, especially the choice of probability distributions (e.g. Bobee 1975, Bobee and Robitaille 1977, Kite 1977, Bobee and Ashkar 1991, Mitosek et al. 2006) and method for parameter estimation (e.g. Arora and Singh 1989). In this study the three parameter (Log) Pearson Type III distribution is chosen because it has widely been applied in extreme flow analysis, can be fit to high and low discharge values, and is a common standard at government agencies in the U.S. and Australia (according to IACWD 1982, and IEA 1998). The deficit volumes calculated as described above are used to form the annual maximum series (Madsen et al. 1997) by selecting the highest deficit volume each year and ranking these according to size. For each grid cell, either the Pearson III or Log Pearson III

distribution is fitted to the annual maximum series based on the underlying data, using the method of moments (Stedinger et al. 1993). The fit of the chosen distribution is checked by an analytical goodness-of-fit test (Kolmogorov - Smirnov test, Rao and Hamed 2000).

The theoretical probability distribution is then used to estimate the probabilities of the hypothetical expected deficit volumes to obtain the drought frequency distribution for T=1 to 200 (drought deficit volumes that are exceeded once every T years). This procedure is carried out for current conditions, as well as the 2070s. Similar to the 100-year flood, which is widely used by engineers as the reference level for the design of dams, reservoirs, etc. 100-year droughts are further examined. As a result, the change in return period of today's 100-year drought is calculated by comparing the current situation with the 2070s.

The statistical significance is evaluated by calculating the 90% confidence intervals (Stedinger et al. 1993) for the estimates of T-year droughts, as exemplary shown in Figure 3-3 and Figure 3-4 for the Danube catchment. The 30-year maximum series is a random sample of the underlying population of annual droughts (expressed in drought deficit volumes) and is used to estimate the frequency curve of that population, which can only be an approximation to the true drought frequency curve (IACWD 1982). In order to evaluate the statistical significance of the change in drought frequencies, an interval of hypothetical frequency curves is constructed that, with a 90% degree of confidence, contains the true population frequency curve. Both the record length N and the specific exceedance probability control the statistical reliability of the estimated frequency curve (IACWD 1982). Figure 3-3 shows the current and A2 2070s drought frequency curves and 90% confidence intervals for the return periods T=2 to 200. If the two bands (curves accompanied by their 90% confidence clouds) do not intersect, statistical significance can be assumed, as is the case for the A2 scenario in comparison to today. The change in 100-year drought deficit volume under the B2 scenario for the 2070s for the Danube catchment is not statistically significant because the two bands intersect (Figure 3-4). In this case, the return deficit volume calculated for the 2070s could also be a random parameter value of the 1961-1990 population.

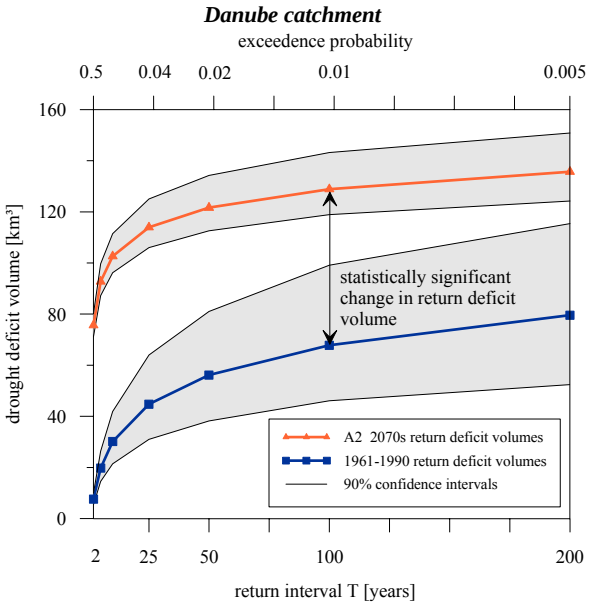

Figure 3-3. 1961-1990 and A2 2070s drought frequency curves with 90% confidence intervals.

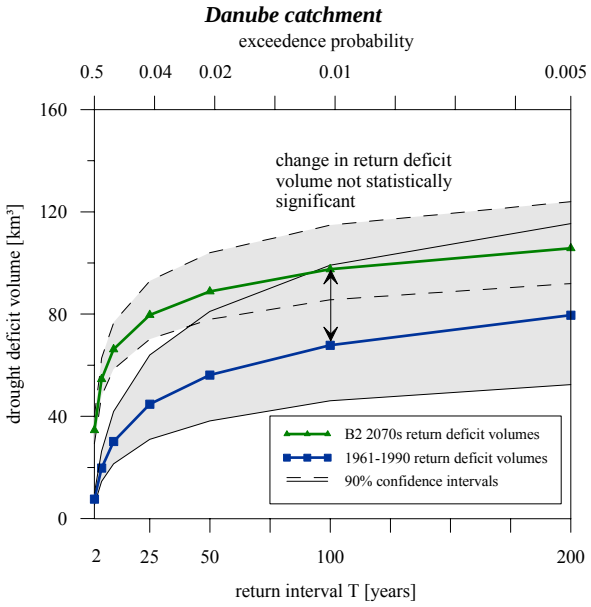

Figure 3-4. 1961-1990 and B2 2070s drought frequency curves with 90% confidence intervals.

3.6 Results

Figures 3-5 and 3-6 show future return intervals of current 100-year droughts in the 2070s for the IPCC A2 and B2 scenarios. The result for the A2 scenario (Figure 3-5) shows very strong increases in frequency over most of Southern Europe, with current 100-year droughts returning once per decade over most of the area. The A2 scenario is based on relatively high greenhouse gas emissions, and therefore has a high rate of climate change. Higher temperatures by itself, or in combination with less precipitation, for example, lead to lower water availability and an increased risk of drought. In 75% of all grid cells, the change in drought frequency is statistically significant. Areas where statistical significance is uncertain are hatched in Figure 3-5.

The B2 scenario (Figure 3-6) shows strong increases in the return frequencies of current 100-year droughts for large areas of Northern Spain, the South of France, Northern Italy and Austria. In the long-term projection for the 2070s, current 100-year drought events are calculated to occur once every 10 years, or more frequently. But also the rest of Europe, especially South-eastern Europe, shows a strong increase in 100-year drought frequency with return intervals of 50 years or more often. In North Africa, only the coast of Algeria faces strong increases in drought frequency, while in the remaining parts current 100-year droughts will occur less frequently. In these areas, precipitation slightly increases, which leads to increasing water availability and decreasing drought intervals. The change in drought frequency is in 69% of the analysed grid cells statistically significant.

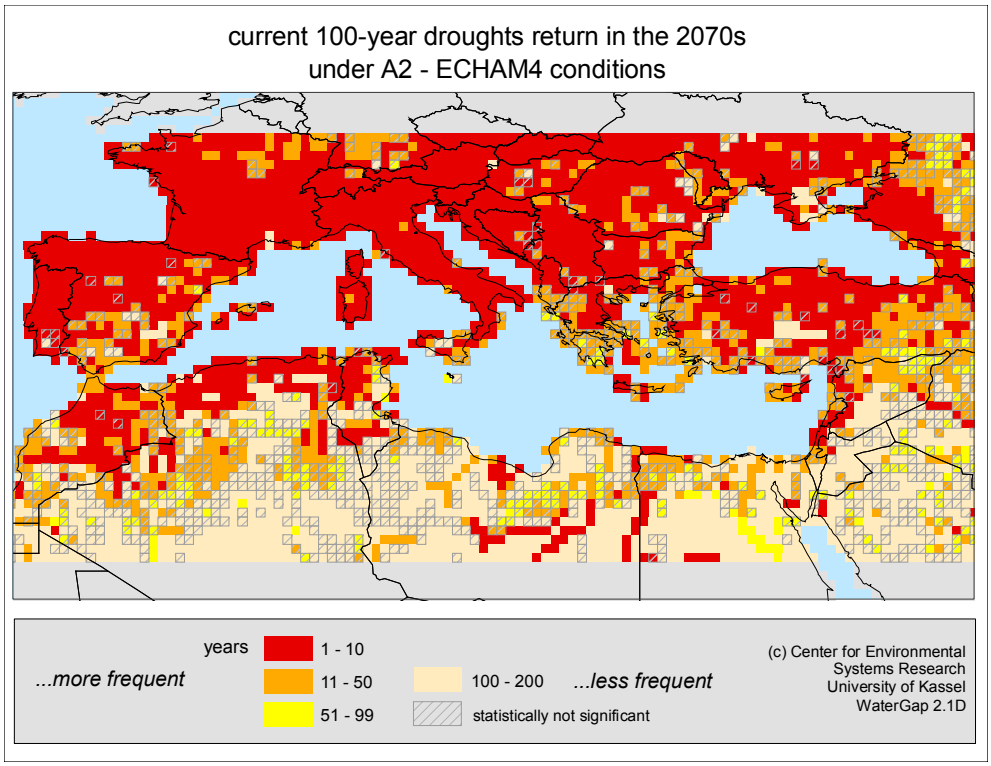

Figure 3-5. Return intervals of current 100-year droughts in the 2070s under the IPCC A2 scenario.

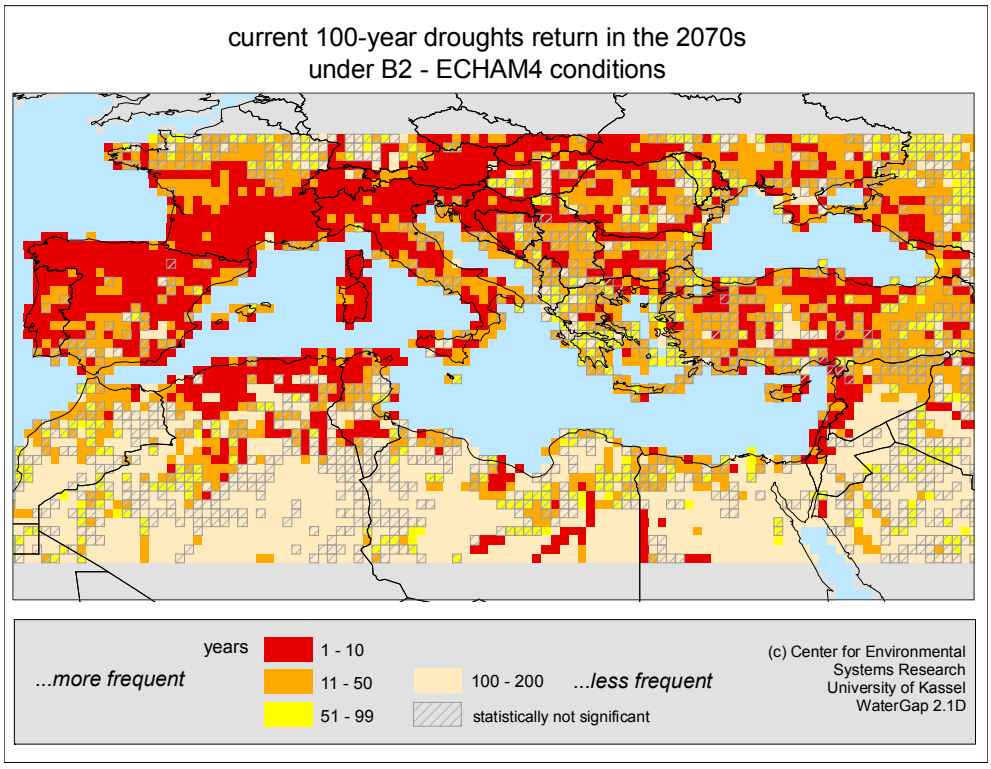

Figure 3-6. Return intervals of current 100-year droughts in the 2070s under the IPCC B2 scenario.

In order to evaluate the impact of the water use sectors on future drought frequencies, the 2070s water consumptions in the industrial, domestic and agricultural sector

for the IPCC A2 scenario are combined with current climate, and drought frequencies are calculated, as before. Increasing industrial activities, strong population growth or higher irrigation demands due to higher temperatures can lead to increasing water demands. If water abstractions in the different sectors fall together with low flow periods, water availability is further reduced and drought conditions can be intensified. In the simulation, the extent of irrigated areas is kept constant to explicitly examine climate-induced changes in irrigation water requirements.

Figure 3-7 shows that increasing water requirements mainly influence drought frequencies in North Algeria, Morocco, Spain, and at the Nile. In these areas, irrigated agriculture plays an important role and elevated water uses follow the projected higher temperatures of the IPCC A2 scenario. Additionally, Africa, the Near East and France are facing population growth rates between 1.1% and 2% in the IPCC A2 scenario, which also leads to increasing water uses in the domestic sector. In countries in Central Europe, where the industry is the sector with the highest water use, the projected technological change in the A2 scenario leads to higher water-use efficiencies. Therefore, water uses decrease in these areas and do not influence droughts. The changes in drought frequencies are in 58% of all grid cells statistically significant.

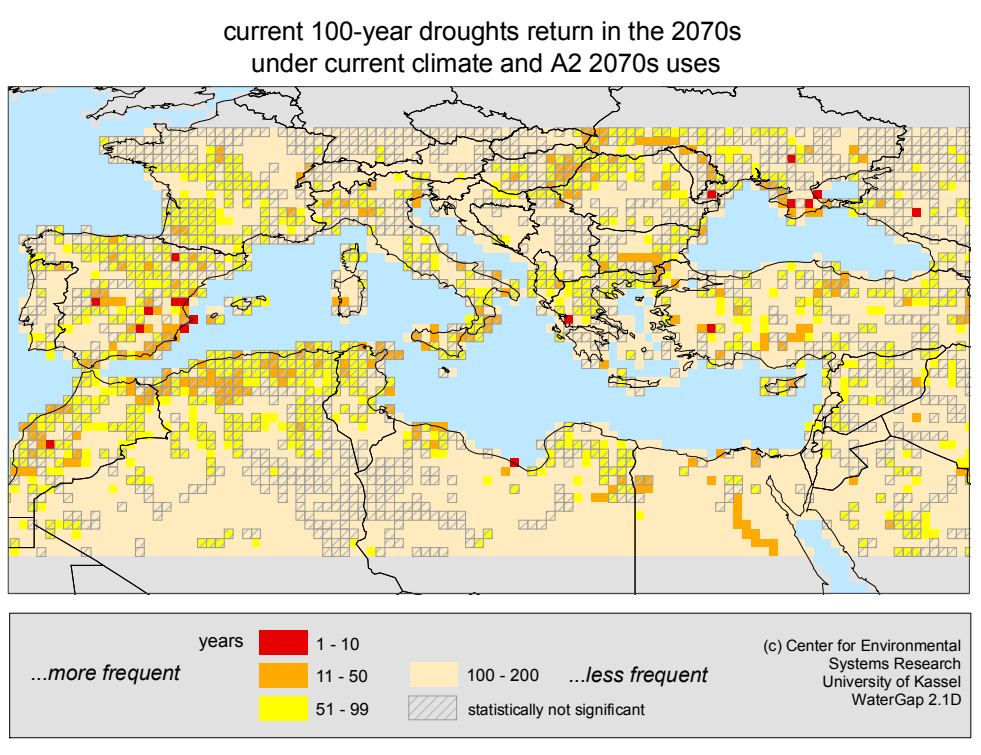

Figure 3-7. Impact of water uses under the A2 scenario on the return interval of current 100-year droughts.

Overall, the statistical significance of the change in future return frequencies decreases from the A2 to the B2 scenario from 75% to 69% and is lowest for the impact of changes in water uses on drought frequencies (58%), based on 90% confidence in-

tervals. Statistical significance is uncertain if the 2070s drought frequency band falls within the 90% confidence interval of the current frequency curve, as the 2070s drought value could also be a random value of the 1961-1990 population. This is for example the case if the difference between the current and 2070s return interval is small (e.g. the current 100year drought returns every 90 years in 2070). The A2 scenario assumes a higher rate of climate change than the B2 scenario and therefore changes in return frequencies are more pronounced, which leads to a higher statistical significance under the A2 scenario. On the other hand, statistical significance is uncertain in areas with generally very low discharges, leaving the calculated drought deficit volumes very small by definition, as for example in North Africa or the near East. It shows that this sort of analysis reaches its limits in arid areas, as a change in drought frequency is less meaningful in the desert.

The reader should be cautious of how to interpret the results of the study in terms of stress and risks for society. According to the method, any shift in low flow occurrence within a year will lead to the calculation of an increased frequency in drought. On the one hand it could be relatively easy for humans to adapt to a low flow, which occurs for example in May in the future as opposed to currently in August. On the other hand this adaptation could be more difficult for aquatic ecosystems that are adapted to a particular seasonal flow regime. In any event the impact of change in drought frequency should be examined carefully.

3.7 Conclusions

The study examined the combined influences of climate and water consumptions on future drought frequencies around the Mediterranean. The results show strong increases in drought frequencies for a belt that stretches from Northern Spain over Southern France towards Northern Italy and Switzerland for the B2 scenario, and strong increase over all of Southern Europe for the A2 scenario. Current 100-year droughts would, under the conditions of the IPCC scenarios, return at least once per decade. In Northern Africa, current 100-year droughts would, except for Northern Algeria, return less frequently. It is shown that climate change has a comparably stronger impact on the change in drought frequency than anthropogenic water uses. Water abstractions can, however, intensify drought conditions. On the other hand, this kind of drought analysis reaches its limits in a dry climate, as drought frequencies cannot increase in deserts and in these areas flows are too low to assume statistical significance of the changes. Overall the study shows a trend towards increasing drought frequencies under both the A2 and B2 scenarios with a statistical significance of 75% and 69%, respectively, and underlines the vulnerability of the Mediterranean to climate change.

CHAPTER 4

QUANTIFYING THE HUMAN APPROPRIATION OF FRESH WATER FOR AGRICULTURAL PURPOSES IN AFRICA

Summary

Human appropriation of renewable freshwater (HARF) is a measure for the influence of human activities on the global water cycle. It describes the fraction of accessible water that is directly used by human-dominated systems. In this section, a comprehensive model-based analysis of HARF for crop production on the African continent is present. The analysis includes the components evapotranspiration from cropland ("green" water fluxes) and water used for cropland irrigation (crop-related fraction of "blue" water fluxes). Model experiments were conducted for two scenarios with a time horizon of 2050, taking into account the combined effect of land-use change, climate change and technological change. For the year 2000, evapotranspiration from Africa's rainfed cropland (green water flux) is estimated to 1,085km³/year, while the abstraction of water for irrigation purposes from the renewable water resources (blue water flux) is estimated to approximately 180km^3/year. Between 2000 and 2050 an area between 1.25 mln km² and 1.56 mln km² of natural biomes is converted to cropland. As a result for the year 2050 evapotranspiration from rainfed cropland is substantially greater than in the year 2000, ranging from 1,870 to 2,040km^3/year, depending on the scenario, while irrigation abstraction increases up to 194 to 330km^3/year. These findings point out the significant role of water appropriated for rainfed crop production in the continental water cycle in contrast to the sum of water appropriated for irrigation, and further suggest that it would be worthwhile to look for opportunities to reduce the amount of water evaporated and transpired from cropland, that is, to increase the "water productivity" of cropland. Furthermore they indicate that under the given scenarios the additional production is very like to be on cost of the extent of natural biomes and

their associated ecosystem services.

4.1 Introduction

According to recent scenarios, Africa is expected to face further expansions of cropland to fulfil the food demand of a growing human population (Alcamo et al. 2005, Rothman et al. 2007). The impact of this development together with climate change and technological innovation is likely to significantly affect the continental water cycle, and therefore the amount of water available to support society and ecosystems. In order to develop a clearer understanding of the complex interactions between land and water and the impact of anthropogenic interference on the continental and regional scale, the concept of "human appropriation of renewable freshwater" (HARF) is applied. It describes the fraction of accessible fresh water that is directly used by human-dominated systems (Postel et al. 1996).

On the African continent rain-fed cropland makes up most of the cultivated area (96.5% in Sub-Saharan Africa). Irrigation plays a prominent role in Northern African countries with irrigation water-uses in the range of 82-85% of total water withdrawals (Rockström et al. 1999, Alcamo et al. 2007). For a comprehensive quantification of HARF, the concept of blue and green water fluxes is utilized. This concept includes not only the fraction of horizontal flow, i.e. surface and subsurface runoff, and renewable groundwater eventually accumulating river discharge, but also the fraction of vertical flow, i.e. evapotranspiration (Falkenmark 1995, Rockström 1999).

Recent studies have estimated current "green water" fluxes from world agriculture to 5,000-7,200 km^3/yr, blue water use in irrigated agriculture to approximately 1,600 km^3/yr, and green water fluxes from grazing lands to 8,000 – 12,000 km^3/yr (Rockström et al. 2007, Rockström et al. 2009) . It is expected that changes in land use and climate will exert a strong influence over regional water balances and hence over green and blue water fluxes. In the past, for example, deforestation has decreased local evapotranspiration and increased surface runoff (Douglas et al. 2005). The expansion of irrigated area, on the other hand, has increased evapotranspiration at the expense of total water available for society's use, but has also lead to increased surface runoff when applied lavishly (Rockström et al. 1999, Scanlon et al. 2007). Up to now, few estimates have been made on finer scales and concentrate on questions related to water availability under current climate and socio-economic conditions (Schuol et al. 2008).

The key question of the model-based analysis presented here is how HARF by cropland will develop during the next decades in Africa, regarding possible changes in climate, land-use and access to modern irrigation technology. To answer this question, two spatially explicit simulation models for hydrology (WaterGAP) and land-use

change (LandSHIFT) are linked to systematically calculate the green and blue water fluxes of African agriculture on continental and country-scale.

In the first step, current conditions (year 2000) are analyzed. Then model experiments for two scenarios with a time horizon of 2050 are conducted, taking into account the combined effect of changes in food production and its resulting land-use change, climate change and technological change on green and blue water fluxes. Estimates of future climate and driving forces of land-use change up to 2050 are taken from the "Policy First" and "Security First" scenarios of the UNEP Global Environmental Outlook-4 Report (GEO-4) (Rothman et al. 2007). The main focus of this study is to give a continental overview of potential future developments. Therefore, the outcome of all the simulation experiments is analyzed on continental level. In order to give a more detailed overview and to establish links to political units, calculated green and blue water fluxes are additionally analyzed on a country basis.

4.2 Methods

4.2.1 Blue and green water

In this paper, green water fluxes on cultivated areas are defined as evapotranspiration, i.e. the sum of water evaporated from the unsaturated soil layer plus that transpired by plants, because this is the amount of water used for crop growth. To compare green water fluxes on cultivated land with green water from natural vegetation, i.e. the fluxes that were present before this land was converted to cropland, green water is defined as the sum of evapotranspiration plus interception. These fluxes make up the theoretically available amount of water to support biomass production in that area.

Blue water required for agricultural production is defined as the amount of water withdrawn for irrigating crops, including conveyance and other losses occurring on the way to, or in the vicinity of crops. It constitutes the amount of water society has to provide to an area that otherwise would not be suitable for crop production due to a water limited climate. Most of this water is converted into green water by consumption. Access water is returned and available for reuse.

Consequently, HARF for crop production is described by the amount of water used in the evapotranspiration process, which is provided by precipitation and irrigation plus the water losses by the irrigation system.

4.2.2 Scenario analysis

Scenarios are plausible descriptions of how the future may unfold (Alcamo 2008). They are used by the scientific community as a research tool for estimating and assess-

ing possible future states of the environment or to examine the effect of alternative policy options. They are based on coherent and consistent sets of assumptions on key driving forces and relationships (storylines). This qualitative description of driving forces is then translated during the scenario analysis into a quantitative description, on the one hand involving the close dialogue with experts, policy makers and stakeholders, on the other hand with model computations. With the key objective of exploring alternative future developments, the storylines are most often characterized by two opposite driving force pathways, e.g. globalization of markets versus regionalization (Alcamo 2008). The scenarios chosen for this study were developed for the fourth Global Environment Outlook: environment for development (GEO-4) assessment (UNEP 2007b). For a description of storylines refer to section 4.3.3.

4.2.3 Land-use change model

LandSHIFT (Land Simulation to Harmonize and Integrate Freshwater availability and the Terrestrial environment) is a spatially explicit dynamic model which simulates land-use change on the continental and global scale. The model has been tested in case studies for India and Africa (Alcamo and Schaldach 2006, Schaldach et al. 2006, Schaldach et al. 2008). Driving variables are provided as input data on the country level and include amount of crop production, increase of crop yields due to technological change and population growth. In this analysis that input data is computed by other models as described in the scenario data section below. The output of LandSHIFT consists of land-use/land-cover grid maps with a cell size of 5 arc-minutes and a set of country level indicators (e.g. area statistics for land-use types and irrigated cropland). The model distinguishes between 14 land-use types. Each grid cell has one dominant land-use type and a fraction that is used for settlement area (which is not available for the dominant type of land use). The land-use type “arable land” is further sub-divided into 9 crops types.

LandSHIFT couples two modules to represent human and environment components of the global land-use system and their linkages:

The *Productivity module* computes potential crop yields under rain-fed and irrigated conditions for each grid cell. This information is used by the LUC-module (see below) for the evaluation of each cells’ suitability for agricultural activities and to determine the amount of crop production that can be allocated there. Major inputs to the module are global yield maps calculated with a grid version of the ecosystem model DayCent (Parton et al. 1998, Stehfest et al. 2007). Rainfed crop yields are adjusted upwards to take into account technological improvements over time, and percent of crop area irrigated.

The *LUC-module* (*L*and *U*se *C*hange) simulates land-use change and the underlying

human decision making processes. The main function of this module is to regionalize the country-level input for crop production and settlement area (based on population growth) to the grid level. In this analysis, these calculations are carried out in two steps by two sub-modules: METRO for settlement area and AGRO for cropland. LandSHIFT assumes that settlement area has higher priority and therefore is allocated first, i.e. it can displace existing cropland. In step one, the suitability of each grid cell for settlement and cropland is determined by a multi-criteria analysis (Eastman et al. 1995). Here, landscape features such as potential crop yields and terrain slope as well as spatial neighbourhood relations and socio-economic factors (e.g. population density and road infrastructure) are evaluated by a weighted linear combination. Additionally land-use constraints prevent the conversion of grid cells that are located within nature reserves to settlement or cropland. In step two, crop production and land requirements for settlement are spatially allocated to the grid cells. The METRO sub-module uses a rule-based approach to calculate changes in settlement area due to population growth. The spatial allocation of crop production (AGRO) is computed with a modified version of the Multi Objective Land Allocation Algorithm (Eastman et al. 1995).

4.2.4 Hydrological model

With a spatial resolution of 30 arc minutes, the WaterGAP model (Alcamo et al. 2003a, Döll et al. 2003) computes current and future water availability by simulating the continental water cycle, taking into account precipitation, snowmelt, interception, evaporation, soil water, groundwater storage and runoff. Surface and subsurface flows are routed through river basins using a directional flow scheme (Döll and Lehner 2002). Current and future water withdrawals and consumptions are calculated for the industrial, domestic and agricultural sectors. The water consumption is abstracted from the natural flow. The remainder forms river discharge. The simulated river discharge is tested against measured runoff time series from the Global Runoff Data Center (GRDC 2004). The WaterGAP model is very well suited for scenario analysis as climate and social-economic drivers can be adapted to scenario conditions. It has previously been applied to a number of scenario studies, e.g. Global Environment Outlook 3 (GEO3), Global Environment Outlook 4 (GEO4), Millennium Ecosystem Assessment (MEA), and Dialogue on Water and Climate (WATCLIM) (UNEP 2002, Alcamo et al. 2005, Alcamo et al. 2007, UNEP 2007b).

WaterGAP is used to calculate green water fluxes from the daily vertical water balance in each grid cell. From the radiation-based calculation of potential evapotranspiration according to Priestley and Taylor (1972), actual evapotranspiration is derived from canopy and soil water balances. The level of crown moisture saturation determines the fraction of incoming precipitation that directly evaporates without reaching the soil, whereby the maximum canopy storage is calculated as a function of the leaf

area index. The remainder accumulates actual soil moisture until saturation. The maximum soil water capacity results from the depth of the effective root zone, and specific water capacity of the particular soil. Excess water is routed to the adjacent grid cell (Alcamo et al. 2003a).

Blue water fluxes on cropland are computed with the irrigation module of WaterGAP (Döll and Siebert 2002) as a function of climate, extent of irrigated area (Döll and Siebert 2000), cropping intensity and crop type with a 30 arc-minute grid cell resolution. Evapotranspiration is crop-specific and depends on the growing stage of the crop. Due to data constraints, the model currently distinguishes rice and non-rice crops. The irrigation requirements are determined in three steps: First cropping patterns and optimal growing seasons are determined based on soil suitability and climate, taking into account multi-cropping if applicable. Next, water consumption of irrigated crops is computed for each day of the growing season. Water withdrawals for irrigation (blue water fluxes) are computed by dividing plant water requirements by irrigation project efficiencies, which account for water distribution losses through seepage and evaporation (Döll and Siebert 2002, Alcamo et al. 2003a). Irrigation project efficiency follows estimates from the Food and Agriculture Organization (FAO 1997) for 84 regions in Africa. Validation of the model with independent data shows a good agreement for modelled irrigation water demand (Döll and Siebert 2002). For scenario simulations, climate, extend of irrigated area, crop type and project efficiency are adjusted to scenario conditions.

In order to take into account inter-annual climate variability, WaterGAP computes both green and blue water fluxes on a monthly basis for a thirty year period. In this study, only long-term average annual results for the thirty year period are reported. For the baseline model experiment (see below) this period is 1971 to 2000. For model experiments concerning "2050" conditions, data from the 1971 to 2000 period are scaled with climate change data to create an artificial future 30 year period. This is explained in Section 4.3.3.

4.2.5 Model coupling

Green and blue water fluxes are computed by soft-linking the WaterGAP and LandSHIFT models, i.e. the models are run in a sequential order. LandSHIFT uses country-scale input information on agricultural production and changing crop yields that are specified in the GEO-4 scenarios. Based on this information, the model computes changing rainfed and irrigated cropland area between 2000 and 2050. For the expansion of irrigated area it is assumed that the fraction of irrigated land for each crop type remains constant on year 2000 levels. If for example in a country 20% of 1000 ha maize area is irrigated in 2000 and the scenario assumes a doubling of maize area until 2050, this will automatically lead to an expansion of irrigated area from 200

to 400 ha. For rice it is assumed that the total area is irrigated.

The resulting grid maps serve as input to the water flux calculations of WaterGAP. Green water fluxes are computed by WaterGAP for grid cells designated as "cropland" in LandSHIFT. Every WaterGAP run uses a representative land-use/land-cover map (i.e. for 2000 or 2050) calculated with LandSHIFT, aggregated to the grid cell resolution of WaterGAP of 30 arc-minutes. Results are presented in this resolution.

In order to give a more realistic spatial picture of blue water fluxes, the changes of irrigated area calculated by LandSHIFT are summed up for each country-level and then redistributed by WaterGAP to the grid cells which are suitable for irrigation. Factors determining this suitability comprise information on area equipped for irrigation (Döll and Siebert 2000) and climate. In the scenario runs, the irrigation project efficiency is adjusted to take into account technological improvements or deterioration over time, consistent with the underlying scenario assumptions (Section 4.3.3).

4.3 Simulation experiments

4.3.1 Underlying assumptions

Four simulation experiments are conducted by running the two models to assess the impact of different components on green and blue water fluxes. These components include climate, land-use change and access to technological progress in terms of crop yield increases (given in metric tons per ha) and irrigation field efficiencies represented in a way that advanced irrigation technologies will result in lower water distribution losses. The change of cropland area is primarily driven by changes of the amount of crop production and increases of crop yields.

- Model Experiment 1 – "Baseline 2000" – computes blue and green water fluxes for a reference climate period (1971 to 2000). Information on climate, cropland area and level of technology are based on year 2000 data.
- Model Experiment 2 – "Climate change 2050" – takes into account only the impact of climate change on green and blue water fluxes. Cropland area and irrigation project efficiency are set to year 2000 values.
- Model Experiment 3 – "Climate change, land use change, and technological change 2050" – takes into account the combined effects of changing climate, changing cropland area and changing irrigation project efficiency on green and blue water fluxes.
- Model Experiment 4 – "Natural vegetation green water fluxes" – computes future green water fluxes under climate change on the area that is converted

to cropland between 2000 and 2050, assuming that they are still covered by the type of natural vegetation as before their conversion. This run provides a reference point for determining whether the expansion of cropland results in an increase or decrease of green water fluxes on the converted land.

Model experiments 2 through 4 pertain to future conditions and were performed for two scenarios from the set of scenarios recently developed as part of the Fourth Global Environmental Outlook Report ("GEO-4") by the United Nations Environment Programme (Rothman et al. 2007). These scenarios were selected because they provide a consistent and even more important, alternative set of socio-economic assumptions for the year 2050 which allow us to explore a large range of future developments.

4.3.2 Data for the Baseline period

The initial land-use map used by LandSHIFT for the year 1992 is based on the global IGBP land-cover dataset (Loveland et al. 2000), derived from AVHRR source imagery data. Additional information on the spatial distribution of crop types is generated by a procedure that merges land cover data with sub-national census data (Heistermann et al. 2006). This map also comprises information on the share of irrigated area for each crop type on country level.

The LandSHIFT routines for suitability assessment and for land allocation use grid-level information on landscape characteristics, zoning regulation and land-use related model variables. Population density is derived from the Global Rural-Urban Mapping Project – GRUMP alpha (CIESIN 2004), while slope data is based on the HYDRO1k data set (USGS 1998). The river network density is calculated via the line density of rivers per grid cell, based on the HYDRO1k data set on streams (USGS 1998). The information on infrastructure is assessed via the VAMP0 data set on roads (NIMA 1997). In order to derive information of zoning regulation, grid cells are mapped to data sets on areas designated as national or international conservation areas (WDPA Consortium 2004).

The year 2000 land-use map, which represents the baseline in this analysis, is calculated by the LandSHIFT model based on these initial map and census input data for population and crop production (FAO 2008) for the year 2000 (Schaldach and Alcamo 2006).

Climate data for the reference period (1971-2000) is taken from the "CRU TS 2.1" gridded dataset for monthly precipitation, air temperature, cloud cover and frequency of wet days (Mitchell and Jones 2005).

4.3.3 Scenario Data

Estimates of future climate and driving forces for land-use change up to 2050 for the experiments 2-4 are derived from the "Policy First" and "Security First" scenarios of the UNEP Global Environmental Outlook-4 Report (GEO-4) (Rothman et al. 2007).

The storyline of the "Policy First" scenario describes a world in which governments implement strong policies to protect the environment and increase human well-being while promoting economic growth through a high level of international cooperation. But the attempt to achieve both economic growth and environmental protection is only partially successful because high population growth, increasing industrial activity and growing energy consumption cannot completely be covered by renewable energy and other resources.

In contrast, the "Security First" scenario describes a world in which natural and regional interests are turned inward, which results in a relatively low level of international cooperation. Government's interests centre on regional security including that of resources. Sustainable development is only an instrument to increase access and use of the environment. The diffusion of technology and information is low and trade barriers limit the movement of goods across borders. Governments lose power as private interests increasingly influence decisions. International climate policy is undeveloped and ineffective.

The quantitative interpretation of the storylines is described in detail by Rothman et al. (2007) In this analysis, quantitative scenario drivers are used for climate, demography, economy, agricultural production and yields, as well as technological change regarding crop yield changes and irrigation project efficiency. In the following paragraphs these scenario drivers are briefly reviewed.

Climate data for 2050 for the "Policy First" and "Security First" scenarios were derived by scaling the reference period's (1971-2000) monthly temperature and precipitation with the differences between years 2000 and 2050 computed by the IMAGE 2.4 model (Bouwman et al. 2006). The climate model component of IMAGE 2.4 is often used in integrated assessments and combines a relatively simple energy balance approach with a consistent scheme for downscaling changes in surface temperature and precipitation to a global grid based on results from more complex dynamic global climate models (Bouwman et al. 2006).

The climate data generated by IMAGE 2.4 for Africa up to 2050 shows only minor differences between the two scenarios because their emission pathways do not lead to significantly different atmospheric greenhouse gas concentrations up to the middle of the 21st century. The continental average surface temperature increase up to 2050 for Africa (relative to pre-industrial) for both scenarios is approximately 2°C. The highest

temperature increases (approximately 3°C under "Security First" and 2.5°C under "Policy First") occur over the North-Western and Southern parts. Long-term annual mean precipitation increases by about 10% over most of the continent. Precipitation decreases by approximately 15% to 20% in small areas of Western and Southern Africa and the coastline of Northern Africa. In general, the climate projections are consistent with those from the Fourth Assessment Report of the Intergovernmental Panel on Climate Change (IPCC 2007).

Demographic change and gross domestic products (GDP) for the GEO-4 scenarios have been calculated by the International Futures model (Hughes and Hillebrand 2006). Total population in Africa in the year 2000 was 795 million. In the "Policy First" scenario, population increases to 1,660 million in 2050 while average national income increases from 702US$cap^{-1}a^{-1} to more than 4,100US$cap^{-1}a^{-1}. Under the "Security First" scenario population increases up to 2,270 million with GDP only increasing up to 1597US$cap^{-1}a^{-1}.

Crop production is calculated by the global agricultural trade model IMPACT (Rosegrant et al. 2002). Under the "Policy First" scenario, production of the major crop types (wheat, maize, other grains, soybeans, millet and sorghum) increases from 77 million metric tons in 2000 to 272 million metric tons up to 2050. Along with this, per capita food availability increases to a level comparable to European standards in 2000 (Rothman et al., 2007). Under the "Security First" scenario, production increases up to 226 million metric tons. Here, a slight decrease of per capita food availability can be observed.

"Technological change" is an important driving force in this analysis because it leads to changes in the magnitude of crop yields (productivity in metric tons per ha) and in irrigation project efficiency during the scenario period. Changes in crop yields are calculated by the IMPACT model as a function of future investments in the agricultural sector and other factors. Since future agricultural investments are assumed to be higher under the "Policy First" scenario as compared to the "Security First" scenario, increases in crop yields are also assumed to be larger under the first scenario. For instance, the average cereal yield increases by a factor of approximately 2.7 between 2000 and 2050 under "Policy First", and by a factor of approximately 2 under "Security First".

Under "Policy First", investments in new technologies lead to increases in irrigation project efficiency in all African regions, increasing from 55% in 2000 to 75% in 2050. In contrast, the "Security First" scenario emphasizes security of water supply but with a low level of investments in the water sector and international trade in water-related technology. Hence, rapidly deteriorating infrastructure and poor management lead to a reduction of irrigation project efficiency under this scenario to an average level of 44%

by 2050. These absolute figures were determined in the scenario analysis procedure of the GEO4 assessment in a mutual effort including stakeholders and modellers.

4.4 Results

4.4.1 Continental level simulation results

Model experiment 1 - Year 2000 Baseline -

The calculated settlement area for 2000 covers only a relatively small fraction of the total continental land area (122,408 km²). Total cropland area is computed to be 2,292,000 km² which is about 7.8% of the total African land area (Table 4-1).

The WaterGAP calculations of "current" green water fluxes in Africa (climate from 1971 to 2000, cropland area and other assumptions from year 2000) amount to 1,085 km³/a while blue water fluxes for irrigation are a magnitude lower, i.e. 179 km³/a (Table 4-2).

Model experiment 2 - "Climate change 2050"-

In this model experiment settlement and cropland area remain constant but the climate input for WaterGAP is adjusted according to the GEO-4 scenarios (see Section Scenario Data). Under these assumptions, the fluxes of green water on the continental level increase by 4% in comparison to the baseline for both scenarios. Although the extent of irrigated area remains constant, the irrigation water requirements of crops on this land (blue water fluxes) also show an increase of 4% because of decreasing precipitation in some areas and/or increasing temperature. The calculated changes on the continental level are very similar for both scenarios because the differences between climate changes under these scenarios up to 2050 are relatively small.

Model experiment 3 - "Climate change, land use change, and technological change 2050"-

In this model experiment, the combined effect of climate change, land-use change and changing irrigation project efficiency based on the respective scenario assumptions (see section Scenario Data) is analyzed. Table 4-1 and Table 4-2 summarize the simulation results of both models.

Table 4-1. Land use data for the baseline and scenario calculations.

Area [1000 km2]	2000	2050 Policy First	2050 Security First
Total Cropland	2,292.0	3,543.0 (+55%)	3,808.0 (+66%)
Rainfed Cropland	2,056.6	3,324.1 (+62%)	3,478.4 (+69%)
Irrigated Cropland	235.4	308.9 (+31%)	329.6 (+40%)

Table 4-2. Continental green and blue water fluxes for Africa as calculated in model experiments 1 and 3.

Fluxes [km3/a]	2000	2050 Policy First	2050 Security First
Green water flux (evapotranspiration from rainfed part of cropland)	1,085	1,870 (+72%)	2,040 (+88%)
Blue water flux (water withdrawals for irrigation)	179	194 (+ 8%)	330 (+84%)

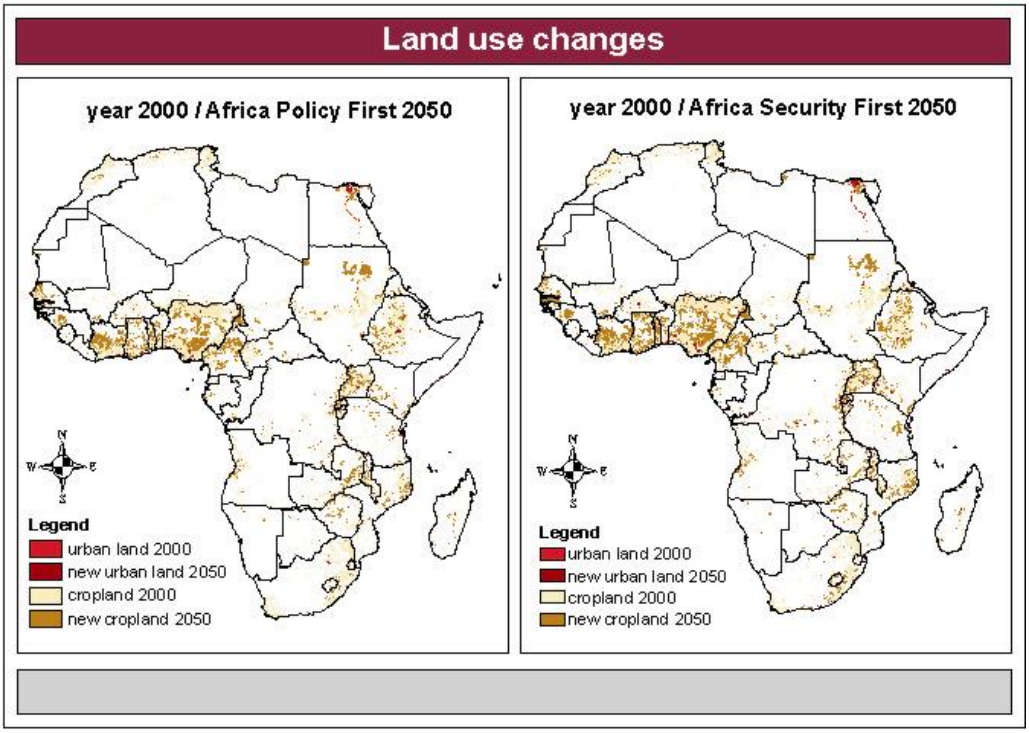

Figure 4-1. Expansion of settlement area and cropland between 2000 and 2050 for the "Policy First" (a) and "Security First" (b) scenario as computed with LandSHIFT.

Figure 4-1 shows the spatial pattern of cropland and settlement expansion between 2000 and 2050 for the two scenarios computed by the LandSHIFT model. Settlement area nearly doubles under "Policy First" and increases by a factor of 2.6 under "Security First". Under "Policy First", rainfed cropland area increases by 62% and irrigated area by 31% during this period. Under the "Security First" scenario, cropland expands by 69% and irrigated area by 40%. The main reason for these differences is the assumption of an overall higher population growth under the "Security First" scenario which leads to a greater need for food-producing cropland. Another factor is that crop yields increase much stronger under "Policy First" and therefore reduce cropland requirements as compared to "Security First". Cropland expands at the expense of natural and semi-natural biomes such as forests, shrubland and savannah. Table 3 summa-

rizes the area of different biome types that is converted to cropland during the simulation.

The resulting spatial distribution of green and blue water fluxes calculated by WaterGAP is shown in Figures 4-2 and 4-3. As a consequence of cropland expansion, green water fluxes increase by 72% ("Policy First"), and 88% ("Security First"), respectively (Figure 4-4). The largest green water fluxes in 2050 occur in regions that face a large increase of cropland area, together with changing climatic conditions that promote evapotranspiration. Examples are parts of Western and Eastern Africa (Figure 4-2a). The largest blue water fluxes correspond to areas with high fractions of irrigated croplands in Africa (Figure 4-3a). Under "Policy First", where very significant improvements of irrigation project efficiency are assumed (see Section Scenario Data), irrigation water withdrawals increase by 8% between 2000 and 2050. By comparison, water withdrawals almost double (+84%) in the "Security First" Scenario because in this scenario irrigation project efficiency decreases due to the lack of financial investments in the water sector (Figure 4-5).

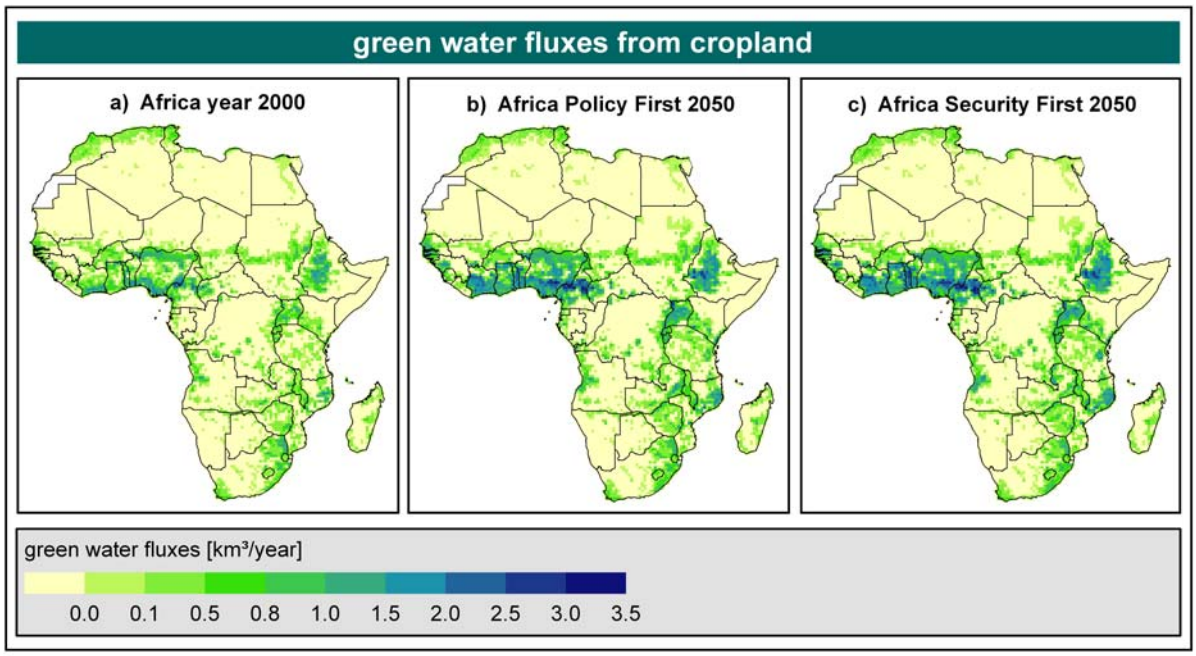

Figure 4-2. Green water fluxes from cropland in Africa for the year 2000 (a) and the GEO-4 Scenarios "Policy First" (b) and "Security First" (c) in 2050.

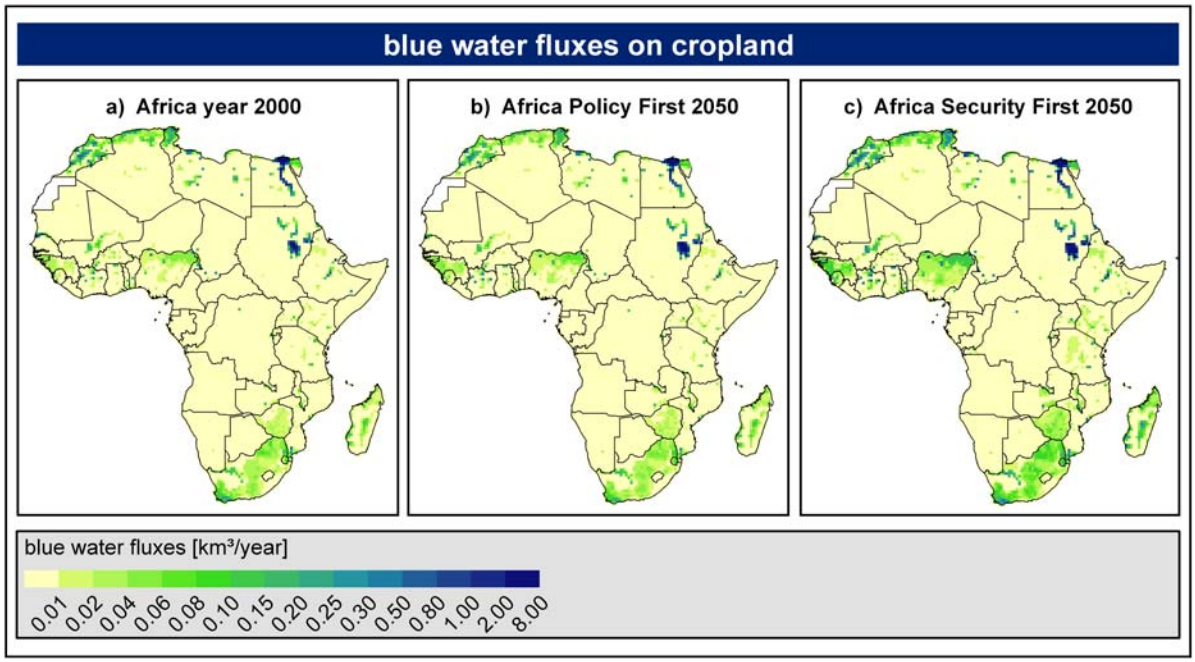

Figure 4-3. Blue water fluxes for crop production in Africa for the year 2000 (a) and the GEO-4 Scenarios "Policy First" (b) and "Security First" (c) in 2050.

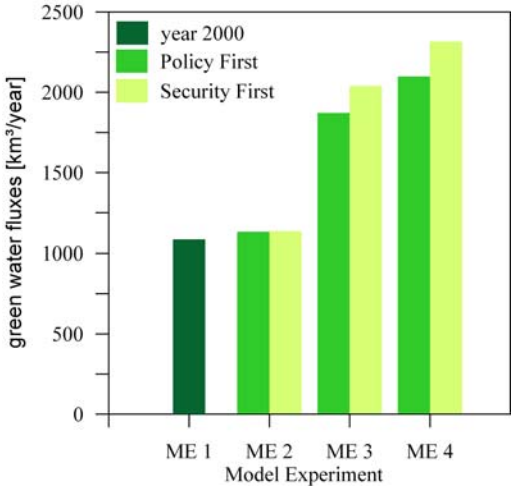

Figure 4-4. Continental green water fluxes from cropland. For description of model experiments see text.

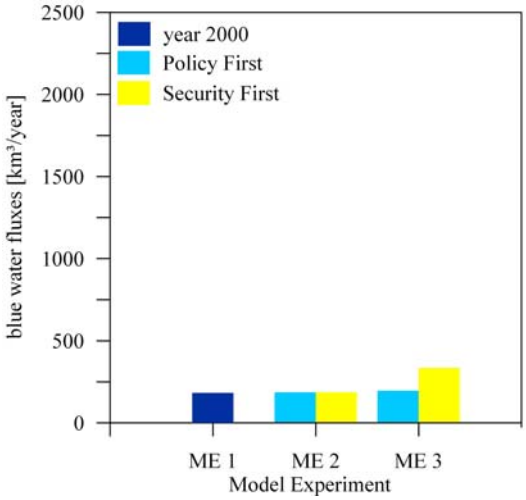

Figure 4-5. Continental crop-related part of blue water fluxes (irrigation withdrawals). For description of model experiments see text.

Model experiment 4 - "Natural vegetation green water fluxes"-

For this model experiment, evapotranspiration from the natural vegetation is computed, which covers the area that is converted to cropland between 2000 and 2050 (Figure 4-1) under the respective climate change scenarios. The calculated area conversions from each biome type to cropland are summarized in Table 4-3. The result is that the green water flux from new cropland is about 12% to 14% lower than the fluxes

from the natural vegetation it has replaced (Figure 4-4).

Table 4-3. Loss of biome area due to the expansion of cropland (biome types are derived from the GLCC land-cover data set).

Area [1000 km²]	Policy First	Security First
Shrubland	24	38
Savanna and Grasslands	648	762
Tropical woodland	280	329
Forest	154	229
Barren	144	157
Sum	1,251	1,516

4.4.2 Country level simulation results

Of the 45 countries analyzed, 44 currently have a larger green water flux than blue water flux. Only Egypt's blue water flux exceeds the green water flux due to its strong dependency on irrigated agriculture.

Except for Algeria and the Comoros, all countries have increasing green water fluxes under both the "Policy First" and "Security First" scenarios up to 2050 (Figure 4-6). Under the "Policy First" scenario, seven countries have a 25% or greater increase, and nine a 50% or greater increase, and 20 a 75% or greater increase. Under the "Security First" scenario, six countries have a 25% or greater increase, six have a 50% or greater increase, and 25 have a 75% or greater increase.

In 18 countries, the blue water flux decreases under the "Policy First" scenario in comparison to current values, while under the "Security First" scenario all blue water fluxes show significant increases (see Figure 4-7).

The country with the largest current and future green water fluxes is Nigeria, followed by Ethiopia and Cameroon. These countries are in this position because of their large cropland areas and partly because of the moist climate over some of this cropland. In Nigeria green water fluxes from cropland increase from 180km³/a in the year 2000 up to 315km³/a in 2050 under "Policy First" and 325km³/a under "Security First". Blue water fluxes, too, show a significant increase from 5km³/a in the year 2000 to 7km³/a in the year 2050 for "Policy First" and 15km³/a in the "Security First" Scenario.

In Morocco, which heavily relies on irrigated cropland, green water fluxes increase from 18 km³/a to 21km³/a, and 24km³/a, respectively. Blue water fluxes decrease in the "Policy First" scenario from 14km³/a up to 11km³/a but increase to 17km³/a in the "Security First" scenario.

Zambia, on the other hand, almost completely relies on rain-fed agriculture. Green water fluxes account for 24km³/a in the year 2000 and increase in 2050 to 51km³/a in the "Policy First Scenario" and 60km³/a in the "Security First" Scenario.

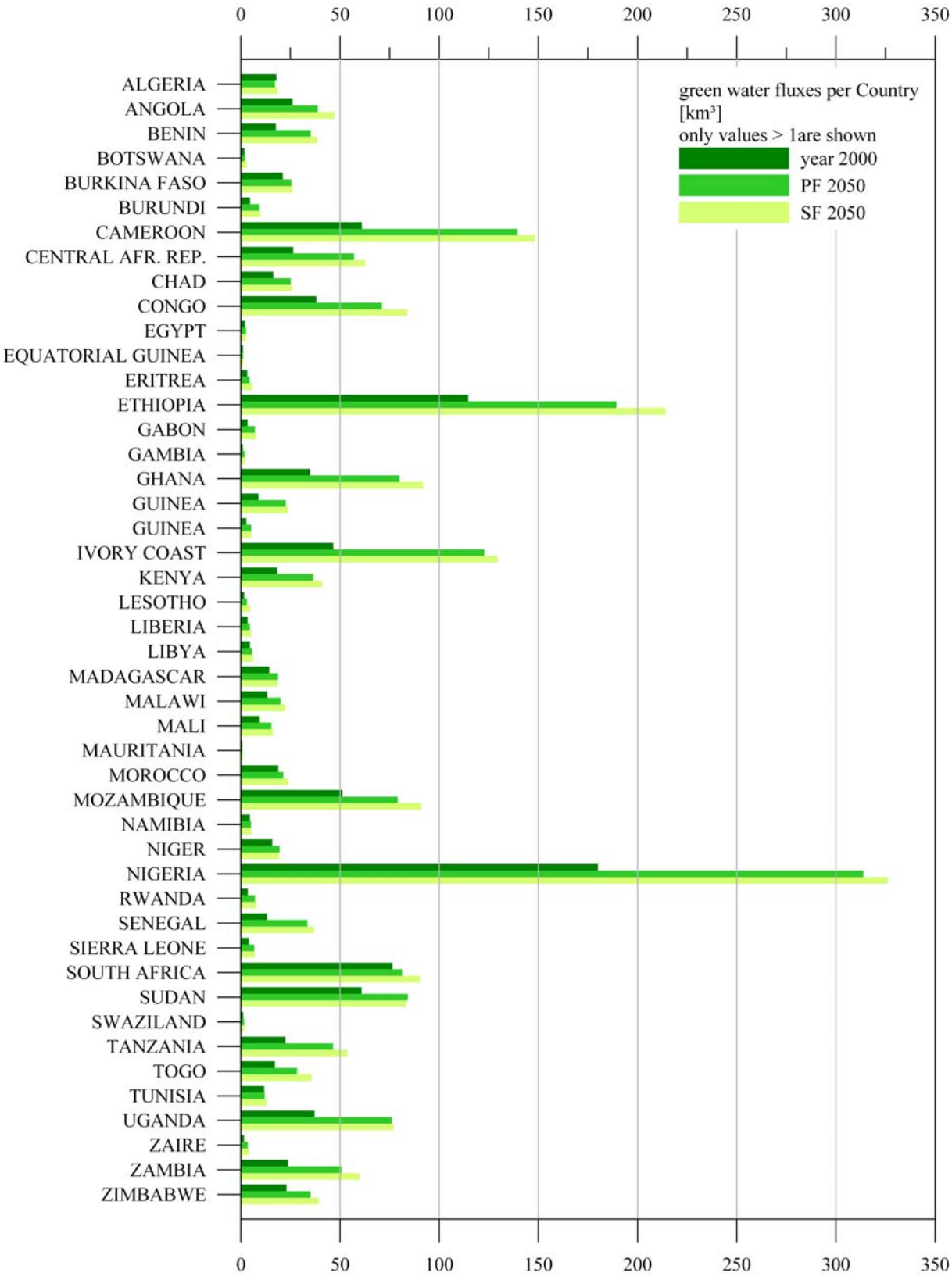

Figure 4-6. Country-level green water fluxes from cropland for the year 2000 and the scenarios "Policy First" and "Security First" for the year 2050.

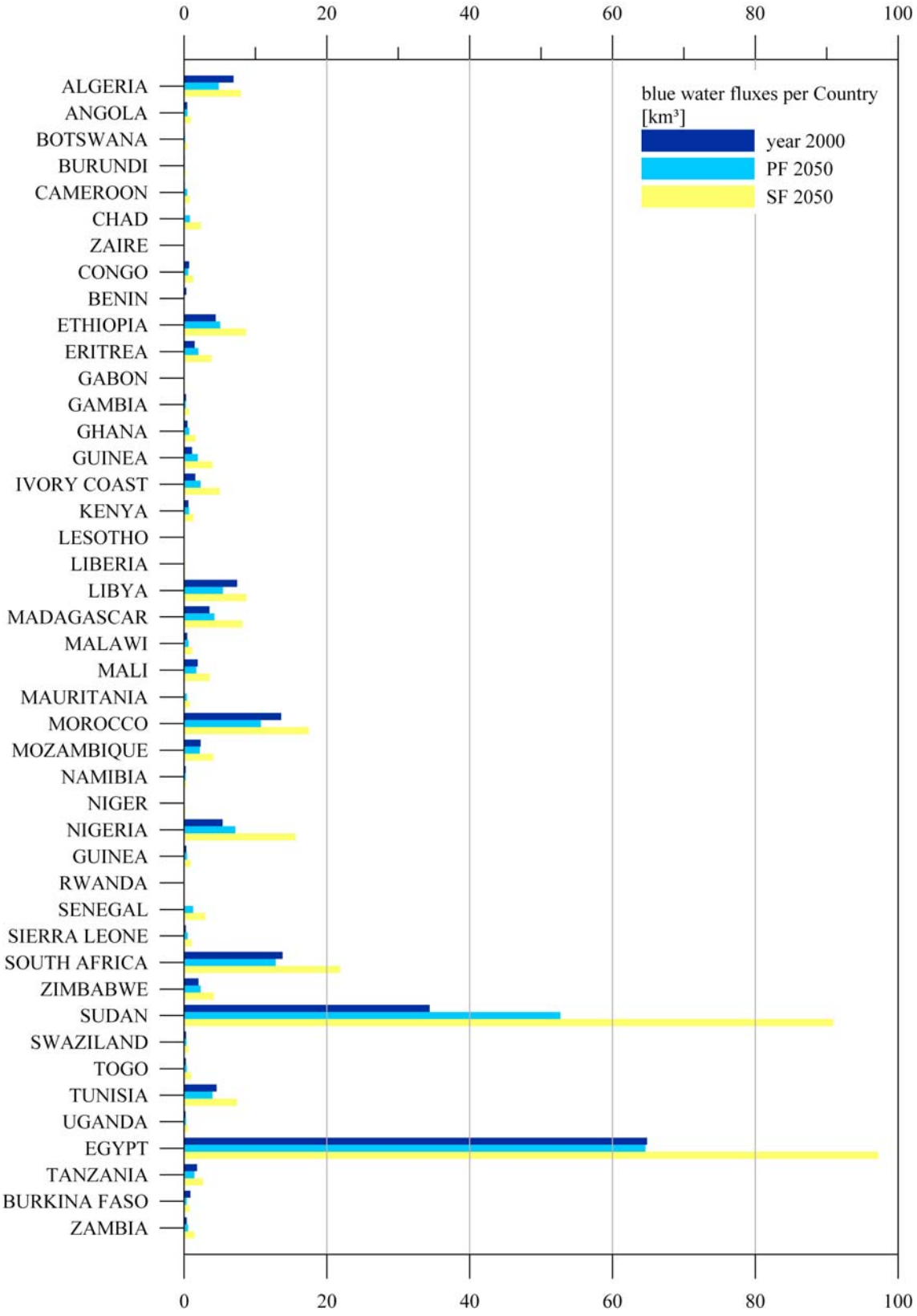

Figure 4-7. Country-level crop-related part of blue water fluxes (irrigation withdrawals) for the year 2000 and the scenarios "Policy First" and "Security First" for the year 2050.

4.5 Discussion and Conclusions

In this study, the spatially explicit land-use change model LandSHIFT and the hydrology model WaterGAP are successfully combined to quantify the appropriation of fresh water by cropland in Africa under current conditions as well as for two internally consistent scenarios.

In order to evaluate the predictive performance of the applied models, the year 2000 simulation outcome for the most important variables of this study is compared to different sources of statistical and literature data. These variables comprise: (1) the extent of cropland, (2) the extent of irrigated land, (3) green water fluxes from cropland and (4) blue water fluxes for irrigation purposes.

The total cropland area computed for Africa by LandSHIFT (2,292,000 km²) compares well to the statistical data of the AQASTAT database (FAO 2003a), where total cropland amounts to 2,214,010 km² (deviation 3.5%). Irrigated area is calculated to be 235,428 km², falling between the values given by the AQUASTAT database for the irrigation potential area of 467,945km² and actually irrigated area of 70,265km². Also the blue water fluxes computed by WaterGAP for 2000 (179km³/a) compare well to the 182km³/a of irrigation withdrawals given in AQUASTAT (FAO 2003a). Although comparisons are difficult due the different underlying scenario assumptions, the simulated cropland expansion until 2050 is in the same order of magnitude as reported in the scenario analysis of the Millennium Ecosystem Assessment, which is between 50% and 60% for Sub-Saharan Africa (MEA 2005). In contrast, deforestation rates are lower. Here, one explanation is that this study does not consider the expansion of grazing land which would put further stress on natural biomes.

To the author's knowledge, currently no other published studies exist, that specifically focus on green water fluxes from cropland for the African continent. However, a recent study by Schuol et al. (2008) has examined total current green water fluxes on the African continent and obtains values of 14,449 to 15,348 km³/a. This number compares well to the WaterGAP calculated value of 14,670km³/a for the African continent.

For further evaluation, values for total green water fluxes from a global model run of WaterGAP are compared to other published global estimates. The global sum of evapotranspiration and interception as calculated with the WaterGAP model for the year 2000 equals 69,000 km³/a. Rockström and Gordon (2001) calculated a global vapour flow of 71,300km³/a based on the spatial coverage of each biome and the annual evapotranspiration of each system. A recent study by Gerten et al. (2005) on green water fluxes with a global dynamic vegetation model resulted in the 63,906km³/a. Shiklomanov (1997) estimated global evapotranspiration in the magnitude of 72,000km³/a. As the results of the WaterGAP model fit very well into this range, it can be concluded

that the estimates of green water fluxes for cropland in Africa, too, are of a reasonable magnitude.

With regards to the methodology, the model experiments in this study have been conducted by soft-coupling two disparate models. The strength of this approach is that the models can be used independently without significant changes of the respective internal structure and source code. Moreover, the simulation outcome can clearly be attributed to the respective model drivers. But this approach can also lead to inconsistencies in how the different models handle different aspects of a specific topic. For example, the LandSHIFT and WaterGAP models deal differently with the spatial distribution and expansion of irrigated area. These disparities had to be reconciled for the model runs by spatially distributing the aggregated country level changes of irrigated area computed by LandSHIFT on the area equipped for irrigation.

The sum of the model experiments indicates that human appropriation of freshwater for the cultivation of crops in Africa has a strong influence on the continental hydrological cycle which, according to the calculated scenarios, is likely to further increase in the coming decades. Current green water fluxes from African cropland area are significant and add up to about one-half of the current continental runoff (4,500 km^3/a). Although the "blue water fluxes" of irrigation water withdrawals make up over 80% of current total African withdrawals (Alcamo et al. 2007), they are overshadowed by moisture fluxes from rainfed cropland; the water evaporated and transpired annually from Africa's rainfed cropland (green water) is 6.6 times greater than the volume of water used in liquid form to irrigate crops (crop-related part of blue water). Furthermore, these model experiments suggest that the magnitude of green water flux will substantially increase over the coming years. Under the expansion of cropland described by the two scenarios in this paper, green water fluxes increase by 72% to 88%. This is proportionately greater than the expansion of rainfed cropland area (62 to 69%) and can be explained by the additional effect of warmer future temperatures stimulating the plants' evapotranspirative processes. The size of green water fluxes in 2050 (1,870 to 2,040km^3/a) can be appreciated by comparing it to current total continental runoff from the African continent (4,500km^3/a). However, runoff in 2050 might be slightly larger (+15%) according to the scenarios examined in this paper. Although blue water fluxes from irrigation will also increase in the future, the overall ratio between green and blue fluxes will remain about the same.

Nonetheless, the additional irrigation water withdrawals for newly converted land, changing climate and changes in efficiencies will compete with water demands of other sectors, e.g. the domestic and manufacturing sectors, which have to be fulfilled by the same water resource. In fact, total anthropogenic water uses increase by 36% under "Policy First" and 170% under "Security First" (based on GEO4 results and re-

sults from this study). Setting this number in relationship to the water that is accessible to anthropogenic uses allows a first estimate of regions suffering from water stress (Alcamo and Henrichs 2002, Alcamo et al. 2005, Alcamo et al. 2007). If the ratio of water withdrawn to water available exceeds 0.4, the region is very likely to experience acute or chronic water shortages, not allowing enough water to maintain environmental flows. The increased re-use of water resources leads to water quality degradations, limiting the functionality of ecosystems and further re-use. While under "Policy First" the situation of the Nile improves, both under "Policy First" and "Security First", the Senegal River, Limpopo River, White Nile and Shebelle River basins additionally fall into the category of severe water stress, endangering especially the wetlands above Lake Victoria.

For both scenarios, the land-use simulations show that substantial areas of natural biomes are converted to cropland (Table 3) with consequences both for the land and water-side. On the one hand the loss of natural biomes has negative impacts on biodiversity leading to a trade-off between crop production and other ecosystem services (MEA, 2005). On the other hand also the impacts on the hydrological cycle become obvious. Especially the replacement of forests and tropical woodlands which, due to their greater leaf area and denser biomass tend to have higher evapotranspiration per unit area than cropland, leads to overall lower green-water fluxes in the model results. This development, accompanied by the withdrawals and consumption of irrigation water induces large changes of local and regional water cycles with potential effects on river discharge and even micro-climatic conditions.

All of these results point to the important role that fresh water appropriated for crop production plays in the continental water cycle, both now and in the future. What implications does this have for agriculture? One conclusion, as Rockström and others have argued (Rockström 1999, Jewitt 2006, Rockström et al. 2007), is that it is worthwhile to not only improve the irrigation water efficiency, but also the efficiency of water used by rainfed crops, given its magnitude. In principle, this could allow the same amount of food to be produced with a reduced amount of water. All other factors remaining constant, more liquid water (surface and groundwater) would remain to maintain freshwater ecosystems and natural flows, and satisfying anthropogenic water uses. This saving potential is reflected in the results by the difference in absolute fluxes under "Policy First" and "Security First". Under the assumptions of accelerated progress in improving crop yields and irrigation field efficiencies under "Policy First", continental-scale green water fluxes increase by 72% versus 88% under "Security First", and blue water fluxes by 8% versus 84% under "Security First".

But all factors, especially climate, are changing during the course of the scenario period. In some countries, increasing precipitation related to global warming will

compensate for increasing evapotranspiration and therefore water availability over a large area may remain the same. In other countries, decreasing precipitation will reduce the productivity of crops and thereby reduce evapotranspiration but also reduce the overall amount of water available. In any event the continental scale relationships between changing green water flux and the water cycle are and will remain complex and merit careful analysis.

CHAPTER 5

A GLOBAL COMPARISON OF FOUR POTENTIAL EVAPOTRANSPIRATION EQUATIONS AND THEIR RELEVANCE TO STREAM FLOW MODELLING IN SEMI ARID ENVIRONMENTS

Summary

This study compares four different potential evapotranspiration equations according to Priestley Taylor, Kimberly Penman, Penman Monteith (FAO-56) and Hargreaves on a global basis to demonstrate their difference, and assess their impact on the calculation of stream flows. The various equations of potential evapotranspiration show great differences in magnitude. But due to the limited availability of validation data, it is difficult to assess which method is the physically most reasonable to be applied. According to this study, the radiation-based Priestley Taylor equation proved to be most suitable for a global application. For the calculation of stream flows, however, the processes involved in the derivation of actual evapotranspiration values from potential evapotranspiration values appear more relevant than the absolute value of the potential evapotranspiration itself.

5.1 Introduction

Limited availability of measured climate and discharge data sets for semi-arid and arid areas restricts the reliability of global hydrological modelling in these regions. Validation with available runoff data sets shows an overestimation of the discharge in semi-arid to arid regions for various global hydrological models (Fekete et al. 1999, Nijssen et al. 2001, Döll et al. 2003). Due to several reasons (Döll et al. 2003), the quantitative simulation of the discharge can lie outside acceptable limits: (1) The quality of the input data sets highly influences the quality of the simulations. Secondly, a

grid-based simulation will not concur with point measurements due to spatial and temporal averaging of input data and processes. (3) Further uncertainty arises from the fact that the selection of representative processes might not be complete and important processes might be ignored. (4) Processes itself might be reproduced with inadequate algorithms. In this study, potential evapotranspiration is examined with respect to the latter case, while the generation of river discharge in semi-arid areas is analysed with respect to case (3).

Evapotranspiration as a major component of the water balance has been identified as a key factor in hydrological modelling and a wealth of methods have been developed for its calculation (e.g. Brutsaert 1982, Jensen et al. 1990). As a first attempt to improve stream flow simulations in semi-arid and areas, the global applicability and results of four potential evapotranspiration equations are compared in magnitude, as well as in their impact on stream flow simulations for the six-year period of 1990-1995. Further, a semi arid to arid study region in the Middle East is chosen to compare calculated potential evapotranspiration values to Class A Pan measurements, and to carry out a model-intercomparison where actual evapotranspiration simulations of a global hydrology model are compared to results from a physically-based regional model that has been developed with special focus on vertical water-fluxes.

5.2 Materials and methods

5.2.1 Equations of potential evapotranspiration

In general, the terms potential evaporation and potential evapotranspiration are to be differentiated. The first is a measure for the atmospheric demand, which is solely meteorologically driven under the assumption of unlimited water supply. The latter combines the rate at which water is removed from wet soils with that from plant surfaces under unlimited water supply. Especially for irrigation scheduling, this definition was further specified to refer to a reference surface consisting of a hypothetical grass with specific characteristics, termed reference crop evapotranspiration (Penman 1956, Doorenbos and Pruitt 1977, Wright 1981, Allen et al. 1998). Empirical crop coefficients are used to relate the reference crop evapotranspiration to crop evapotranspiration under non-standard conditions (Allen et al. 1998). It has, however, become common practice to use the terms potential evaporation and potential evapotranspiration interchangeably in the literature despite their different definition in terms. The output of various potential evapotranspiration equations will be compared on a global basis.

Noteworthy definitions of potential evaporation include the radiation-based formulation of Priestley and Taylor (1972), which is termed reference crop evapotranspiration by Jensen et al. (1990) and Maidment (1992):

$$E_p = \alpha_{PT}\left(\frac{\Delta}{\Delta+\gamma}\right)(R_N - G)\ [\text{mm/d}] \qquad \textbf{(5-1)}$$

with R_N = net radiation [mm/d], G = soil heat flux [mm/d] (can be neglected according to Maidment (1992)), Δ = gradient of saturated vapour pressure [kPa/°C], and γ = psychrometric constant [kPa/°C]. The α_{PT} factor [-] has the value of 1.26 and accounts for the aerodynamic component. Jensen et al. (1990) showed that the value of 1.26 is valid for humid areas, only. For arid areas, the value of 1.7 to 1.75 is more appropriate, in order to account for advection. The influence of a constant α_{PT} = 1.26 (‘*PT 1.26’*) will be compared to the differentiation into humid and arid areas with α_{PT} = 1.26, and 1.74, respectively (‘*PT’*), as suggested by Maidment (1992).

Penman (1948) was the first to introduce a combination equation to calculate reference crop evapotranspiration, termed this way as it combines the theoretical energy balance with the mass transfer method (Burman and Pochop 1994). Here, the modified Kimberly Penman (‘*KP’*) version is used to calculate reference crop evapotranspiration for alfalfa (Wright 1982), which additionally features a seasonally variable wind function. The wind function is used as cited in Allen et al. (1989).

$$E_P = \frac{R_N\Delta}{\Delta+\gamma} + \left(\frac{6.43\gamma W_f d}{\Delta+\gamma}\right)/\lambda\ [\text{mm/d}] \qquad \textbf{(5-2)}$$

with d = vapour pressure deficit [kPa], W_f = wind function , λ = latent heat of vaporization [MJ/m²d], all other parameters as defined in (5-1). The wind function takes the form

$$W_f = (a_w + b_w u_2) \qquad \textbf{(5-3)}$$

with u_2 = wind speed at 2m [m/s],

$$a_w = 0.4 + 1.4\exp[-((J-173)/58)^2], \qquad \textbf{(5-4)}$$

$$b_w = (0.007 + 0.004\exp[-((J-2432)/80)^2)])(86.4) \qquad \textbf{(5-5)}$$

where J is the Julian day of the year. In southern latitudes, J is incremented or decremented by 183, respectively (Allen et al. 1989).

Another extension of the Penman equation is the Peman-Monteith equation, which will be applied in the FAO 56 recommended form (Maidment 1992):

$$E_P = \frac{R_N\Delta}{\Delta+\gamma} + \left(\frac{\gamma u_2}{\Delta+\gamma}\right)\left(\frac{r}{T+273}\right)\ [\text{mm/d}] \qquad \textbf{(5-6)}$$

with T = air temperature [°C] and r = resistance term [-]. The aerodynamic and surface resistances of the original Penman Monteith equation have been set according to the particular reference crop and are included in the constant number r, which has a

value of 900 for grass (*'PM grass'*) and 1600 for alfalfa (*'PM alfalfa'*). All other parameters apply as defined in (5-1) and (5-3).

The temperature-based evapotranspiration equation defined by Hargreaves et al. (1985) is further applied in this study (*'HG'*). It is solely temperature-based and was initially developed for the semi-arid and arid area of California.

$$E_P = 0.0023 S_0 \sqrt{\delta_T} (T + 17.8) \qquad \textbf{(5-7)}$$

with S_0 = water equivalent of extraterrestrial radiation [mm/d], T = air temperature [°C], δ_T = daily air temperature range [°C]. δ_T accounts for effects of cloudiness, correlates with relative humidity and vapour pressure and negatively with wind speed (Hargreaves and Allen 2003). The authors make no comment for the case of $T \leq -17.8$ °C, which is necessary for a global application. In this case, E_P is set to zero.

Many other equations could not be applied globally, because for certain days of the year, the equations are mathematically not defined and the authors give no recommendations for these cases. This clearly results from the fact that most equations were developed for a specific climatic region, or specific time of the year (e.g. growing season for reference crop evapotranspiration). For example, the Turc method is valid for temperatures above 0°C and for humid climates, only (Maidment 1992, DVWK 1996). The Thornthwaite method is only recommended for monthly sums of evapotranspiration and has been demonstrated to give unrealistic values for Europe (DVWK 1996).

For simplicity, the output of Equations (5-1), (5-2), (5-6), and (5-7) will be termed potential evapotranspiration. For its calculation, only the grid-routine of the WaterGAP model is used, consisting of 66 896 grid cells. No model specific procedures are relevant for the results; they solely depend on the input data and the chosen equations. The CRU TS 2.1 gridded climate data set is used for climate input. It provides time series of monthly precipitation, air temperature, cloud cover and wet day frequency (Mitchell and Jones 2005). Wind information, when applicable, was used from the long-term average gridded climatology data set CRU CL 1.0 (New 1999). In this study, only evaporation and transpiration from the land fraction of a cell is considered, as evaporation from open waters (e.g. lakes and wetlands) is not included in the above definitions and its calculation is based on slightly different fundamentals. The evaluation period is 1990-1995.

5.2.2 The global model

The analysis is based on one of the current state-of-the-art global hydrological models, WaterGAP (Water - Global Assessment and Prognosis), which computes current and future water availability and water use (Alcamo et al. 2003a, Döll et al. 2003). For calculations of water availability, the daily vertical water balance (Figure 5-1) is calcu-

lated for each grid cell (0.5° x 0.5° geographical latitude and longitude). In a standard run, potential evapotranspiration is calculated according to Priestley Taylor. The distinction between arid and humid after Jensen et al. (1990) foresees a classification based on the month with the peak evapotranspiration at the arbitrary threshold of a relative humidity (RH) of 60%. Since the month with the peak evapotranspiration cannot be determined prior to the calculation itself, a classification based on land cover is implemented in WaterGAP, where grassland/steppe, hot desert, scrubland, and savanna are considered as arid, the remaining land cover classes are humid. From the potential evapotranspiration, actual evapotranspiration is derived based on a canopy and soil water balance. Potential evapotranspiration is hereby reduced according to the ratio of current canopy water storage to maximum canopy water storage based on an internally calculated leaf area index. Interception evaporation occurs as long as the canopy water storage is greater zero. Soil evapotranspiration is derived in a similar way based on the level of soil moisture saturation, which is a function of soil and vegetation specific field capacity. From the throughfall, which is precipitation reduced by interception, groundwater storage and surface runoff are calculated. The latter is routed through the respective river basin according to a global drainage direction map (Döll and Lehner 2002) to form river discharge. WaterGAP is calibrated and validated against measured discharges from the Global Runoff Data Centre (GRDC 2004). As climate input the CRU TS2.1 gridded climate dataset (Mitchell and Jones 2005) is used. Further, the FAO Soil Map of the World (FAO 1995) is used, as well as the global land cover grid as modelled by IMAGE 2.1 (Alcamo et al. 1998). Further input is specified in Döll et al. (2003).

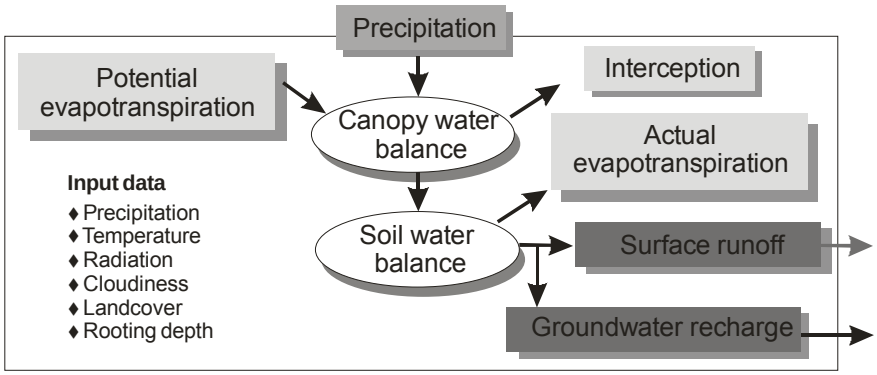

Figure 5-1. Schema of the daily vertical water balance that is calculated for each grid-cell in WaterGAP.

5.2.3 The regional model

TRAIN (Menzel et al. 2007) is a physically-based, spatially distributed model which includes information from comprehensive field studies on the water and energy balance of various land cover types, including natural vegetation and agricultural land. It has been designed to simulate the individual water budget components at different

spatial and temporal scales with focus on the soil-vegetation-atmosphere interface. The vertical water fluxes are calculated as follows: evapotranspiration follows the Penman Monteith equation (Monteith 1965), interception is simulated according to Menzel (1997), and the calculation of the soil water balance and percolation follow a modified version of the conceptual approach from the HBV-model (Bergström 1995). The application of TRAIN for agricultural land includes an automated irrigation process. When the soil water content falls below a critical limit, the model assumes irrigation until field capacity is reached. Since the model is especially designed to simulate vertical water fluxes in great detail, horizontal water flow from one cell to another is not considered. The model was initially developed for the humid environments of Central Europe and has been extensively validated with experimental data (e.g., actual evapotranspiration data determined with micrometeorological methods or lysimeter measurements) (Menzel 1999). It is currently adapted to the arid and semi-arid regions of the Jordan River: The major land-use types of the region and their typical annual development were introduced as well as some basic irrigation practices in agriculture. The model has been validated with data from several experimental sites along the climatic gradient (Sect. 0) covered with natural vegetation, forest and agricultural crops. A first application of TRAIN to the region can be found in Menzel et al. (2007).

For this study, TRAIN was run with a temporal resolution of one day and a spatial resolution of 18km x 18km (see Figure 5-2) based on the resolution of the climate input. Meteorological time series (precipitation, air temperature, air humidity, wind speed and solar radiation) were used as calculated by the regional climate model MM5 (2007) from the Institute for Meteorology and Climate Research IMK-IFU. The assumed land cover came from the Global Land Cover Characterization (USGS 2007). Further input data is described in Menzel et al. (2007). The following table (Table 5-1) compares the main elements of the two models as they have been applied in this study

Table 5-1. Comparison of the main features of the global model (WaterGAP) and the regional model (TRAIN).

Feature	WaterGAP	TRAIN
Spatial resolution	0.5° x 0.5° isogonal	18km x 18km isometric
Spatial coverage	global	regional
Climate Input	CRU TS 2.1	MM5
Land cover input	IMAGE	GLCC
PET equation	Priestley Taylor	Penmann Monteith
Irrigation	not assumed	based on expert knowledge

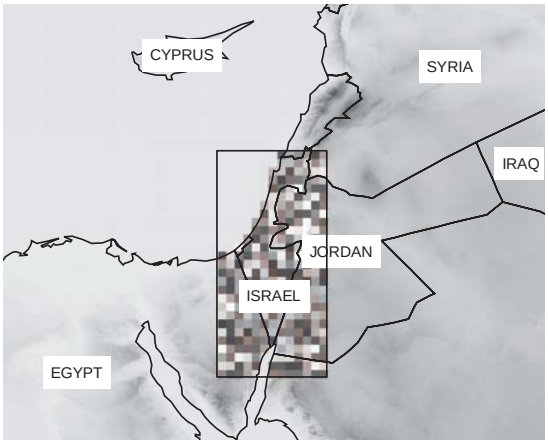

Figure 5-2. TRAIN simulation grid in the semi-arid to arid study region, situated along the Jordan River.

5.2.4 The regional study area

The study region (Figure 5-2), situated in the area of the Jordan River, is one of the most critical regions of current and future water scarcity. The strong climatic gradient from sub-humid in the north to arid in the south condenses many different climatic conditions into a small region, which turns this area into a unique study region with high transferability of results gained here. This strong climatic gradient is also an important factor for water availability. Sources of water are concentrated in the north of the region. The main precipitation falls during winter (November-January), with approximately 800 mm/ year in the north and 100 mm/year in the south. The Jordan River and its aquifers are trans-boundary resources, and the scarcity of water is used as a political issue between rivalling states.

5.3 Results: Comparison of potential evapotranspiration values

5.3.1 Intercomparison of different potential evapotranspiration equations

Figures 5-3 to 5-8 show average annual sums of potential evapotranspiration calculated with Equations (5-1) to (5-7). Lakes are depicted in blue because evaporation from open water is not calculated in this study. It appears that the Priestley Taylor (Figure 5-3) equation yields the highest values of evapotranspiration. The distinction between arid and humid areas can be recognized in a mosaic-like structure, where very high potential evapotranspiration values are calculated for arid areas due to the α_{PT} -factor. For a constant α_{PT} = 1.26, lower values as shown in Figure 5-4 result.

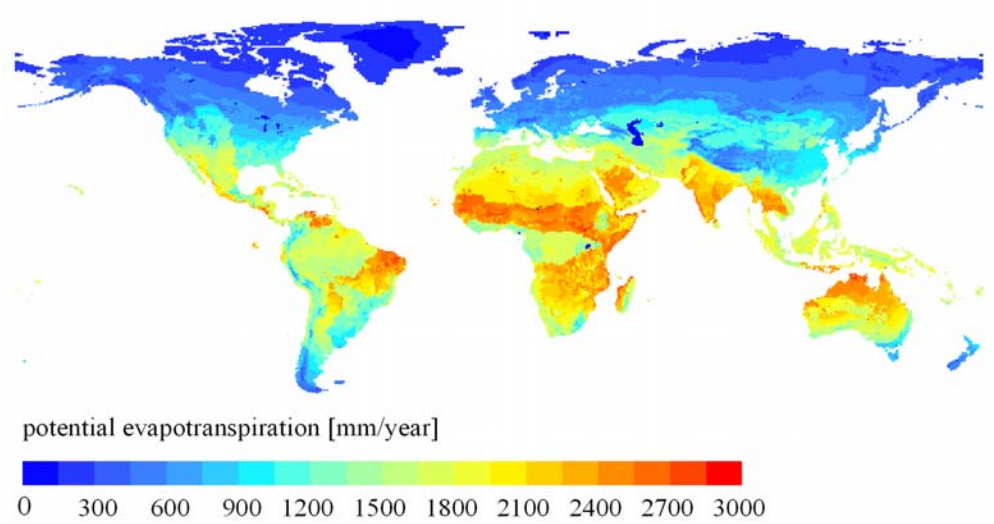

Figure 5-3. Average annual potential evapotranspiration (1990-1995) of land areas based on the Priestley Taylor equation with a variable α_{PT} for humid (1.26) and arid (1.74) areas.

The Kimberly Penman equation led to the second highest potential evaporation values (Figure 5-5) of all methods applied. Noteworthy are the elevated values in northern South America and the Congo basin, and higher values in Europe, in comparison to the Priestley Taylor equation with a variable α_{PT} .

The evaluation of the FAO 56 Penman Monteith equation, both for reference grass and alfalfa evapotranspiration (Figure 5-6 and Figure 5-7) showed unexpected low values, especially when compared to a study by Droogers and Allen (2002), who evaluated the same equation for grass based on CRU CL data (long term monthly averages 1961-1990) and obtained values nearly twice as high.

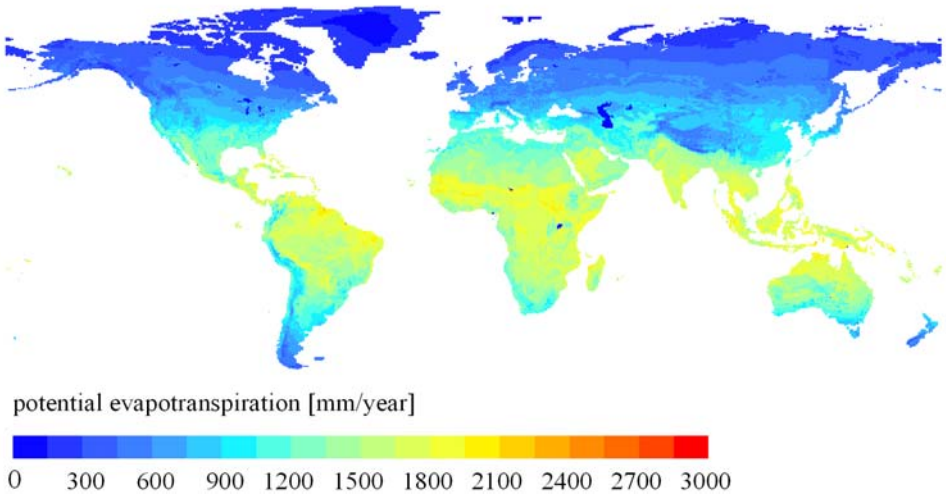

Figure 5-4. Average annual potential evapotranspiration (1990-1995) of land areas based on the Priestley Taylor equation with α_{PT} =1.26.

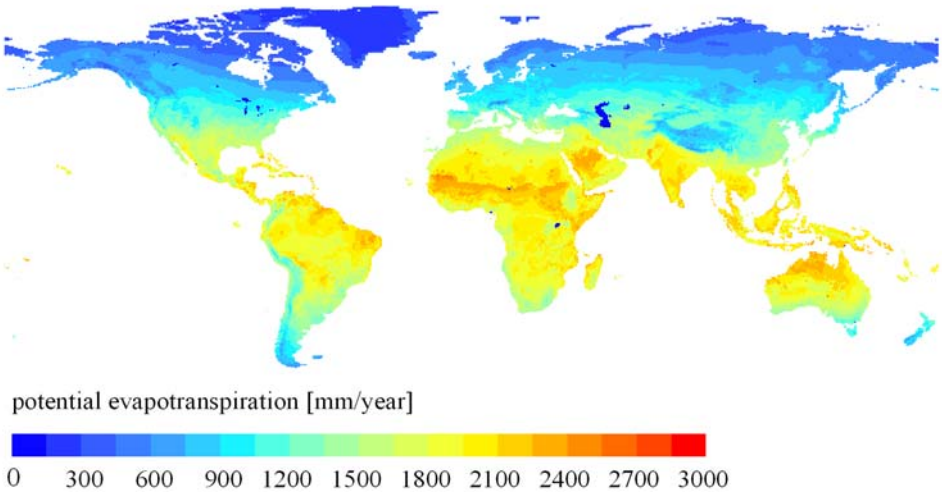

Figure 5-5. Average annual potential evapotranspiration (1990-1995) of land areas based on the Kimberly Penman equation.

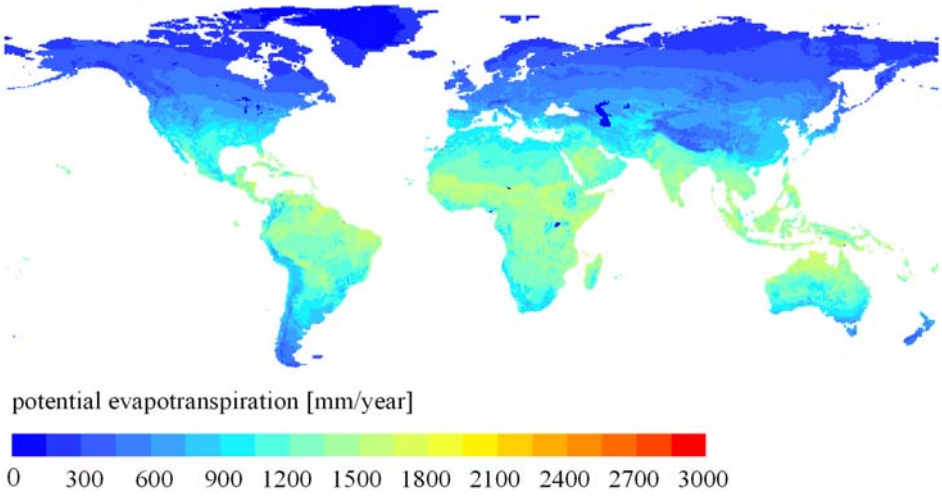

Figure 5-6. Average annual potential evapotranspiration (1990-1995) of land areas based on the FAO 56 Penman Monteith equation for grass.

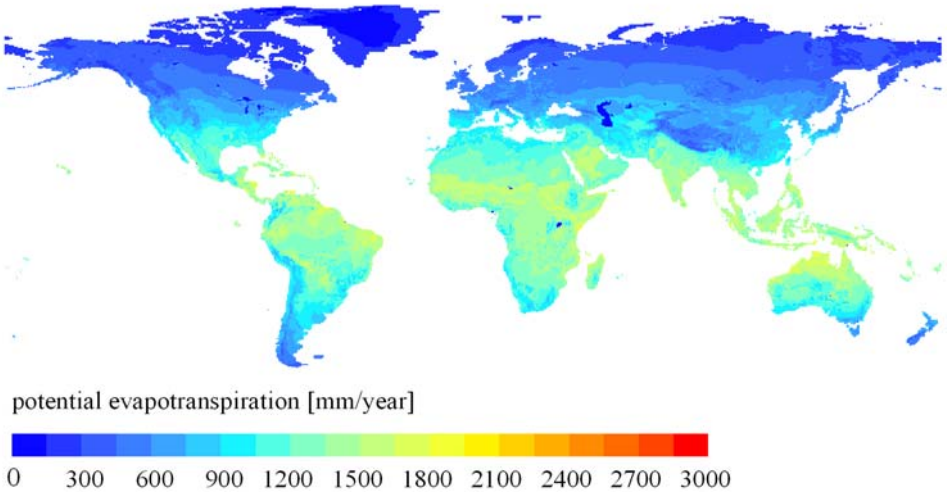

Figure 5-7. Average annual potential evapotranspiration (1990-1995) of land areas based on the FAO 56 Penman Monteith equation for alfalfa.

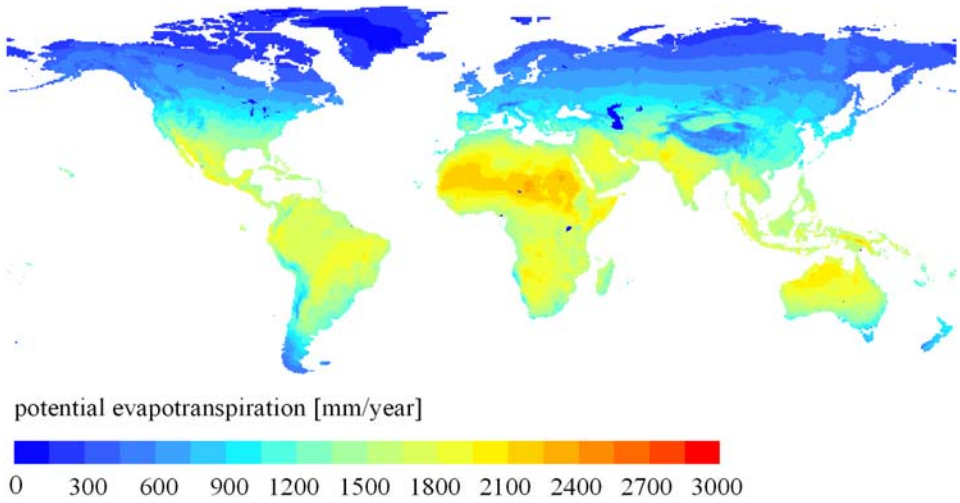

Figure 5-8. Average annual potential evapotranspiration (1990-1995) of land areas based on the Hargreaves equation.

The Hargreaves equation led to overall higher values than Priestley Taylor (arid/humid based on land cover) except for those areas classified as arid (Figure 5-8). Remarkable is the temperature-based cloud-like pattern of evaporation zones. The lag of peak estimates has to be noted with this equation, which becomes visible when looking at daily or monthly values due to the lag of temperature in comparison to radiation, which was also found by Jensen et al. (1990).

A comparison of the absolute values of potential evapotranspiration calculated with the various equations for the GEO4 regions (UNEP 2007a) is shown in Figure 5-9 . The graph reveals that the Kimberly Penman equation results in the highest potential evapotranspiration values in the global sum, as well as for all continents, except for Africa, where the Priestley Taylor equation results in higher values. This can be explained by the fact that Priestley Taylor differentiates arid and humid areas, with a significantly higher evapotranspiration in arid areas. Since a large part of Africa is classified as arid, the total value of potential evapotranspiration is high. For the other continents, the second highest values are calculated with the Priestley Taylor equation. In contrast, the Penman Monteith equation gives rather low values, even if adjusted to alfalfa vegetation.

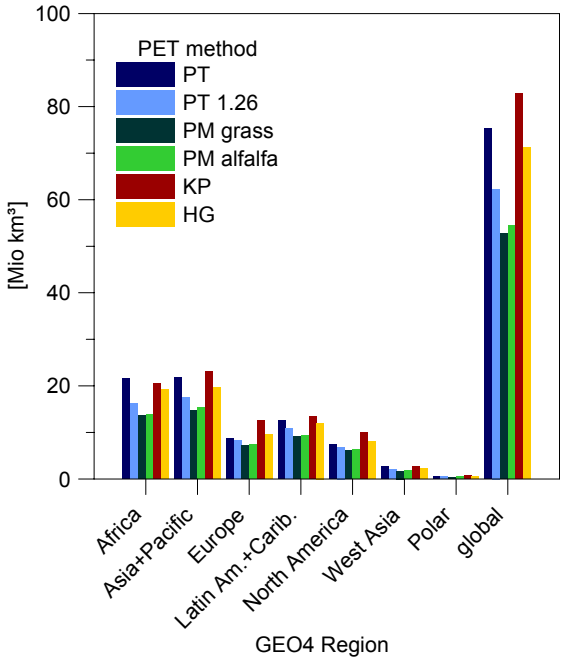

Figure 5-9. Regional (GEO-4 regions) and global potential evapotranspiration (PET) sums based on various PET equations.

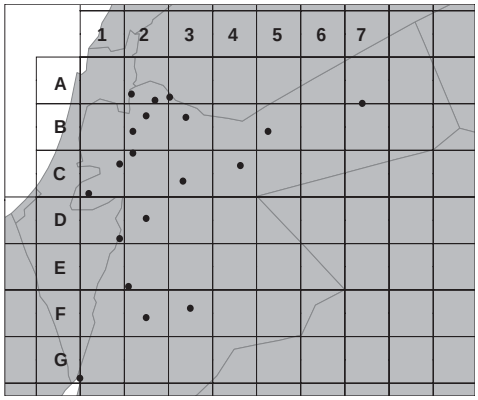

Figure 5-10. WaterGAP grid with Class-A pan evaporation measurement locations in the study region.

5.3.2 Comparison of calculated potential evapotranspiration values to measured pan evaporation data in the study region

Currently, no consistent global data set is available to validate potential evapotranspiration. For a first approximate comparison, pan evaporation data from 23 Class-A pan measuring stations in the Jordan River region are compared to simulated data at each of the locations. The measured data was available in monthly or daily resolution. It was aggregated to yearly values and then averaged over a minimum of 5 years, whereby the evaluation period could not be limited to the years 1990-1995 due to lack of data. Instead, values between 1980 and 2005 were used under the assumption that a general change of local evapotranspiration values over the decades can be neglected.

Figure 5-10 shows the WaterGAP grid for the study region and the location of the stations. Preferably, an averaged value over a number of stations should be used and compared to the value of a grid-cell, which itself represents an averaged value for the grid cell. Unfortunately, too little data was available and most of the grid cell values are compared to a single point measurement. Table 5-2 contains (averaged) pan evaporation measurements, corrected (averaged) pan evaporation measurements, the number of stations over which this value was averaged, and the calculated values based on Equations (5-1) to (5-7).

Problems with pan evaporation measurements arise from the difficulty of accurate measurements during rainfall, or poor maintenance of the pan causing inaccurate measurements (Bloemen 1978) as cited in (Linacre 1994). In general, pan evaporation measurements are of higher magnitude than reference crop evapotranspiration (Jensen et al. 1990). According to Linacre (1994), they can be adapted by using a correction factor of the value of 0.7, which was applied to the measured values.

All calculated values stay well below measured values. If compared to the corrected measurements, the Priestley Taylor method with a variable α_{PT} for arid and humid areas shows the best results with an averaged deviation of -5.9% in the examined study region. The second closest calculation was obtained with the Kimberly Penman method with a deviation of -9.1%. Hargreaves method showed a deviation of -19.8% whereas Priestley Taylor with a constant α_{PT} of 1.26, and Penman Monteith FAO 56 showed deviations of -30% - -40%.

Table 5-2. Comparison of average annual (1990-1995) measured pan evaporation rates versus calculated potential evapotranspiration, and percentage deviation of calculated value from corrected measured values, with avg. Pan = average measured Class A pan evaporation, corr. pan = corrected pan evaporation, PT = Priestley Taylor with α_{PT} = 1.74 in arid areas and α_{PT} = 1.26 in humid areas, PT 1.26 = Priestley Taylor with a constant α_{PT} = 1.26, PM grass = Penman Monteith grass reference evapotranspiration, PM alfalfa = Penman Monteith alfalfa reference evapotranspiration, KP = Kimberly Penman, and HG = Hargreaves.

Grid cell	Avg. pan [mm]	Corr. pan (*0.7)	No. of pan stat.	PT [mm]	PT [%]	PT 1.26 [mm]	PT 1.26 [%]	PM grass [mm]	PM grass [%]	PM alfalfa [mm]	PM alfalfa [%]	KP [mm]	KP [%]	HG [mm]	HG [%]
A2	2069.3	1448.5	2	1877.7	(29.6)	1359.7	(-6.1)	1154.4	(-20.3)	1193.0	(-17.6)	1727.8	(19.3)	1352.8	(-6.6)
A3	2729.2	1910.5	1	1844.3	(-3.5)	1335.6	(-30.1)	1137.3	(-40.5)	1180.2	(-38.2)	1711.5	(-10.4)	1480.9	(-22.5)
A7	3589.6	2512.7	1	1605.0	(-36.1)	1162.3	(-53.7)	1008.5	(-59.9)	1062.0	(-57.7)	1640.8	(-34.7)	1579.9	(-37.1)
B2	2217.2	1552.1	3	1898.4	(22.3)	1374.7	(-11.4)	1160.0	(-25.3)	1196.5	(-22.9)	1734.0	(11.7)	1339.6	(-13.7)
B3	2456.7	1719.7	1	1473.4	(-14.3)	1066.9	(-38.0)	925.3	(-46.2)	968.0	(-43.7)	1503.2	(-12.6)	1490.4	(-13.3)
B5	3541.7	2479.2	1	1523.4	(-38.6)	1103.1	(-55.5)	954.0	(-61.5)	1001.3	(-59.6)	1575.0	(-36.5)	1591.8	(-35.8)
C1	1973.8	1381.6	2	1971.2	(42.7)	1427.4	(3.3)	1199.6	(-13.2)	1233.2	(-10.7)	1771.8	(28.2)	1381.0	(0.0)
C2	2404.6	1683.2	2	1979.8	(17.6)	1433.7	(-14.8)	1208.3	(-28.2)	1246.2	(-26.0)	1802.4	(7.1)	1422.5	(-15.5)
C3	2479.2	1735.5	1	1498.0	(-13.7)	1084.8	(-37.5)	930.7	(-46.4)	970.0	(-44.1)	1519.1	(-12.5)	1436.6	(-17.2)
C4	3169.5	2218.7	1	1561.9	(-29.6)	1131.0	(-49.0)	976.6	(-56.0)	1022.5	(-53.9)	1596.5	(-28.0)	1570.8	(-29.2)
D1	2342.2	1639.5	2	1577.7	(-3.8)	1142.5	(-30.3)	983.6	(-40.0)	1023.0	(-37.6)	1581.8	(-3.5)	1473.8	(-10.1)
D2	2017.4	1412.2	2	1958.2	(38.7)	1418.0	(0.4)	1194.8	(-15.4)	1234.1	(-12.6)	1783.4	(26.3)	1396.0	(-1.1)
E2	1767.9	1237.5	1	1495.9	(20.9)	1083.3	(-12.5)	934.2	(-24.5)	978.1	(-21.0)	1521.1	(22.9)	1428.3	(15.4)
F2	3602.7	2521.9	1	1532.6	(-39.2)	1109.8	(-56.0)	962.7	(-61.8)	1013.4	(-59.8)	1566.9	(-37.9)	1520.2	(-39.7)
F3	3589.6	2512.7	1	1605.0	(-36.1)	1162.3	(-53.7)	1008.5	(-59.9)	1062.0	(-57.7)	1640.8	(-34.7)	1579.9	(-37.1)
G1	4831.9	3382.3	1	1631.2	(-51.8)	1181.2	(-65.1)	1036.4	(-69.4)	1097.9	(-67.5)	1676.2	(-50.4)	1575.4	(-53.4)
Avg. deviation [%]					(-5.9)		(-31.9)		(-41.8)		(-39.4)		(-9.1)		(-19.8)

5.3.3 The impact of different potential evapotranspiration equations on the stream flow simulation

The comparison with pan evaporation measurements suggests that the currently implemented algorithm for the calculation of the potential evapotranspiration according to Priestley Taylor produces the most reasonable results. This comparison was, however, restricted to a rather small study region. For the overall aim of improving stream flow calculations and a wider approach, the above-described potential evapotranspiration equations were utilized in WaterGAP runs for the calculation of stream flows, which were then validated with measured runoff data form the Global Runoff Data Centre (GRDC 2004). In this comparison it was not possible to detect a consistent improvement of modelled river discharges in 14 evaluated catchments. In humid areas, where the simulation of stream flow is good in general, no effect on the river discharge was noted under application of the various potential evapotranspiration equations. In semi arid and arid catchments, a minor impact on the modelled stream flow was visible but the equation that caused the closest agreement of simulated with measured stream flow data was a different one for the different catchments. Overall, none of the equations was capable to improve the calculated river discharges effectively. Therefore it is concluded that it is very worthwhile to further examine the algorithms involved in the derivation of actual evapotranspiration values from potential evapotranspiration values.

5.4 Comparison of long-term average monthly actual evapotranspiration as calculated with a global and a regional model

Since potential conditions are only met during and shortly after precipitation, condensation or on irrigated fields (ASCE 1996), the amount of actual evapotranspiration, which describes the evapotranspiration that occurs under natural constraints, is more relevant to the global modelling of the hydrological cycle. Actual evapotranspiration is usually calculated model-specifically from potential evapotranspiration based on various storage balances, taking into account plant parameters and field capacities.

In order to make a first attempt in assessing the performance of this calculation with the WaterGAP model in the study region, actual evapotranspiration rates were compared to those calculated with the regional model TRAIN. With the aim of facilitating the comparison of two models that rely on different algorithms and input data, long-term average monthly (1961-1990) cumulated values are compared, and the overall behaviour of functions over the extend of the TRAIN simulation grid (Figure 5-2). In Figure 5-11 and Figure 5-12, grey bars depict the long-term regional average monthly actual evapotranspiration values from the (1961-1990) WaterGAP and TRAIN runs (*monthly aet*).

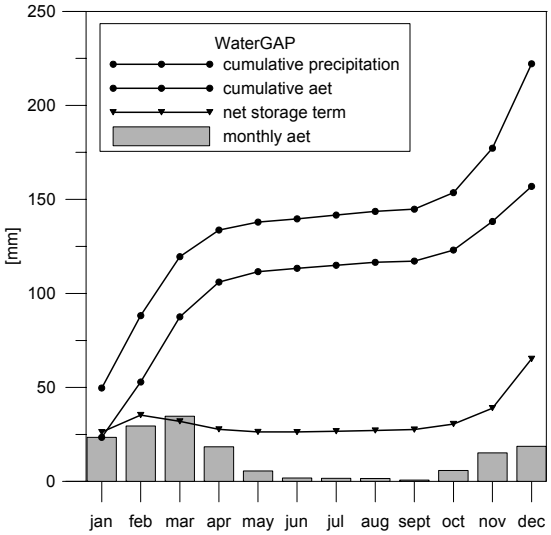

Figure 5-11. 1961-1990 long-term average monthly water balance as calculated with WaterGAP for the TRAIN simulation grid, with cumulative aet = cumulative actual evapotranspiration, net storage term = cumulative precipitation – cumulative aet.

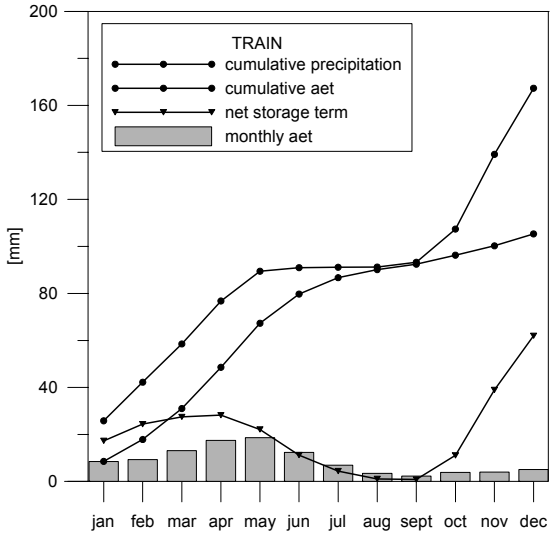

Figure 5-12. 1961-1990 long-term average monthly water balance as calculated with TRAIN for the TRAIN simulation grid, with cumulative aet = cumulative actual evapotranspiration, net storage term = cumulative precipitation – cumulative aet.

It has to be noted that in TRAIN, irrigation is included, which is treated similar to precipitation input. Further, the cumulative precipitation curve (*cumulative precipitation*) and cumulative actual evapotranspiration (*cumulative aet*) curves are shown. The *net storage term* is the remainder of the cumulative balance of precipitation minus actual evapotranspiration and is thus composed of soil water and surface runoff. These two processes have to be regarded as one in this comparison because in TRAIN the horizontal water balance is not accounted for.

It appears that the actual evapotranspiration in WaterGAP is strongly correlated to precipitation with a priority on discharge generation over evapotranspiration generation. Calculations of actual evapotranspiration with TRAIN are stronger related to the level of soil water storage with emphasis on the vertical water fluxes as the horizontal water balance is not considered. The net storage term almost completely falls dry in the TRAIN simulations while the net storage term in the WaterGAP simulations remains above an average threshold of 25mm. This indicates that the calculated values of actual evapotranspiration in WaterGAP are too small, which could explain the overestimation of discharge values in semi-arid and arid catchments that was also found by Döll et al. (2003) for this model.

5.5 Discussion and conclusions

In this study, four different formulations for the calculation of potential evapotranspiration were compared on a global basis. The author applied one radiation-based method (Priestley Taylor), two combination equations (Kimberly Penman and Penman Monteith) and one temperature-based method (Hargreaves), which all showed great differences in magnitude. Due to the fact that the radiation-based equation showed the closest agreement with Class A pan evaporation measurements for a semi-arid study region, and for its overall low input requirements it was found to be most appropriate for global applications.

It has, however, to be noted, that the evaluation with measured data was carried out for a, although covering a large climatic gradient, small study region, with a rather low density of measuring stations. Of the four applied potential evapotranspiration equations that yield an upper limit of potential evapotranspiration, three were initially developed for irrigation scheduling and therefore perform best for agricultural areas. Usually, empirical crop coefficients are used to relate the reference crop evapotranspiration to non-standard conditions. The usage of these coefficients was neglected because they were not available for the variety of global land cover types. Furthermore, crop coefficients for various agricultural areas have a value close to 1.0, with values below 1.0 for the most part of the growing season. It is therefore assumed that the difference is not significant in comparison to the great difference in magnitude of the formulations itself.

Further, the application of the two combination equations relies on wind data, which had to be taken from a climatology data set, as time series in the required resolution of 0.5 degrees are not available yet. This impairs the performance of the combination equations as the wind function is degraded to a wind factor. The combination equations might therefore lead to improved values if an appropriate wind product is available. This, however, further underlines the current advantages of the application of a radiation-based equation.

Since in most parts of the world, the process of evapotranspiration is rather water-limited as opposed to radiation-limited, the processes involved in deriving values of actual evapotranspiration from potential evapotranspiration is of higher relevance to the simulation of surface runoff and stream flows than the initial magnitude of the potential evapotranspiration itself. To date, too little process-knowledge is available, turning the calculation of actual evapotranspiration into a model-specific process, related to various storage balances. Therefore, a comparison between two models was carried out, where a global hydrological model was compared to a regional model. Both rely on different process algorithms and different input data that are both physically-based descriptions of the current state. The comparison of the behaviour of the

storage functions revealed that it is worthwhile to examine the various storage balances in more detail rather than varying the potential evapotranspiration equations in order to improve stream flow simulations in semi-arid environments.

CHAPTER 6

REGIONALISATION OF THE PRIESTLEY TAYLOR COEFFICIENT FOR USE IN GLOBAL HYDROLOGICAL MODELLING

Summary

The Priestley-Taylor equation is a widely accepted approach to calculate potential evapotranspiration due to its low input requirements. The equation contains an α-coefficient, which was initially introduced at the value of 1.26 by Priestley and Taylor, but has since been adapted to site-specific conditions in many small-scale studies. A global application of the Priestley Taylor equation was, up to now, limited to a single, fixed value of α, or when differentiating arid and humid areas, to the use with two α-values. The objective of this study was to parameterize the α-coefficient for a global application by using pan evaporation measurements supplemented by α-values from existing small-scale studies. The parameterization was carried out within the boundaries of climate zones, which were initially introduced by Köppen and Geiger. The available data enabled a differentiation of 12 α-classes for which potential evapotranspiration was simulated. The best agreement between measured and simulated values was achieved in cooler climates, while in warmer and drier climates, measured pan evaporation values were characterized by greater variability. The new α-parameterization, when fed into a global hydrological model, lead to improved discharge simulations in all climates.

6.1 Introduction

For the simulation of water resource systems, a correct estimation of magnitude and variation of evapotranspiration is critical, as it constitutes a major component of the water cycle. Numerous equations of evapotranspiration have been developed that dif-

fer largely in their data requirements for parameterisation (Weiß and Menzel 2008). The Penman Monteith equation (Monteith 1965), for example, following a physically-based approach, requires a large amount of detailed information, such as aerodynamic resistance, stomatal resistance and wind speed that are difficult to acquire in high resolution for the entire globe. Especially for use in global hydrological models, where the calculation of potential evapotranspiration often represents an upper limit to the evaporation rate and actual evapotranspiration is calculated by canopy and soil water balances, a simpler approach that accounts for the atmospheric demand can alternatively be used.

Priestley and Taylor (1972) proposed a simplified version of the combination equation (Penman 1948) as an example of a radiation based approach, which has proven to be remarkably accurate and theoretically robust. It consists of an energy term multiplied by a coefficient to account for the aerodynamic component. In its original version this α-coefficient was set to 1.26. A great number of regional studies have since attempted to adjust the α-coefficient for site specific conditions (McNaughton and Black 1973, De Bruin and Keijman 1979, Viswanadham et al. 1991, Castellvi et al. 2001, Engstrom et al. 2002, Komatsu 2005). A study for the entire globe, considering different vegetation zones has, to the author's knowledge, not yet been carried out. The most widely used parameterization, in this case, is a distinction between arid and humid areas that was introduced by Jensen et al. (1990). They suggest a value for humid areas of $\alpha = 1.26$ and an increased α value for arid areas (1.74) to consider advection (Maidment 1992). The solely differentiation between two zones seems no longer appropriate, especially for large-scale distributed modelling. Further, an abrupt augmentation by 50% between neighbouring regions, or – expressed from a modeller's perspective – from one grid cell to the next, seems unrealistic.

Therefore, this study aims at regionalising the Priestley Taylor coefficient by comparison of calculated potential evapotranspiration values with measured pan evaporation and supplementing these with values from local studies for those areas where pan values are not available. It is further show that the regionalised Priestley Taylor coefficient leads to improved discharge simulations when applied to a global hydrological model.

6.2 Materials and Methods

6.2.1 The global hydrological model WaterGAP

The WaterGAP model is an integrated global water model for the simulation of current and future water availability and water use (Alcamo et al. 2003a, Döll et al. 2003). It simulates the water balance in each grid cell over a continental grid with 30 arc-

minutes spatial resolution in a daily time step and routes flows along surface and subsurface pathways using a directional flow scheme (Döll and Lehner 2002).

The water balance takes into account climate parameters from the CRU TS2.1 gridded climate dataset (Mitchell and Jones 2005) consisting of time series of monthly mean temperature, precipitation, number of wet days and cloud cover. These are used to calculate, amongst others, potential and actual evapotranspiration, surface and subsurface runoff. From the natural flow, anthropogenic water uses are subtracted on a grid cell level. The remainder forms river discharge. The simulated river discharge is calibrated and tested against measured discharge data from the Global Runoff Data Center (GRDC 2004). The global water use module calculates water withdrawals and other metrics for several water using-sectors, taking into account e.g. population, industrial and agricultural production and GDP (Alcamo et al. 2003a, b, Alcamo et al. 2007).

6.2.2 The Priestley Taylor equation for potential evapotranspiration

The Priestley Taylor equation (eq. 1) is based on the concept of equilibrium evaporation (McNaughton and Black 1973, Monteith 1981, as cited in Eichinger et al. 1996). Air passing over a saturated surface will gradually decrease in saturation deficit until an equilibrium evaporation rate is reached (Eichinger et al. 1996). The potential evaporation rate E_p then becomes a function of available energy and air temperature specific saturation vapour pressure. As equilibrium conditions are rarely met in natural environments, and based on experimental evidence, Priestley and Taylor (1972) suggested an empirical coefficient α_{PT} (here referred to as α-coefficient) with an invariable value of 1.26 which accounts for the aerodynamic component of the evaporation process (Eichinger et al. 1996, Engstrom et al. 2002). Jensen et al. (1990) later differentiated arid and humid areas with an α-coefficient of 1.74 and 1.26, respectively.

$$E_p = \alpha_{PT}\left(\frac{\Delta}{\Delta+\gamma}\right)(R_N - G)\,[\text{mm/d}] \qquad \textbf{(6-1)}$$

with RN = net radiation [mm/d], G = soil heat flux [mm/d], Δ = gradient of saturated vapour pressure [kPa/°C], and γ = psychrometric constant [kPa/°C]. G is assumed to be small in comparison with RN on a daily basis and therefore neglected.

To simulate the net radiation flux, R_N, global solar radiation flux and net long wave radiation flux are calculated as functions of day of the year, latitude, sunshine hours and albedo (Kaspar 2004).

Albedo values hereby follow the study by Rechid et al. (2008) who developed dynamic values for the snow-free land surface albedo as a function of vegetation phenology and background albedo in 30 arc-minutes spatial, and monthly temporal resolu-

tion, based on MODIS data. For application in the WaterGAP model, this dataset of land albedo is combined with the value of 0.08 for lakes, and a value for snow cover depending on underlying vegetation. The reflective properties of snow vary depending on age of the snow, particle size, density and composition, impurities, etc., which cannot reliably be modelled by a global model that reads monthly climate input. Tanskanen and Manninen (2007), however, have found snow albedo further depending on the vegetation above snow and give values for various land-cover types, such as evergreen needle leaf forests, deciduous needle leaf forests, woodlands, grasses, croplands and bare land.

As the calculation of albedo values now is combined with the model-internal procedure for the calculation of the leaf area development, as stated above, this procedure was also modified as part of this study. A certain threshold of minimum rain fall now has to be exceeded for the onset of optimum growing conditions. Previously, this was associated with certain potential evapotranspiration conditions, which could no longer be used since the sequential order of calculating potential evapotranspiration and vegetation development within the model was reversed. The second condition for the onset of the growing season is a temperature threshold, which has to be exceeded by a certain number of days, depending on type of vegetation. This threshold was set to 8°C instead of previously 5°C, based on a sensitivity analysis, in order to reach a more realistic representation of the onset of vegetation development within the year.

6.2.3 Pan evaporation measurements

To the author's knowledge, no global pan evaporation data set is available. Data used in this study were compiled from various sources as given in Table 1. The data base was compiled with emphasis on semi-arid and arid areas as the reliability of the α-coefficient in humid areas has thoroughly been proven in previous studies (Priestley and Taylor 1972, Davies and Allen 1973, Stewart and Rouse 1976, Mukammal and Neumann 1977, Brutsaert 1982, Jensen et al. 1990, Parlange and Katul 1992). The location of pan measuring stations is shown in Figure 6-1.

The significance of results deduced from pan evaporation data depends on the reliability of the historical pan evaporation measurements which, as for all meteorological data, can be affected by non-climatic factors, for example changes in observing practices, station relocations, or changes in exposure (Easterling and Peterson 1995).

The Australian dataset was provided by the Australian Bureau of Meteorology as a quality checked data set and changes of observing practice, for example, were indicated. The Australian observation systems were successively transferred to Class-A Pan observing systems in the middle of the 20th century. If the difference in measured values before and after change of observation system was statistically significant, val-

ues that were not derived with Class A pans were omitted in this study.

For the other sources used here (Table 1), these factors could not as easily be detected, as background information on the site history was difficult to retrieve. Pan measurements were therefore quality-ranked based on available background information, reliability and reasonability of absolute values. The high quality data was given more emphasis than the low quality data. But due to the fact that long-term means of each station were used in the generation of the α-coefficient, some of the discontinuities should have levelled out.

Table 6-1: Sources of the pan evaporation dataset compiled for this study.

Country	Period*	No. of stations	Temp. resol.	remark	source
Australia	1901-2002	580	daily	high quality, quality checked by the Bureau of Meteorology Australia	Australian Daily Evaporation, Product code: IDCJDC05, National Climate Centre, PO Box 1289, Melbourne, 3001 (retrieved 21.05.2008)
U.S.	1901-2002	110	monthly avg.	high quality - long-term monthly averages	• http://hydrology1.nmsu.edu/Pan_Evaporation/ • http://www.sjd.water.ca.gov/landwateruse/evaporation/#Bakersfield • http://www.ocs.orst.edu/page_links/comparative_climate/evap.html • http://www.dnr.sc.gov/climate/sco/Publications/pan_evap_tables.php#1 • http://www.stormwaterauthority.org/assets/110MMegginnis.pdf (accessed 01.11.2008)
Jordan	1963-2002	20	hourly/ daily/ monthly, depending on station	medium to low quality – measuring practices do not comply with standards	Data made available to the GLOWA Jordan River Project (http://www.glowa-jordan-river.de, accessed 01.01.2008)
Russia	1978-1983	5	10 day means	low quality – small record of measured values	http://climate.envsci.rutgers.edu/soil_moisture/DOWNLOAD/RUSWET-GRASS-6STA/forcing/ (accessed 28.02.2008)
Thailand	1982-2002	3	daily	low quality - no indication of Pan method	PUB Research Database, PWRI Memorandum No.4003, http://www.icharm.pwri.go.jp/html/network/index.html (21.04.2008)

* The longest period in a dataset is given, many stations having shorter or discontinuous measuring periods

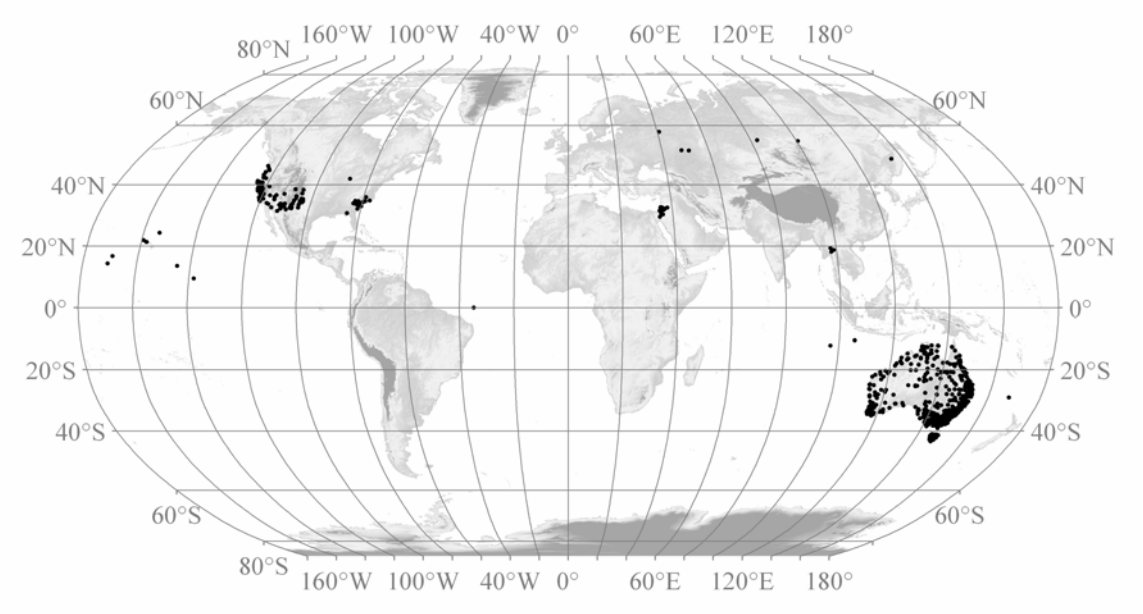

Figure 6-1: Location of pan measuring stations shown as black dots.

As the available pan evaporation data is insufficient to examine temporal variability of the α-coefficient, this study is limited to the spatial variability of α. For each grid cell of the WaterGAP model with a pan measuring station (Figure 6-1), an average α-value is determined by solving the Priestley Taylor equation for α. If more than one station is located in one grid cell, measured values are averaged.

In general, measured pan values have been shown to be of higher value than prevailing potential evapotranspiration in the area surrounding the pan due to e.g. significant differences in the pan water temperature from the surrounding air temperature or different exchange rates of air masses over the pan than in the surrounding area. Therefore, pan evaporation reduced by a factor is used equivalent to potential evaporation to solve the equation for α. A factor of 0.8 is applied to the measured pan data, a value that has been proven adequate in previous studies. (Jensen et al. 1990, Linacre 1994).

The distribution of α-values within climate zones was then used to find the optimum α-value in each zone. Since some of the classes are characterized by a wide span of α-values, the median is used rather than the average. Pan measuring stations covered 14 of the 30 Köppen climate zones. The *A* and *B* climates were completely covered. For the uncovered *C*-subclasses (temperate rain climates), mainly the well-established value of 1.26 for humid areas was used. The *D*-climates were partly covered by pan measuring stations, for the remaining stations values from small-scale studies were used. The α-values for the *E*-climate were derived from literature.

6.2.4 Köppen climate zones

The transferability of results derived from measured pan evaporation station data to the rest of the world is achieved through the link with climate zones. The division into climate zones hereby follows the updated Köppen-Geiger climates as presented by Kottek et al. (2006). Kottek et al. (2006) base their classification scheme on the work of Wladimir Köppen and Rudolf Geiger, a quantitative classification of world climates based on vegetation, temperature and precipitation. Five major vegetation groups are differentiated: plants of the equatorial zone (*A*), the arid zone (*B*), the warm temperate zone (*C*), the snow zone (*D*), and the polar zone (*E*).

Subtypes are further differentiated by a second and third letter following the mean annual precipitation and temperature cycles: (*W*) only in combination with (*B*) – desert, (*S*) only in combination with (*B*) – steppe, (*f*) humid, (*m*) monsoon, (*s/w*) summer/winter dry; (*a*) hot summer, (*b*) warm summer, (*c*) cool summer, (*d*) extremely continental. In order to ignore short term spatiotemporal variations in the extent of climate zones, the climate classification is based on a period of 30 years (1961-1990). The original differentiation results in 30 classes. During the process of this study, these were grouped into 12 categories of unique α-values.

The applicability and advantage of the Köppen climate zones in global hydrological and climate modelling studies has been proven in previous studies by Peel et al. (2007) and Lohmann et al. (1993) who examined continental-scale variability in annual runoff, and validated GCM control runs, respectively. Since this climate classification is, per definition, linked to environmental conditions, it should also be an adequate classification for potential evapotranspiration.

6.2.5 Efficiency of model simulations

In order to evaluate the agreement between modelled and measured evaporation as well as modelled and measured discharge, the following efficiency indicators are applied,

$$R^2 = \left(\frac{\sum (Q_{\mathrm{mod}} - \overline{Q_{\mathrm{mod}}})(Q_{obs} - \overline{Q_{obs}})}{\sqrt{\sum (Q_{\mathrm{mod}} - \overline{Q_{\mathrm{mod}}})^2 \sum (Q_{obs} - \overline{Q_{obs}})^2}} \right)^2 \quad [-] \qquad \textbf{(6-2)}$$

$$bias = \frac{\sum (vol_{\mathrm{mod}} - vol_{obs})}{\sum vol_{obs}} \qquad [-] \qquad \textbf{(6-3)}$$

$$NSE = 1 - \frac{\sum (Q_{\mathrm{mod}} - Q_{obs})^2}{\sum (Q_{obs} - \overline{Q_{obs}})^2} \qquad [-] \qquad \textbf{(6-4)}$$

where R^2 is the well-known coefficient of determination, with Q_{mod} being the mean monthly modelled streamflow, or modelled evaporation, respectively, Q_{obs} the mean monthly observed streamflow or observed pan evaporation, and $\overline{Q_{obs}}$ the average of the mean monthly observed streamflow values or observed pan values. A value of 1.0 indicates that all variance in the model can be explained by the variance in measured data. As second criterion the bias is examined, defined as the difference of simulated and observed volumes of river discharge or values of evaporation. A value of zero represents a perfect simulation of the observed flow volume/evaporation, a negative or positive value an under- or overestimation of the flow volume/evaporation. The third examined criterion is the Nash Sutcliffe efficiency (NSE) (Nash and Sutcliffe 1970). A NSE of 1.0 indicates that the model results correspond to observations; possible values of NSE may include a range between $-\infty$ and 1.

The efficiency of modelled potential evapotranspiration is determined with data from Australia because only this data set contains high quality time series of measured pan evaporation.

For measured values of river discharge, data provided from the Global Runoff Data Center (GRDC 2004) is used. From the provided approximately 1200 stations a total of 960 stations were applicable for model testing, as stations with measuring periods shorter than five years were excluded, as well as those, where the shape of the hydrograph pointed to intense river regulation, e.g. near the outlet of a reservoir, because this study aims at modelling natural flows.

6.3 Results and discussion

6.3.1 Regionalized α-values

Table 6-2 gives the regionalized α-values for the different Köppen classes as derived from pan evaporation measurements. The α-values range from 1.0 in polar climates to 2.0 in tropical climates and deserts. Their spatial distribution is shown in Figure 6-2.

Arid climates and the monsoon and humid classes of the tropical rain climate, as well as hot, summer dry areas of the temperate rain climates have the highest α-values (1.65-2.0). These values compare well to those found in other studies. A value of 2.0 is suggested in (Verma et al. 1978) for dry areas under the influence the advection, while (Jury and Tanner (1975) suggest a value of 1.57 for the same conditions. Viswanadham et al. (1991) found α to vary from 1.28 to 3.12 during stable conditions and daylight hours for the Amazon forest. Castellvi et al. (2001) determined α to be in the range 1.4 to 1.8 for region in north-east Spain, which falls into the *Csa*- climate class

(α=1.65).

Still higher than the initial value of 1.26 is the α-coefficient for the savanna climate and the humid climates of the temperate rain and boreal forest climates (1.3-1.45). Castellvi et al. (2001) found α to be in the range of 1.3 to 1.44 during summer for a region situated in the *Cfa*- climate (α=1.45). Shuttleworth and Calder (1979) found α–values for forests in England to be in a wide range(0.53-2.08) with an average value of 1.3 (*Cfb*- class).

The lowest α-values are assigned to the polar climates and the cool summer and continental climates of the boreal forest/snow climates (1.0-1.2). Comparable values were found by McNaughton and Black (1973) for a Douglas-fir forest (1.05-1.18). Shi et al. (2008) use α with a value of 1.18 for a pine forest in the Changbai Mountains in China, which is situated in the *Dwc*- climate (α =1.1). Eaton et al. (2001) have found an average α of 1.07 for several sites in Canada including shrub tundra vegetation, wetland, upland tundra and coniferous forests (ET and *Dfc*- class, α=1.1). This value is also supported by Saunders et al.(1997) and Rouse et al. (1977).

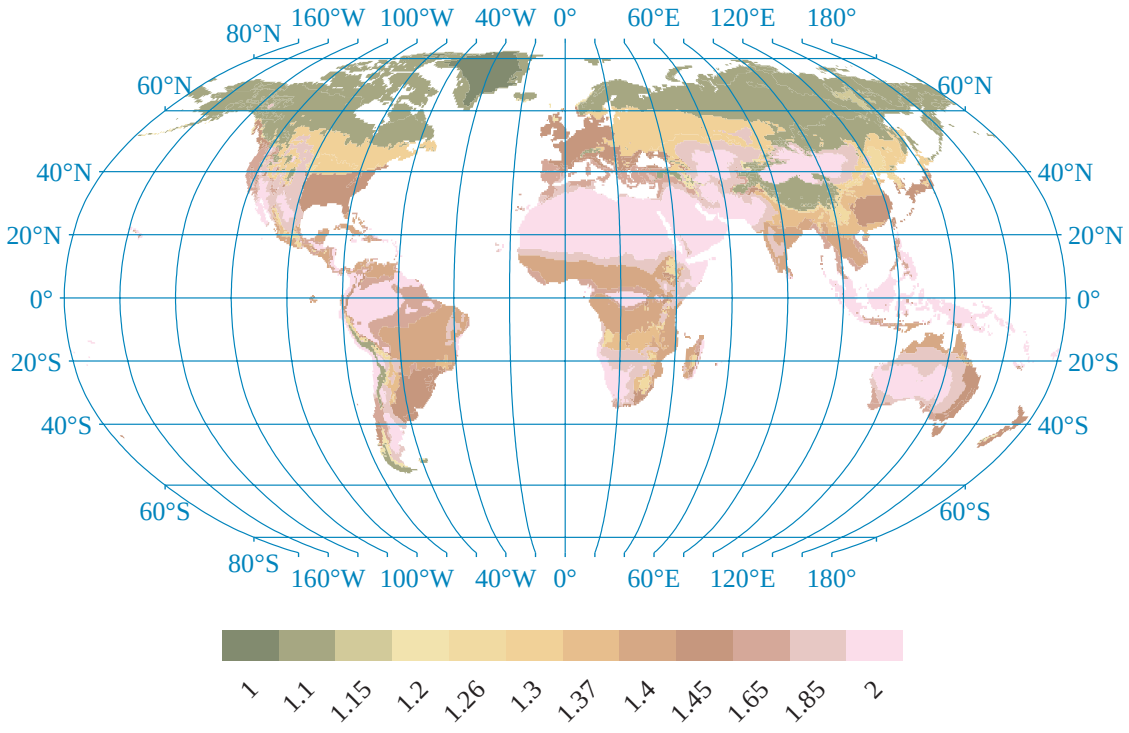

Figure 6-2. Spatial distribution of regionalised α-coefficients.

Table 6-2: α-values for different Köppen classes as derived from pan evaporation measurements.

Basic class	Sub-class	Pan station	Vegetation *	α
A	Af	x	Tropical evergreen rain forest	2.0
Tropical rain climates	Am	x		1.65
	Aw/As	x	Savanna	1.4
B	BW	x	Desert	2.0
Arid climates	BS	x	Bush to grassland	1.85
C	Cfa	x	Deciduous broad-leafed forest, areas with mild winters evergreen broad-leafed forest	1.45
Temperate rain climates	Cfb	x		1.45
	Cfc		Needle tree forest	1.45
				1.2
	Csa	x	Cs: Evergreen broad-leafed forest	1.65
	Csb	x		1.65
	Csc			1.65
				1.26
	Cwa	x	Cw: Only in mountain heights above Aw, evergreen forest vegetation	1.37
	Cwb			1.26
	Cwc			1.26
D	Dfa	x	Deciduous broad leafed forest	1.3
Boreal forest and snow climates	Dfb	x		1.3
	Dfc		Needle tree forest	1.1
	Dfd			1.1
	Dsa			1.2
	Dsb			1.1
	Dsc			1.1
	Dwa		Deciduous broad leafed forest	1.26
	Dwb	x		
	Dwc	x	Needle tree forest	1.3
	Dwd			1.1
				1.15
E	EF		Polar desert	1.0
Cold snow/polar	ET		Tundra, dwarf tree species and mosses	1.1

* as given in Lamb (1972)

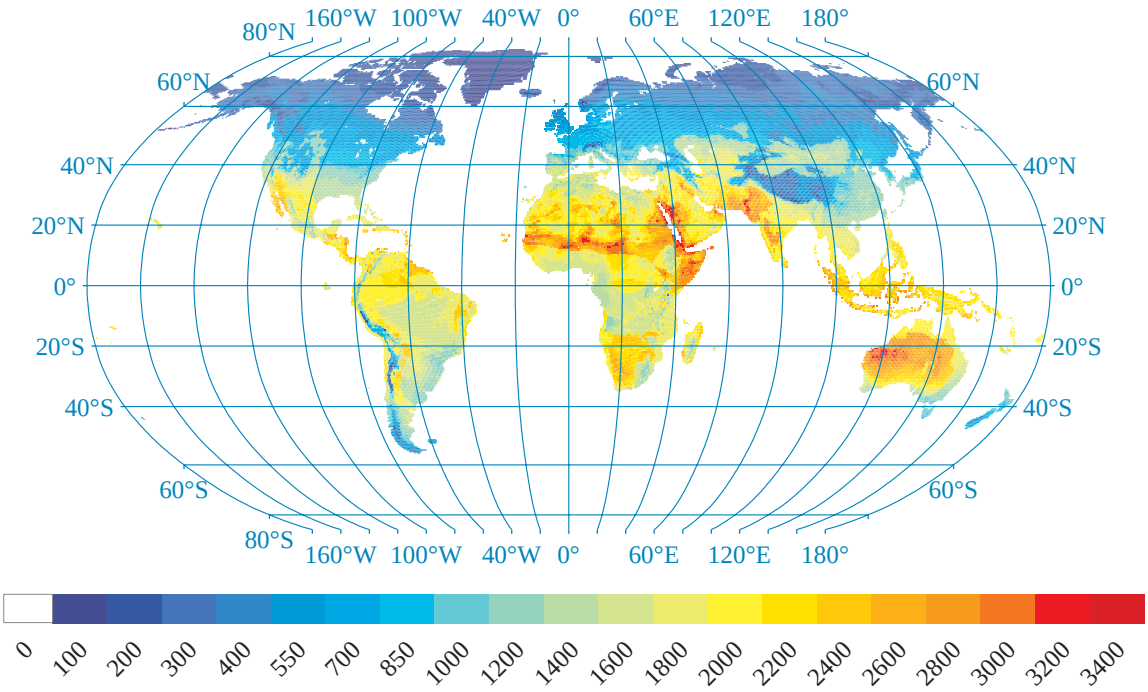

Figure 6-3. Average annual potential evapotranspiration (1990-1995) of land surfaces according to Priestley Taylor with regionalised α-coefficient.

In Figure 6-3 the resulting annual potential evapotranspiration for land surfaces is presented, averaged over the period 1990-1995. A time series comparison of simulated potential evapotranspiration with Australian daily pan evaporation measurements shows a good agreement, expressed in R^2 and bias. R^2 is calculated following equation (6-2), with Q = potential evapotranspiration. The bias is calculated according to equation (6-3) with *vol* = evaporation in mm. The distribution of efficiency indicators for the pan measuring stations is shown in Figure 6-4 in form of a box-whisker plot, ordered by climate class.

For the bias, values at an average of 0.16 to 0.26 are found, with higher values for the classes *Aw*, *BW* and *Cwa*. Overall, the measured pan values are higher than modelled potential evapotranspiration values, which can be attributed to the fact that a rather small reduction factor for pan values (0.8) is used, in comparison to values found in other studies, ranging from 0.6 to 0.9 (Linacre 1994, Roderick and Farquhar 2004). This reduction factor could have been further adjusted to the different climate zones, but it is believed that the background data is not strong enough to allow for such a procedure.

The averages of R^2 values for all climate classes are above the value of 0.8 except for the classes *Aw* and *Cwa*. The *Cwa*- climate is located in Australia in a very small area at the north-east coast, and is represented by four pan measuring stations, only. The sample size is too small to support any conclusions for this climate zone.

The rather low mean R²-value of 0.62 in the *Aw/As*- class with a spread of R² from 0.2 to 1, as well as the wider spread in the *BW*- class indicate that there could be a general problem with pan evaporation measurements in these climate classes. This is also supported by the fact that especially in the *BW*- class, a wide spread of α-candidates is found. As a consequence, these two classes could require a subdivision. This is further supported by the fact that measured pan evaporation values from North America are significantly higher than those measured in Australia for the same climate class. But since this deviation could also be attributed to differences in observing systems, a division into sub-classes seems not appropriate for the scope of this study, due to limited data availability.

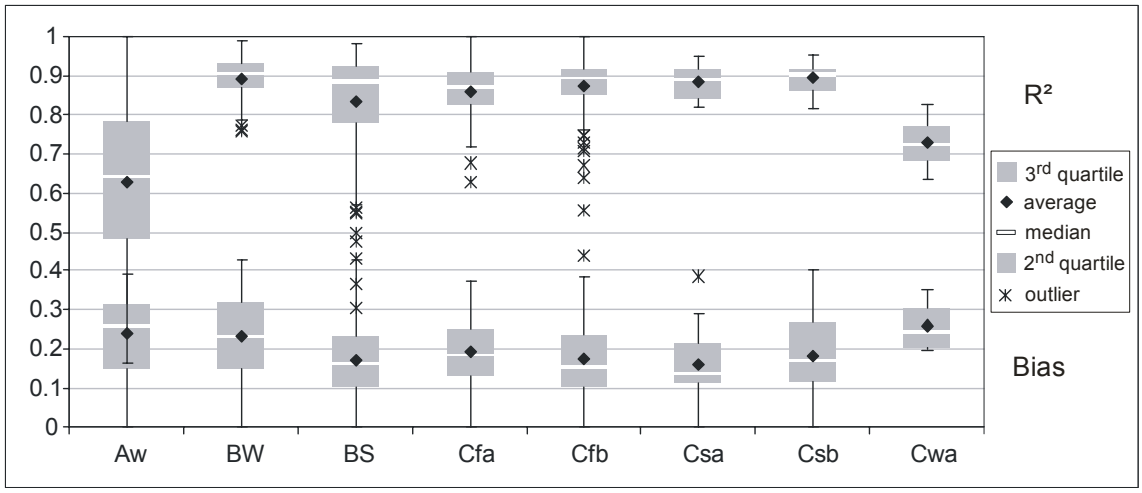

Figure 6-4. Distribution of R² and bias of potential evapotranspiration simulation in comparison to pan evaporation measurements from Australia, sorted by Köppen zones.

6.3.2 Discharge simulation efficiency

With the regionalized α-values improved discharge simulations were achieved when compared to previous simulations, as shown in Table 3. The best improvement is achieved in snow and polar climates with increased efficiencies for most indicators and all basins. The *D* and *B*- climates show slight increases in all efficiency indicators. Basins in the *A*- climate show a slight increase in average NSE and bias, while the average R² remains constant. In the *C*- climate the efficiency of discharge simulation increases in some basins, but decreases in other basins, leading to an overall slight decrease in efficiency.

Table 6-3: Efficiencies for discharge simulations in the five main Köppen climates as simulated with the WaterGAP model using previous α-values (alpha_ah), differentiating arid and humid areas only, and new, regionalized α-values (alpha_reg).

Köppen climate		R^2 [-]		bias [-]		NSE [-]	
		alpha_ah	alpha_reg	alpha_ah	alpha_reg	alpha_ah	alpha_reg
A	average	0.60	0.60	0.06	0.05	0.32	0.33
	median	0.63	0.63	0.01	0.00	0.50	0.50
B	average	0.48	0.48	0.12	0.09	0.17	0.20
	median	0.49	0.49	0.03	0.02	0.39	0.39
C	average	0.60	0.59	0.02	0.01	0.46	0.45
	median	0.61	0.59	0.00	0.00	0.52	0.50
D	average	0.57	0.59	-0.07	-0.05	0.45	0.48
	median	0.61	0.63	-0.03	-0.03	0.53	0.56
E	average	0.52	0.62	-0.22	-0.11	0.38	0.50
	median	0.53	0.63	-0.13	-0.05	0.41	0.52

The validation of components of the hydrological cycle, however, is a general problem in global water balance modelling due to the fact that the model is fed with erroneous climate input (Legates and Willmott 1990), complicating the evaluation of hydrological simulations. Further the limitations of efficiency indicators have to be acknowledged. The NSE, for example, is more sensitive to peak values, while the R^2 is known to be insensitive to proportional differences between model simulations and observations (Harmel and Smith 2007). Therefore, a set of indicators should be used for model evaluation. The efficiency of the WaterGAP model is also influenced by its specific set-up: natural water availability is calculated from vertical and lateral water balances, while river discharge is then calculated considering anthropogenic water abstractions. Water uses are available on a country or basin level and are then allocated to the respective grid-cell. Although accurate as a spatial average, this methodology adds further uncertainty when comparisons with point measurements are carried out. The fact that the overall efficiencies in the A and C climate do not improve significantly indicates that the simulation efficiency is governed by other processes of the hydrological cycle, which additionally would have to be examined if model efficiency was to be further increased.

6.4 Conclusions

The present regionalization of the Priestley Taylor coefficient for the calculation of potential evapotranspiration was designed to consider the deviation from equilibrium conditions in the different climate zones. It provides a more realistic estimation of potential evapotranspiration, based on pan evaporation measurements, supplemented by knowledge gained form existing local studies. It is intended for use in large-scale studies rather than in point studies where the appropriate α-value should be determined for site-specific conditions.

When previously applied in global studies, the Priestley Taylor equation was used with a constant α-value, or a combination of two different values for humid and arid conditions, respectively. It is, however, more appropriate to allow for a stepwise increase between cold and hot, and wet and dry zones.

The division into climate zones, and hence α-zones, hereby followed the updated Köppen climate classification with a reduced number of classes, which was also useful for the transferability of pan measurements. The new α-values lead to improved potential evapotranspiration and river discharge simulations when carried out with a global model, as compared to those obtained with previous α-values, thus increasing model efficiency.

Especially in the dry climates, however, a wide spread in measured pan values and consequently a wide spread in possible α-values was found. This lead to a lower modelling efficiency than in the other classes for time series simulation of both potential evapotranspiration and river discharge. It is concluded that a) general problems in the observation of pan values exist in this zone and b) a subdivision of the appropriate classes is suggested in order to reduce the spread. With the available data, this could not be carried out as part of this study.

Nonetheless it is believed that the regionalized α-coefficients provide the basis for a more realistic assessment of potential evapotranspiration on the global scale, which could also be of interest to other large-scale hydrologic or climate modellers.

CHAPTER 7

A SYSTEMATIC APPROACH TO ASSESSING THE SENSITIVITY OF WATER AVAILABILITY TO CLIMATE CHANGE IN EUROPE

Summary

The new trend towards ensemble climate modelling systems and multi-model simulations for generating future climate projections calls for a systematic approach in analyzing possible climate change impacts. In this study the response surface method is introduced to systematically, consistently and objectively examine impacts of climate change on water availability. As part of the study 18 European river basins are ranked according to their sensitivity to climate change. The use of climate change projection from six RCMs for the year 2100 under the IPCC A1B scenario in combination with societal vulnerability thresholds enables further a vulnerability ranking of the basins. Overall, a strong climate sensitivity of the Nordic basins is found based on the snow-dominated flow regime. When looking at the vulnerability, however, southern European basins together with some central European basins are highest in the ranking due to the violation of low flow and water stress thresholds.

7.1 Introduction

Examining climate change and its effects now has a history of almost three decades. A wide variety of scenarios (e.g. Arnell and Liu 2001, Carpenter et al. 2005, UNEP 2007b) has since been developed to qualify and quantify required model drivers and set the context for carrying out climate change scenario analysis. Profound advances have been made in both climate models and impact models, generating complex projections of potential environmental and socio-economic consequences and setting the scene in the planning of adaptation and mitigation strategies.

Impact analysis has hereby mostly followed the conventional way of a cause-effect analysis (Bruckner et al. 1999). Based on a consistent set of socio-economic drivers, emission paths for various greenhouse gases are developed, which are then used to simulate future climates that constitute the basis for impact analyses (e.g. IPCC 2000). Although including largely divergent drivers, this type of scenario analysis only provides insight into the consequences of concrete action along rigid pathways.

The urge to address erroneous climate model sensitivities and imperfections due to the intrinsic chaotic nature of the climate system and inherent uncertainties in the climate modelling process has recently resulted in developing ensemble climate model systems consisting of a number of models that lead to a wide range of projected changes (Collins 2007). Impact analysis for projected ranges can become cumbersome, especially when carried out with a complex impact model in the cause-effect analysis mode, as impact model simulations have to be carried out for each of the climate change projections.

For the applicability of impact analysis results, for example providing scientific support for policy makers, the absolute value of an impact might not be of much interest, as for the planning of adaptation and mitigation strategies it is rather the sensitivity of a system towards change that is relevant, and how close the system moves towards thresholds of unacceptable limits.

For the above stated reasons, this study introduces a systematic sensitivity analysis of water availability to climate change applied to 18 river basins in Europe, in which response surfaces are constructed for each basin. These show the response of water availability to climate change for temperature in the range of -1°C to +6°C of current conditions, in combination with changes in precipitation in the range of -40% to +100% of current conditions. Different aspects of the response are then analyzed, covering the nature of the system itself, as well as human impacts on the system. The study concludes with a vulnerability ranking, for the first time objectively comparing basins throughout Europe under consideration of a future climate cycle as projected by six different RCMs for the year 2100 under the A1B scenario.

7.2 Materials and Methods

7.2.1 Modelling water availability

The sensitivity of the water availability to climate change is assessed by means of one of the current state-of-the-art integrated global hydrological models, WaterGAP (Alcamo et al. 2003a, Döll et al. 2003), which has been applied in a wide range of scenario studies including IPCC (Arnell and Liu 2001), Global Environment Outlook Assessments 3 and 4 (UNEP 2002, 2007b), and the Millennium Ecosystem Assessment

(Alcamo et al. 2005, Carpenter et al. 2005).

Simulations of river discharge are forced by a thirty-year period of monthly climate time series from the CRU gridded dataset of monthly precipitation, air temperature, cloud cover and wet day frequency (CRU TS 2.1, Mitchell and Jones 2005), which are model–internally disaggregated to daily values. In each grid cell (0.5°×0.5° geographical latitude and longitude) the daily vertical water balance is calculated, quantifying each of its components evapotranspiration, interception, groundwater storage and surface and subsurface runoff. Hereby, water availability is defined as the total renewable water resource. River discharge is defined as the water availability reduced by anthropogenic consumptive uses.

The consumptive uses are computed with the water use modules for the domestic, industrial and agricultural sectors. The domestic sector includes municipal and household uses; the industrial sector is subdivided into electricity production and manufacturing facilities; the agricultural sector is subdivided into irrigation and livestock uses (Alcamo et al. 2005). The water uses are abstracted from the water availability in the respective grid cell. The remaining forms river discharge, which is routed through the respective river basin according to a global drainage direction map (Döll and Lehner 2002). WaterGAP simulations of river discharge are tested for the reference period to measured discharges from the Global Runoff Data Centre (GRDC 2004) at currently 1235 stations world-wide.

7.2.2 Climate impact response surfaces

The response surface method is extensively covered in the literature (Box and Wilson 1951, Box and Draper 1959, Hill and Hunter 1966, Cornell 1987, Myers et al. 1989, Myers 1999) as a standard approach in system sciences with a focus on system behaviour and large-scale optimization of operating conditions. Applications to the field of climate change impact analysis have mainly been carried out under the ICLIPS (Integrated Assessment of Climate Protection Strategies) framework (van Minnen et al. 2000, Füssel and van Minnen 2001, Füssel et al. 2003) with only few studies covering the potential impact of climate change on water resources (Fowler 1999, for New Zealand).

Response surfaces (RS) express the response of a system to the variation of two or more driving variables. The RS is hereby derived by individual system simulations for each combined incremental change in the driving variables, forming discrete data points in the 3-d response space, which are then interpolated to a continuous surface. The resulting surface can be graphically presented in three-dimensional diagrams or as two-dimensional contour plots, with isolines connecting all those points on the surface that take the same value.

In this study, RS are used to assess the sensitivity of water availability to climate change. With respect to the impact model, temperature and precipitation are selected as representative climate change components. These are modified at predefined increments of 1°C in the range [-1°C, +6°C] for temperature (T), and at increments of 10% in the range [-40%, + 100%] for precipitation (P), resulting in a 8 x 15 matrix. The chosen ranges reflect the envelope of changes as projected for Europe by the currently available regional climate models (see below) up to the year 2100 and beyond.

Based on the model-internal disaggregation of monthly precipitation input to daily values, two approaches of adding delta changes are differentiated. On the one hand, increased precipitation values can be achieved by increasing the intensity of precipitation while keeping the number of raindays per month constant. On the other hand, the number of rain days per month can be increased, while maintaining rainfall intensities. Obviously the second approach is confined by the number of days per months. Once all days in a month are assigned rain days, the intensity of precipitation will increase. Both approaches will be analyzed.

Modelling climate change is still subject to significant uncertainty. Therefore, the average of the results of six different Regional Climate Models (RCM) for 2071-2100 (Table 7-1) is calculated to distribute average annual changes the months of the year. Hereby, the average annual change is broken down to varying monthly changes by calculating normalized monthly scaling factors from the difference of scenario climate data to the reference period data set. Thus, the projected future climate cycle is taken into account in each grid cell. For each of the six RCMs, a period of 30 years is used both for the reference period (1961-1990) and the scenario period (2071-2100) to construct mean monthly scaling factors.

Table 7-1. Regional Climate Models as applied in this study.

RCM	Driving GCM	Scenario	reference
C4I-RCA3	HadCM3-e1	A1B	http://ensembles-eu.metoffice.com/index.html
DMI-HIRHAM5	ARPEGE	A1B	http://ensembles-eu.metoffice.com/index.html
ETHZ-CLM	HadCM3Q0	A1B	Böhm (2006)
KNMI-RACMO2	ECHAM5	A1B	http://ensembles-eu.metoffice.com/index.html
MPI-M-REMO	ECHAM5	A1B	Jacob (2001), Jacob et al. (2001)
SMHI-RCA	BCM	A1B	Kjellström and Rummukainen (2005)

7.2.3 Spatial aggregation and selected river basins

The impact model works with a spatial grid cell resolution of 0.5 degrees and is driven by climate data on that same resolution. Resulting water availability is examined at river basin level.

The European climate varies from cold temperate, potentially subarctic in the north to temperate with mild wet winters and hot, dry summers in the south. Water resources and precipitation are unevenly distributed: precipitation is highest in the western part and in mountain areas. Annual average run-off ranges from 3000mm in western Norway to 100-400mm over much of central Europe and less than 25mm in southern Spain. 18 climate-representative river basins across Europe have been selected (Figure 7-1). Figure 7-2 shows current long-term annual precipitation and temperature averages in the selected river basins according to the 1961-1990 CRU TS 2.1 climate dataset (Mitchell and Jones 2005).

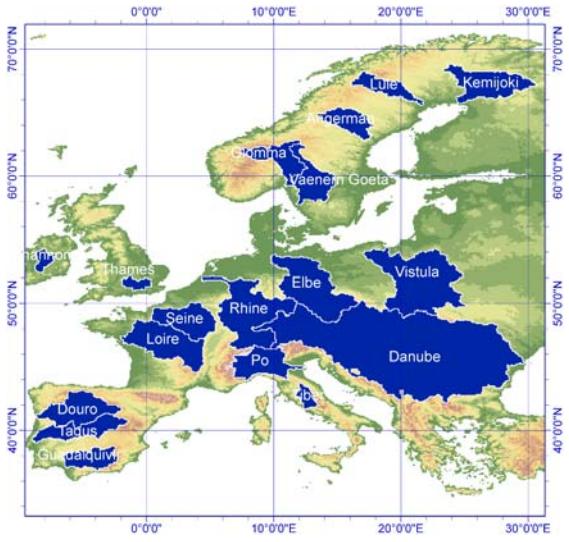

Figure 7-1. Selected European river basins.

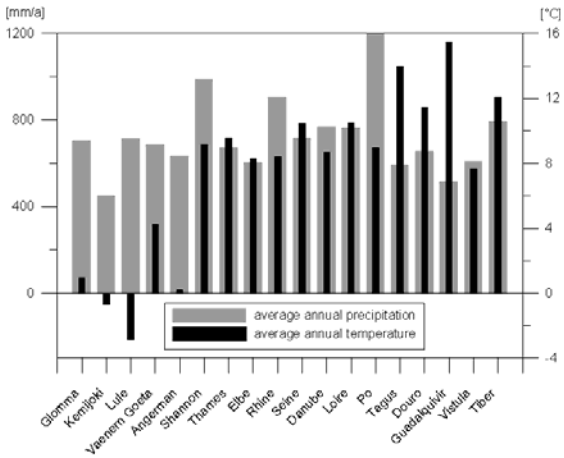

Figure 7-2. Long-term average annual precipitation and temperature in the selected river basins (1961-1990).

7.2.4 Sensitivity assessment

Here, the nature of the system itself is examined, i.e. the shape of the response surfaces, and their position in the 3-d space as well as in relation to each other. Since the same increments are used in all catchments to generate response surfaces for normalized water availability, we can directly compare the results. The first indicator analyzed is the volume below the surface, as shown in Figure 7-3. It is assumed that the greater the volume, the more sensitive the system responds to climate change.

As second indicator we examine the stability of the flow regime under climate change. The natural flow regime has been identified as critical to the ecological integrity of a system (Richter et al. 1996, Poff et al. 1997, Gibson et al. 2005). A delay in the occurrence of the peak month can, for example, severely affect freshwater biodiversity (Tockner and Stanford 2002).

The flow regime is analyzed by Pardé-coefficients (Pardé 1933, Krasovskaia et al. 1994, Bower et al. 2004), which are defined as the monthly stream flow normalized by the longterm mean flow. For each combination of climate change parameters, we calculate thirty-year mean Pardé-coefficients to neglect short-term fluctuations. The stability of the flow regime under climate change is expressed as area between the Pardé-coefficient curves for the reference period in comparison to a perturbed T and P combination, normalized by the area under the reference curve and summarized for all discrete climate change combinations (see Figure 7-4).

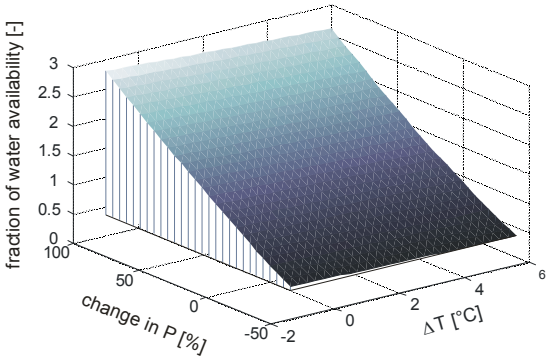

Figure 7-3. Volume below the response surface as a measure of a basin's response to climate change.

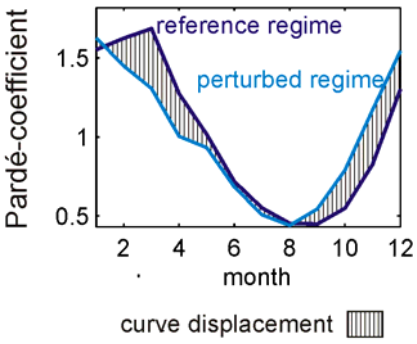

Figure 7-4. Calculation of the displacement of the flow regime curve caused by temperature and precipitation perturbations.

7.2.5 Sensitivity classification

In order to rank the basins according to their sensitivity, the volume is normalized by the mean volume of all basins, revealing which basins react stronger than average (value >1.0) and basins with a response weaker than average (value < 1.0). Similarly, the displacement value is averaged by the mean displacement to facilitate intercomparison of basins. Both indicators are then equally weighted and the basins are ranked according to the average of both indicators.

7.2.6 Vulnerability assessment

Here, we use the response surfaces to investigate whether societal thresholds will be exceeded under various climate change scenarios. In this way, the vulnerability of human population in the river basins can be estimated, as opposed to the sensitivity of a basin itself, as estimated above.

We examine a high flow and a low flow indicator (Bruckner et al. 1999, Toth et al. 2000, Smakhtin 2001, Laaha and Blöschl 2008), as well as two indicators of water stress (Falkenmark and Widstrand 1992, Postel 1997, Henrichs et al. 2002, Alcamo et al. 2003b, Flörke and Alcamo 2007), as described below. We quantify thresholds for these indicators in form of normalized values. Thresholds are assumed to mark the critical state in a system, beyond which the proper functioning and integrity of the system might not be guaranteed.

The response of a system to the exceedance of a threshold can either be linear, or non-linear, i.e. the system is pushed in gradual steps past a defined critical limit, or the incremental increase of the trigger causes an abrupt, disproportionate jump in response (Arnell 2000, Groffman et al. 2006). The combination of the threshold analysis with response surfaces supports impact analyses in two ways: In a linear response system, pre-defined thresholds reveal unacceptable limits of change. In a nonlinear system, the response surface reveals a threshold, hence unacceptable limit of change, by a sudden bend in the surface.

As high and low flow indicators we use the Q80 and Q20 flows (Clausen and Biggs 2000, Olden and Poff 2003, Monk et al. 2007), which represent the flow that statistically is exceeded 80%, or 20% of the time, respectively, determined from flow duration curves.

With regards to water stress, we use the water availability index (w.a.i.), defined as the amount of annual renewable fresh water per capita accessible to anthropogenic uses. The following thresholds are commonly used: Below 1700m³ per capita and year, periodic high water stress could be experienced. Below 1000m³ per capita and year, chronically high water stress could be experienced, that could negatively influences economic development and human health. Below 500m³ per capita and year, absolute water scarcity is often experienced (Falkenmark and Widstrand 1992, The World Bank 1992, Gleick 1993, Postel 1997). We convert these values to thresholds of water availability by multiplication with data on population per basin provided by the Center for International Earth Science Information Network (CIESIN 2005).

As an alternative to the indicator “freshwater per capita” that overemphasizes densely populated areas, we further apply the withdrawal-to-availability ratio (w.t.a), i.e. the sum of water withdrawn in the domestic, industrial and agricultural sectors di-

vided by the total annual renewable water resource of a basin. Categories of water stress are low for a w.t.a. < 0.2, medium for a w.t.a. between 0.2-0.40 and severe for a w.t.a. > 0.4 (Alcamo et al. 2007). Again we convert theses values into thresholds of water availability by reversing this equation and solving for water availability at constant withdrawals. Withdrawals are used as calculated with the WaterGAP water use model for the year 2000.

7.2.7 Vulnerability classification

The vulnerability classification is carried out based on the absolute number of climate modelling projections under which the above described thresholds would be violated in 2100. See Table 7-2 for a key to the vulnerability classification with the high/low flow indicator.

The key to the vulnerability classification with the water stress indicators w.a.i and w.t.a is given in Table 7-3. Hereby, the current state of the basin is of relevance to the vulnerability classification. For example, a basin that is currently not stressed will be classified (+), if the low water stress threshold is violated according to 1-3 or 4-6 RCM simulations. If the medium water stress threshold is violated by 1-3 or 4-6 RCM simulations for that same basin, it will be classified (++). As another example we look at a basin which is currently classified as medium water stressed. If RCM simulations suggest that this medium water stress threshold is violated by only 1-3 simulations in the future, a relaxation of the water stress situation will take place and the basin will be classified (+). If it remains in its medium water stressed class (according to 4-6 RCM simulations) it will be classified (++) and if it moves up into the next (high) water stress class it will be rated (+++). See Table 7-3 for any other constellation of current and future water stress class.

For the vulnerability ranking we then only use that water stress indicator that results in the higher stress class. The water stress indicator is then equally weighted with the high/low flow indicator and based on the sum of plus-signs, we are able to rank the basins from highest to lowest vulnerability.

Table 7-2. Key to vulnerability classification with high/low flow indicator.

indicator	Threshold violated by number of scenarios (tvns)			
	0	1	2-3	4-6
High/low flow	0	+	++	+++

Table 7-3. Key to vulnerability classification with water stress indicators.

future / current	no tvns*	low 1-3	low 4-6	med 1-3	med 4-6	high 1-3	high 4-6
no	O	+	+	++	++	+++	+++
low	O	O	+	++	++	+++	+++
med	O	O	O	+	++	+++	+++
high	O	O	O	+	++	++	+++

* tvns= threshold violated by number of scenarios

7.3 Results

7.3.1 Sensitivity analysis

In the method section we introduced two alternative approaches to apply delta changes to precipitation, which were 1) increasing the rainfall intensity at constant number of rain days and 2) increasing the number of rain days and thus maintaining the rainfall intensity. The results of both alternatives will now be shown for a basin in a cool climate (Kemijoki) and one in a warm climate (Guadalquivir). In Figures 7-5 and 7-6, contour plots show the response of water availability to climate change based on both approaches for the Kemijoki and Guadalquivir basins.

For both approaches we find an over-proportional increase in water availability in comparison to the initial perturbation in precipitation at the Kemijoki basin, as well as for the Guadalquivir under approach 1. For approach 2, the same pattern becomes more pronounced the higher the change in precipitation, while for small delta changes, a delayed response in water availability is observed. This should not be mistaken as an incorrect representation of the water balance. Instead, the additional water is partitioned differently between the various moisture storages. Table 7-4 shows the water balance for both basins and both approaches of disaggregating delta changes for a parameter perturbation of Δ T = +6°C and Δ P = + 100%. It confirms that the mass balance with respect to volume of water is preserved.

This pattern can be explained by the fact that all basins are situated in a mostly humid climate and water storages are filled on average throughout the year. Adding rainfall on an already wet day tends to exceed soil water capacity, converting the additional water almost entirely into direct runoff. In the further analysis, we will therefore use the assumption that additional rain will be distributed to additional rain days, thus maintaining intensity at reference level until the maximum number of days per month is reached, as this approach apparently adds less bias to simulations of water availability.

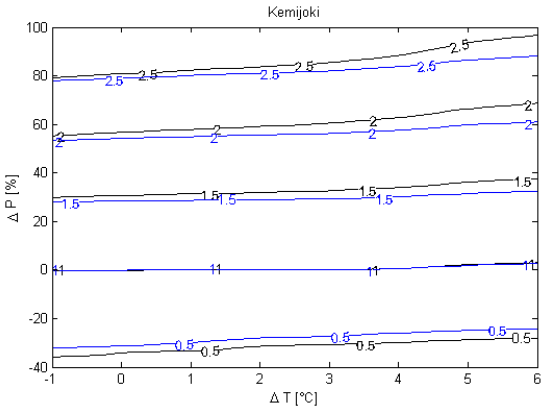

Figure 7-5. Contour plots of water availability for the Kemijoki basin, based on two approaches of applying precipitation delta changes, in blue increasing rainfall intensity at constant number of rain days, in black increasing the number of rain days while maintaining rainfall intensity.

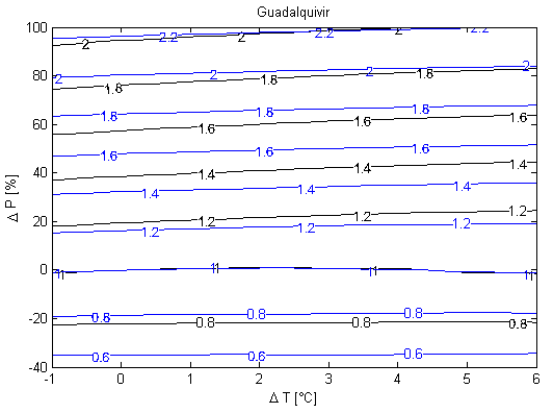

Figure 7-6. Contour plots of water availability for the Guadalquivir basin, based on two approaches of applying precipitation delta changes, in blue increasing rainfall intensity at constant number of rain days, in black increasing the number of rain days while maintaining rainfall intensity.

Table 7-4. Water balance components for parameter perturbations of Δ T = +6°C and Δ P = + 100% for the Kemijoki and Guadalquivir, with delta changes of precipitation added either by increasing the number of rain days ('*NRD*') or by increasing intensity at constant number of rain days ('*intensity*'). Precipitation, AET (actual evapotranspiration, including interception)and surface and groundwater runoff are given as 30-year sums, averaged over all grid cells of a basin. Change in storages is assumed to be close to zero for a period of 30 years and therefore not stated.

River basin	Delta change	Precipitation [km³]	AET [km³]	Surface + groundwater runoff [km³]	Water balance, deviation in [km³]
Kemijoki	NRD	32.9	4.7	28.4	**-0.20**
Kemijoki	intensity	32.9	2.9	30.1	**-0.18**
Guadalquivir	NRD	76.4	15.9	60.7	**-0.18**
Guadalquivir	intensity	76.0	9.7	65.9	**0.05**

Figure 7-7 shows response surfaces for the 18 analyzed European catchments, representing the sensitivity of annual water availability to changes in the key climate parameters temperature and precipitation. To enable a comparison between basins, water

availability is normalized by its reference value (1961-1990). Figure 7-7 indicates that the response of the selected basins is quite similar, differing mainly in magnitude; water availability increases linearly with precipitation and decreases linearly or exponentially with temperature. The reason for the similarity is that the annual response curves average out opposing tendencies observed in monthly (and presumably smaller time scale) flows of the river basins. Below we show the much stronger responses of the monthly time scale.

Two metrics to compare response curves are used, i.e. the "volume below surface" (abbreviated "volume") which indicates the response of annual water availability, and the "displacement of Pardée curves" (abbreviated "displacement") which reflects the response of the monthly flow regime. (See Figures 7-3 and 7-4 for an explanation of these metrics).

Figures 7-8 and 7-9 show that the normalized volume ranges from 0.7 (Guadalquivir) to 1.25 (Elbe), while the normalized displacement ranges from 0.3 (Guadalquivir) to 2.0 (Lule). Apparently there is a much wider range of responses of the monthly flow regimes than of annual water availability. These figures also show that the monthly flow regimes of some basins might have a strong response to climate change while their annual water availability has a weak response (e.g. Lule), or the other way around (e.g. Elbe). If we give equal weight to the sensitivity of annual water availability and monthly flow regime, we obtain the ranking of basins according to their sensitivity shown in Table 7-5. The first four are northern basins heavily influenced by snowpack and snowmelt. The last two are the Douro and Guadalquivir, located in semi-humid areas of the Iberian Peninsula. Falling in the middle of the ranking are the Elbe and Rhine.

To understand their sensitivities it is helpful to examine the response surfaces of monthly flows shown for three selected basins: the Kemijoki for northern Europe, the Elbe for central Europe, and the Douro for southern Europe. The Kemijoki basin (Figure 7-10), strongly affected by snowmelt, shows significantly different forms of response for different months. Already at first glance it is apparent that monthly responses are much more pronounced than the curves for annual water availability. In June, water availability declines exponentially as temperatures become warmer because the snowmelt, which currently feeds June discharge is then shifted to earlier in the year. It is apparent that much of the snowmelt and resulting high river flows are shifted to April, which shows a very sharp peak in water availability as precipitation and temperature increase. A similar but milder effect is observed in the curve for March.

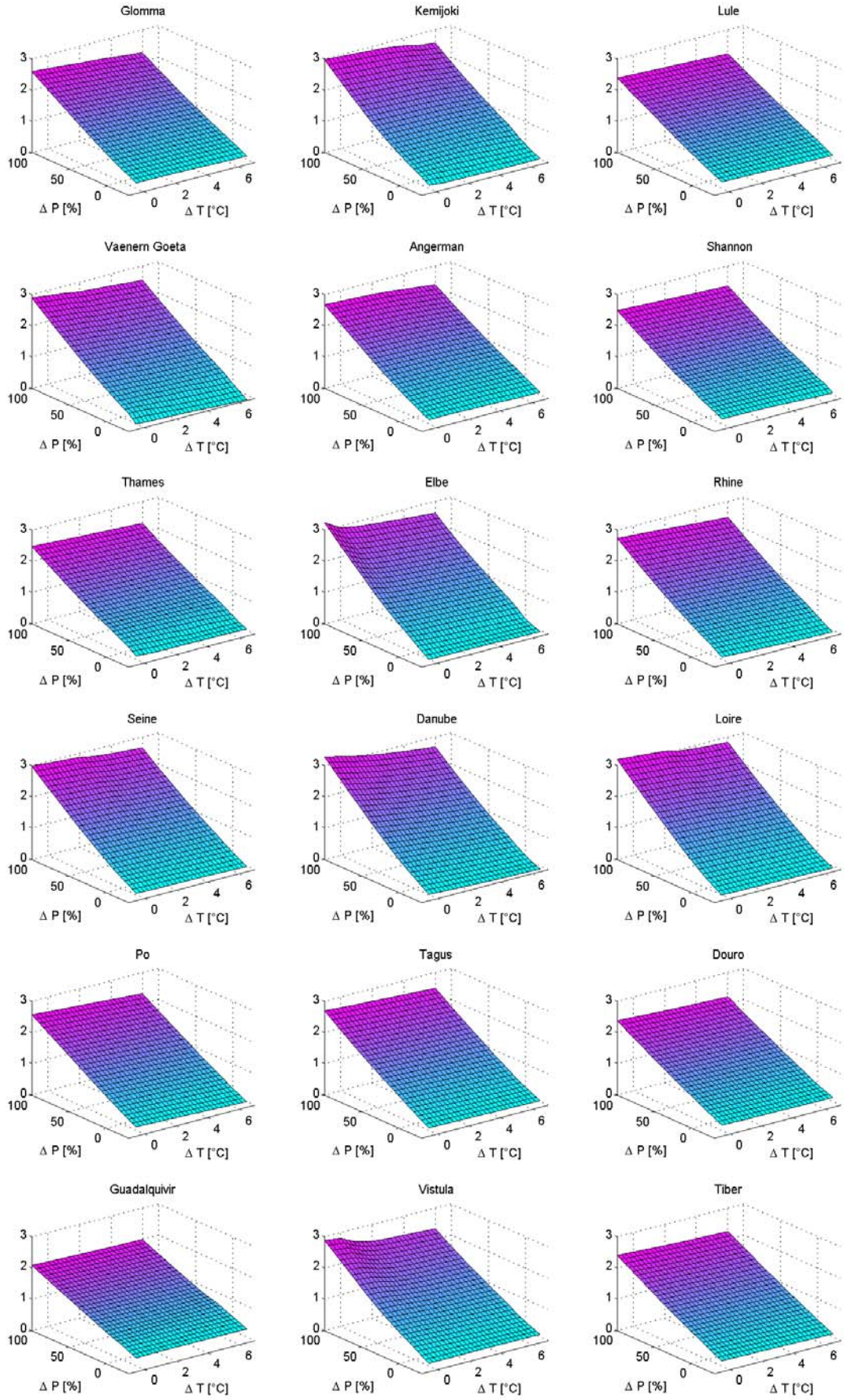

Figure 7-7. Response surfaces of the fraction of annual water availability resulting from temperature and precipitation perturbations for 18 European river basins.

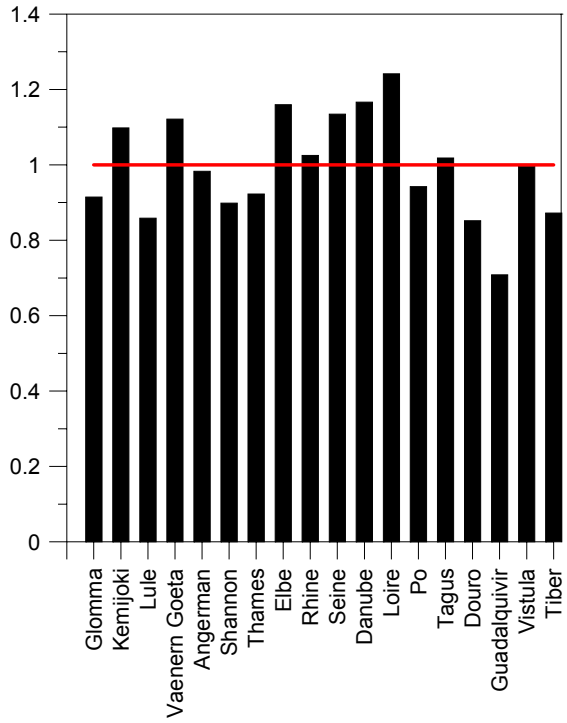

Figure 7-8. Volume below the response surface for each of the 18 analyzed catchments.

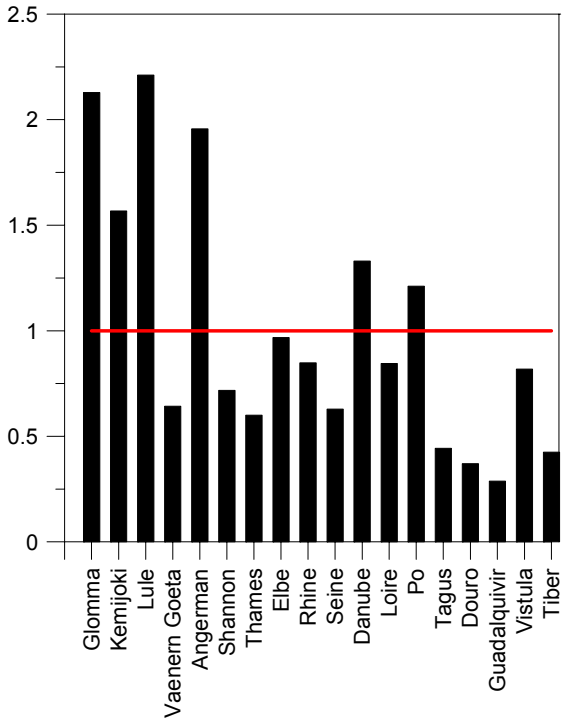

Figure 7-9. Displacement of the flow regime curve in percentage of the area below the curve under reference conditions.

Table 7-5. Sensitivity ranking of 18 European basins based on two indicators of system behaviour, i.e. "volume" and "displacement"

River basin	Volume	Displacement	**sum**
Lule	0.86	2.21	**3.07**
Glomma	0.91	2.13	**3.04**
Angerman	0.98	1.96	**2.94**
Kemijoki	1.10	1.57	**2.67**
Danube	1.17	1.33	**2.50**
Po	0.94	1.21	**2.15**
Elbe	1.16	0.97	**2.13**
Loire	1.24	0.84	**2.09**
Rhine	1.03	0.85	**1.87**
Vistula	1.00	0.82	**1.81**
Vaenern Goeta	1.12	0.64	**1.76**
Seine	1.13	0.63	**1.76**
Shannon	0.90	0.72	**1.62**
Thames	0.92	0.60	**1.52**
Tagus	1.02	0.44	**1.46**
Tiber	0.87	0.43	**1.30**
Douro	0.85	0.37	**1.22**
Guadalquivir	0.71	0.29	**1.00**

The Elbe (Figure 7-11) is also influenced by snowmelt (especially because of its high montane headwaters), but not as strongly as northern European basins because of the moderate climate along most of its length. Accordingly, the snowmelt effect observed in Kemijoki is also present, but not as strongly, and with a seasonal shift. While snowmelt declines in June in Kemijoki, it diminishes much earlier in the Elbe basin. This is apparent from the April response curve of the Elbe basin which bears a distinct resemblance to the June curve of Kemijoki. As the Kemijoki curve for April, the Elbe curves for December, January, and February show sharply increasing water availability with increasing precipitation and temperature, reflecting a shift in snow accumulation and snowmelt to earlier in the Northern Hemisphere winter. However, water availability in the Elbe does not peak as sharply as in Kemijoki because when temperature increases above roughly 2 degrees in the Elbe basin, increased evapotranspiration compensates for the increase in precipitation and slows the rise of water availability.

The Douro (Figure 7-12) shows a smaller response than the snow-influenced basins of northern and central Europe chiefly because warmer, sunnier conditions here promote the evaporation of a larger fraction of additional precipitation and various water storages are filled to a lower degree than in humid areas, and access water can be buffered before it is converted to runoff.

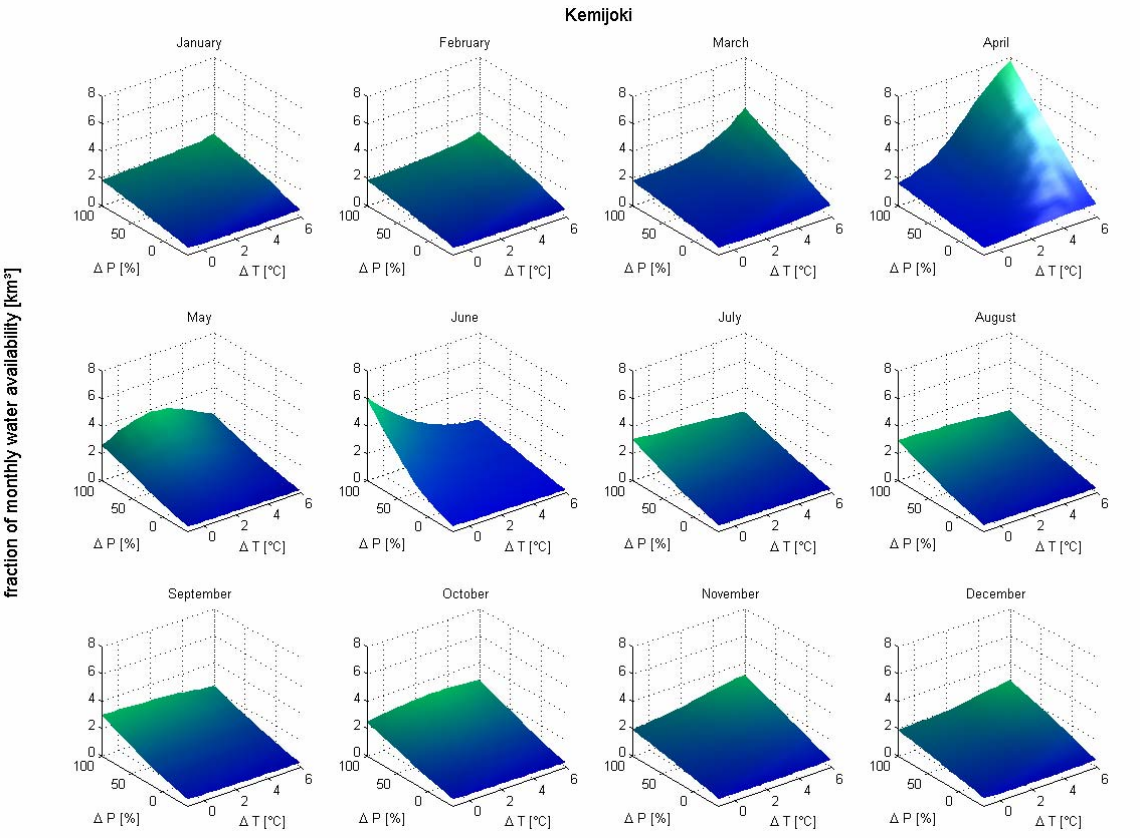

Figure 7-10. Response surfaces of normalized monthly water availability for the Kemijoki basin.

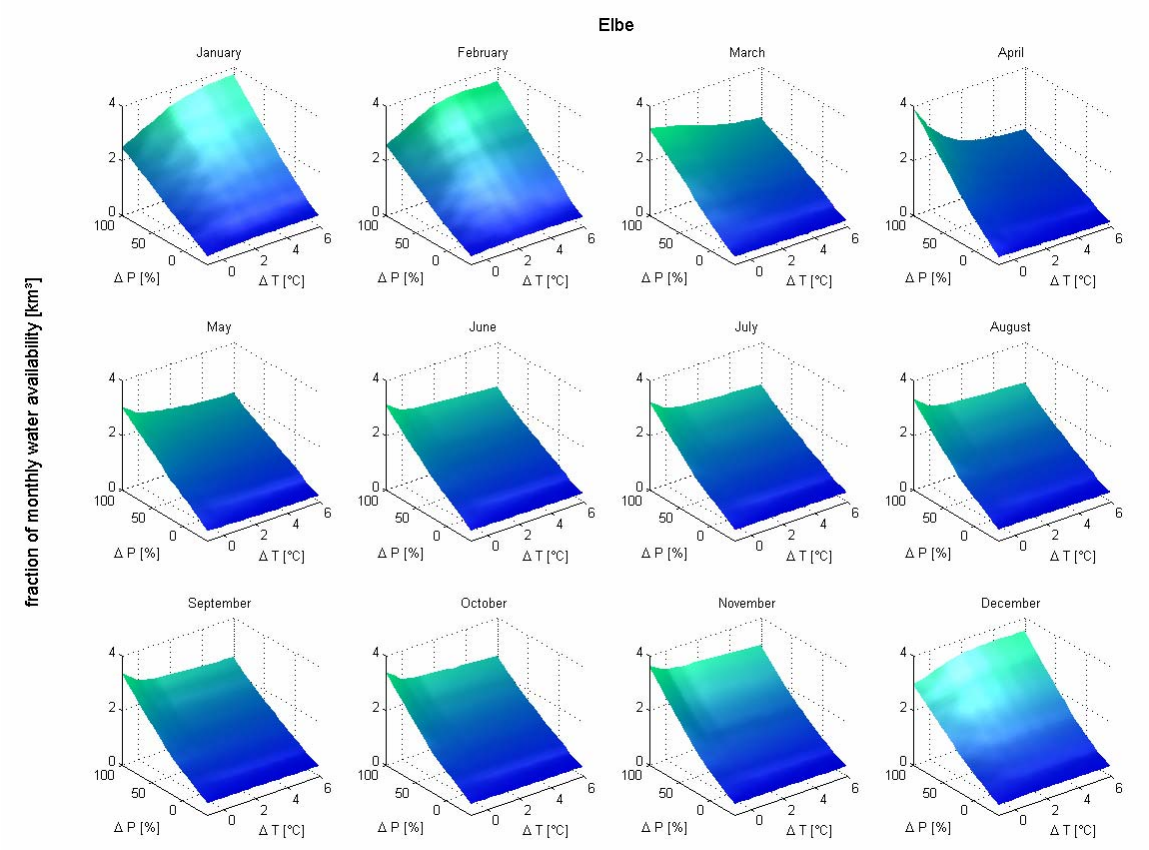

Figure 7-11. Response surfaces of normalized monthly water availability for the Elbe basin.

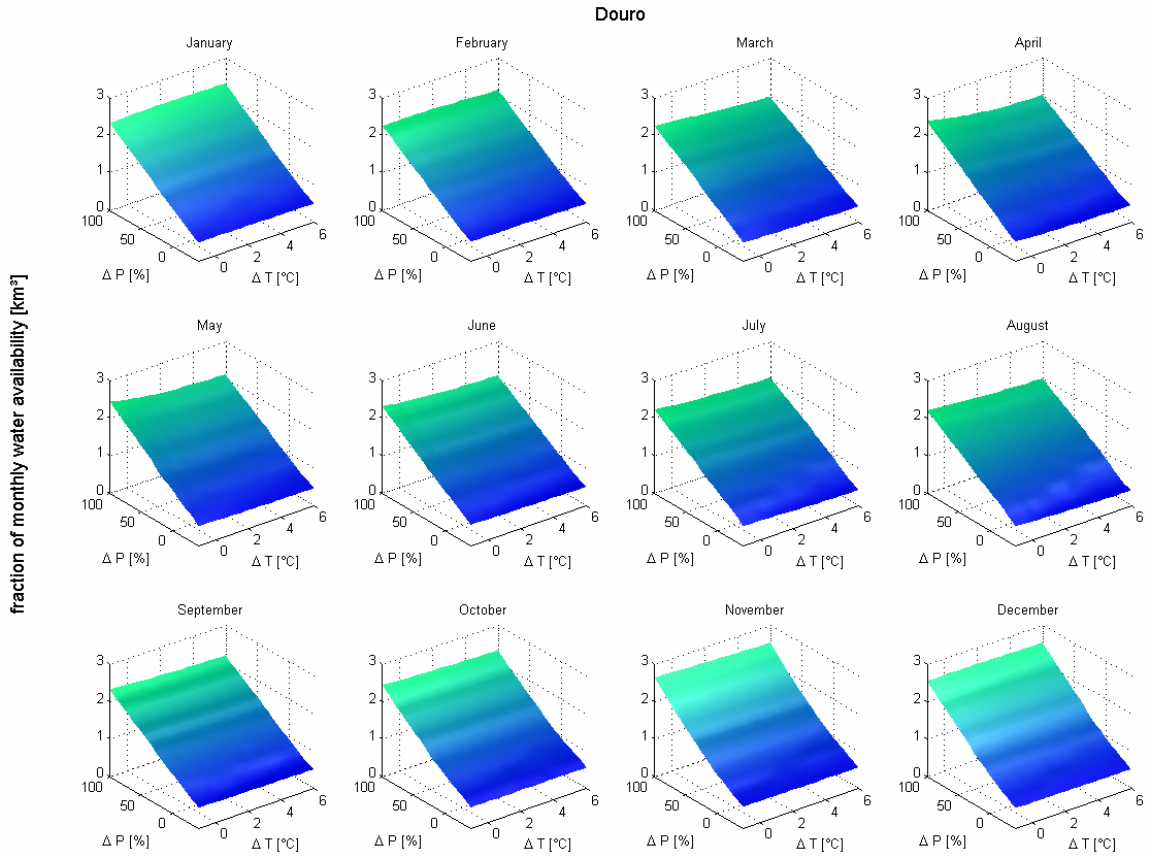

Figure 7-12. Response surfaces of normalized monthly water availability for the Douro basin.

7.3.2 Vulnerability results

Although the surface response curves are visually interesting, they are difficult to interpret numerically. Therefore we represent the data of Figure 7-7 in two-dimensional contour plots (Figure 7-13). Further, we superimpose the positioning of 6 climate scenarios as explained in section 7.2.2 for the period 2070-2099 onto the temperature and precipitation space. This gives us a general method for looking at the implications of any particular climate scenario at any juncture in the future, as long as it fits on the given temperature and precipitation domain. With this diagram we combine an estimate of the future pressure on water resources (the climate changes represented by the climate scenarios) with the sensitivities of the river basins (as represented by the response surface diagrams) in order to assess the vulnerability of the river basins to climate change. Furthermore, we also indicate various thresholds for extreme flows and water stress relevant to the populations living in these basins (Figure 7-13). These thresholds were explained in Section 7.2.6.

As described earlier we define different vulnerability classes for the river basins according to how many of the climate scenarios violate different thresholds. (See Tables 7-3 and 7-4 for the definition of these vulnerability classes). The resulting vulnerability ranking (Table 7-6) is quite different from the sensitivity ranking (Table 7-5). The relatively insensitive southern river basins such as Douro and Guadalquivir are much higher in the vulnerability ranking because expected changes in precipitation and temperature according to the climate scenarios lead to higher water stresses. Other river basins such as the Vistula, which have a medium sensitivity ranking, are at the top of the vulnerability list because of the combination of moderate sensitivity and unfavourable climate changes according to the scenarios. On the other hand, the Shannon, which has a moderate sensitivity ranking, has the lowest vulnerability because the given climate scenarios do not lead to large unfavourable changes in water availability.

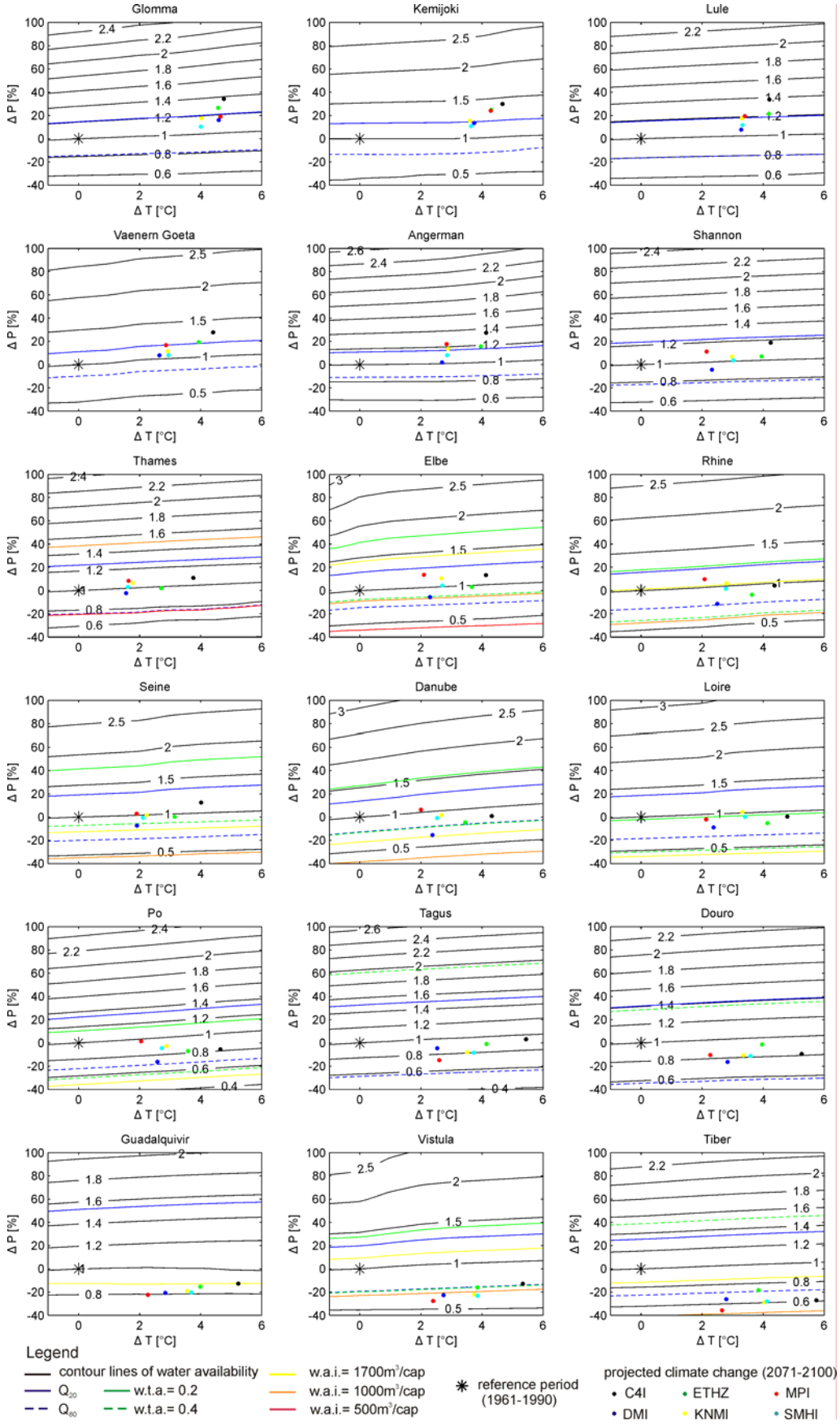

Figure 7-13. Contour plots and societal thresholds of water availability for 18 European catchments. Scenario-states of basins are indicated by dots of projected climate change for 2100 under the IPCC A1B scenario.

Table 7-6. Vulnerability ranking of 18 European basins based on equal weighting of the two indicators high/low flow and water stress (of the two water stress indicators, only the indicator with the 'higher' score is counted).

River basin	**High/low flow**	Water stress w.a.i.	**Water stress w.t.a.**	**sum**
Vistula	+++	++	+++	**6**
Tiber	+++	+	+++	**6**
Danube	+	o	+++	**4**
Kemijoki	+++	o	**o**	**3**
Thames	**o**	++	+++	**3**
Seine	**o**	o	+++	**3**
Tagus	**o**	o	+++	**3**
Douro	**o**	o	+++	**3**
Guadalquivir	**o**	+	+++	**3**
Angerman	+++	o	**o**	**3**
Lule	++	o	**o**	**2**
Rhine	**o**	+	++	**2**
Elbe	**o**	+	++	**2**
Vaenern Goeta	++	o	**o**	**2**
Glomma	++	o	**o**	**2**
Loire	**o**	o	++	**2**
Po	**o**	o	++	**2**
Shannon	**o**	o	**o**	**0**

The span of projected percentage changes in water availability based on the different scenario calculations is shown as box-whisker plots in Figure 7-14 for all 18 river basins. These are derived from the response surfaces by computing water availability at the intersection of the T and P change as given by each RCM. The length of the whiskers represents the spread in water availability caused by the different results of the RCMs for each basin. Overall, we find a gradient in changes that starts in northern Europe with increasing water availabilities and ends in southern Europe with a decrease in water availability. In central Europe, the results are inconclusive. The direction of change depends on the respective RCM.

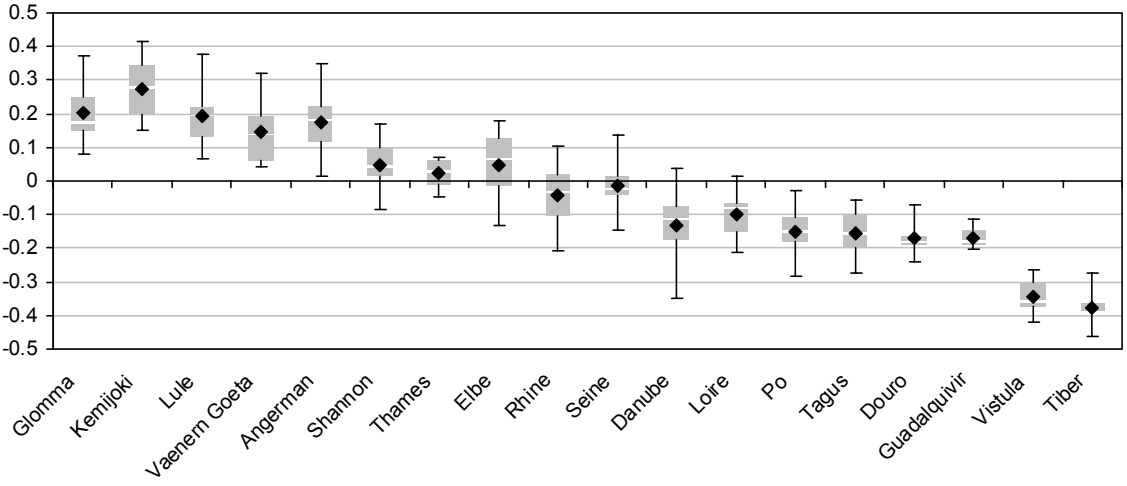

Figure 7-14. Projected percentage change in water availability as calculated with the WaterGAP model: Box whisker plots show the direction of change in long-term average water availability between current conditions (1961-1990) and 2100 (2070-2099). Percentages give the span of changes that result from the use of six RCMs. The black diamond indicates the mean, the boxes the second and third quartile, the white line the median.

7.4 Discussion and conclusions

Using the response surface method enabled us, for the first time, to consistently and objectively compare the sensitivity of European river basins to climate change, and carry out a vulnerability assessment based on the results of six RCMs for the IPCC A1B scenario in combination with societal windows of tolerance for water availability levels. The most sensitive to climate change were the Nordic basins, e.g. Lule, Glomma and Angerman, followed by more central European basins, while southern European basins, e.g. Tagus, Douro and Guadalquivir were least sensitive.

The high sensitivity of the Nordic basins can be explained by the fact that they are characterized by a mostly snow-dominated regime. Temperature increases directly affect the onset of high discharges due to snowmelt, and therefore the stability of the flow regime. Southern European basins are found to be least sensitive under the chosen indicators because evaporation makes up a major component in the water balance and increasing precipitation can be counterbalanced by increasing evaporation, especially under rising temperatures.

In the ranking of basins, we see no contradiction to previous studies, because all basins respond to climate change, as was found in regional studies, e.g. for Greece (Mimikou et al. 1991, Mimikou et al. 2000), Spain (Avila et al. 1996), the Rhine (Kwadijk and Rotmans 1995, Middelkoop et al. 2001), the UK (Mansell 1997, Arnell

1998, Limbrick et al. 2000) and Scandinavia (Bergström et al. 2001). Due to the difference in selected indicators, impact models, baseline periods and scenarios, a European-wide comparison was difficult with the majority of these regional assessments.

The vulnerability ranking is quite different from the sensitivity ranking and sees the southern European basins much higher ranked than in the sensitivity ranking based on higher water stress levels they might be facing in the future. Comparably highest vulnerable in Europe are the Vistula, Tiber and Danube basins due to the fact that both the high-low flow threshold and water stress thresholds are violated under all of the climate scenario simulations.

The sensitivity of sectors under the influence of human management is closely associated with the development level, institutional capacities, and technological capabilities of society and can therefore be adapted within certain boundaries. The applied thresholds have been chosen based on current knowledge and do not consider adaptive capacity of society, or possible changes in population densities. Thresholds might be subject to change, for example due to improving technologies, shifting the sensitivity of a basin to a lower level. On the other hand, the interpolation of an average intra-annual cycle has levelled out extreme monthly changes, and therefore might have lead to a smaller response in some of the basins.

The use of different RCM simulations for the same scenario addresses only some uncertainties associated with projections of climate change and it is quite possible that future climate change might put another area of the response surface into focus. But due to the flexibility of the response surface method, new indicators or additional climate change frequencies could easily be included, once they become available.

The response surface method itself introduces some uncertainty caused by the fitting method, especially when extracting absolute values of projected water availability. The increased accuracy of the response surface with the increased number of generated points obviously collides with the desire of reducing the number of model runs and simulation time.

When looking at the contour plots it becomes apparent that the response of water availability is stronger than the initial perturbation in precipitation in almost all basins. This should not be mistaken as an incorrect water balance. Instead, the incoming water is partitioned differently between the various moisture storages. Overall, the considered basins are situated in a mostly humid climate and water storages are filled on average throughout the year. However, looking at the Guadalquivir, the most southern basin, we find a delayed response in water availability, i.e. precipitation perturbation is greater than the response in water availability, especially for increasing temperatures. Here, more water can be stored, and thus evapotranspire during residence time, before

the additional water is transformed into runoff.

On the whole, this procedure offers a consistent way of judgment for current and future conditions. It provides an immediate visual comparison of the relative impact of unit changes in temperature and precipitation and enables the direct identification of hot spots, which might require further detailed analysis.

CHAPTER 8

SYNTHESIS

The objective of this thesis was to integratively model the impact of global change on the hydrological system, with special focus on droughts, evapotranspiration and long term water availability under consideration of anthropogenic interference with the natural system. The state-of-the-art global hydrological model WaterGAP was used to answer identified research questions, each in a specific regional context.

The overall aim was to gain new insights into hydrological processes under current and global change conditions as water resources can easily become a limiting factor for development and preservation of population, economic activity and ecosystems.

As part of this thesis, the impact of global change on return intervals of Mediterranean droughts was analysed. A study on green and blue water fluxes assessed the impact of global change on the appropriation of fresh water for African agriculture. In order to enhance model simulations in semi-arid to arid environments, the implemented semi-physical approach to simulate potential evapotranspiration according to Priestley Taylor was regionalised to better represent prevailing conditions in different climate classes. Finally, a method was developed to assess both sensitivity and vulnerability of river basins to global change.

In the following sections, the five research questions posed in the introduction are revisited to present answers and the main results of the chapters. A concluding section will summarize the major findings of this thesis. The chapter will end with an outlook on potential future research.

8.1 What is the impact of climate change on droughts in the Mediterranean, and how is the impact affected by anthropogenic interference?

Chapter 3 examined the combined influences of climate change and changes in anthropogenic water consumptions under IPCC SRES scenario conditions on future drought frequencies in the Mediterranean. The analysis was based on a statistical evaluation of the annual maximum series of deficit volumes, i.e. the volume of water the monthly discharge falls short of in comparison to the average monthly flow.

The modelling results show strong increases in drought frequencies for the 2070s in comparison to today for a belt that stretches from northern Spain over southern France towards northern Italy and Switzerland under the IPCC B2 scenario, and a strong increase over all of Southern Europe under the IPCC A2 scenario. Under consideration of both climate change effects and the impact of water abstraction, current 100-year droughts would return up to once per decade in the 2070s in these regions. Around the Black Sea, the 100-year drought would occur twice as often under the B2 scenario. Only in North Africa, current 100-year droughts would, except for North Algeria, return less frequently under both scenarios.

The study shows that climate change has a comparably stronger impact on the change in drought frequency than anthropogenic water uses. Increasing return frequencies are mainly caused by a combination of rising temperatures and decreasing precipitation, while decreasing return frequencies can mainly be attributed to increasing precipitation. Overall, the impact of anthropogenic water abstractions on drought frequencies is comparably low, with a statistical significance of 58%. Only in some scattered regions, anthropogenic water abstraction would cause the 100-year drought to return twice as often. These areas are characterized by very high water uses, as for example the Nile area with high irrigation water needs. Yet, anthropogenic water abstractions can intensify hydrological drought conditions because they further reduce already low stream flow. Increasing water use in the domestic sector, for example, which is caused by the projected increase in population, influences drought frequencies in Africa and the Middle East. On the other hand, industrial water use decreases in some central and eastern European countries due to more efficient technologies. Therefore, more water remains in the river system and hydrological droughts return slightly less frequently.

Similarly, Stahl (2001) has found a significant positive trend for parts of Spain analysing trends in European drought series, looking at the 1962-1990 period. Vicente-Serrano et al. (2004) found that drought increased significantly in the mid to northern

area of Spain between 1951 to 2000. In a global study, Sheffield and Wood (2008) analyzed changes in drought occurrence using soil moisture data for the IPCC SRES B1, A1B and A2 future climate scenarios, and found large increases for long-term frequencies in the Mediterranean, too.

In comparison to the number of documents underlining the vulnerability of the Mediterranean to droughts, the actual number of analyses of projected climate change on hydrological drought frequencies is low. To the author's knowledge, no other study currently exists that analyses future hydrological drought frequencies for the Mediterranean. One reason could be that river flows in the Mediterranean are rather erratic, which turns modelling into a difficult task, especially if statistical significance is to be assumed. The study in Chapter 3 showed a trend towards increasing drought frequencies under both the A2 and B2 scenarios with a statistical significance of 75% and 69%, respectively, for the combined impact of changes in climate and water uses, and a statistical significance of 58% for the impact of anthropogenic water abstraction. On the one hand, this underlines the vulnerability of the Mediterranean to climate change. On the other hand it confirms the urgent need for modelling tools to become more reliable in large-scale assessments of semi-arid to arid environments. One step towards fulfilling this need is carried out in Chapters 5 and 6 (see section 8.3).

8.2 What is the human appropriation of water for agriculture in Africa in the form of irrigation water compared to evapotranspiration? How is this appropriation affected by land cover change, climate change and technological change?

Chapter 4 assessed, for the first time, separately as well as combined the effect of climate change, land use change and technological change on human appropriation of fresh water for African agriculture. The concept of green and blue water was applied in this study to account for both irrigation water withdrawals (blue water), and water that evaporates and transpires from cropland (green water).

Model experiments were conducted by soft-coupling two disparate models, one land use change model (LandSHIFT) to quantify and locate the spatial extent of agricultural land to satisfy yield requirements under scenario conditions, and one global hydrology model (WaterGAP) to analyse effects on hydrological processes on a grid, country and continent level. For that reason, the two internally consistent scenarios 'Policy First' and 'Security First' of the UNEP Global Environmental Outlook-4 Report (GEO-4) with a time horizon of 2050 were applied.

For the year 2000, evapotranspiration from Africa's rainfed cropland ('green water flux') is calculated with the WaterGAP model to 1,085km^3/year, while the abstraction of water for irrigation purposes from renewable water resources ('blue water flux') is computed to 180km^3/year. Based on simulations with the LandSHIFT model, an additional area of approximately 1.25 mln km² to 1.56 mln km² of natural biomes is converted to cropland during 2000 and 2050, depending on the scenario considered. As a result for the year 2050, simulated evapotranspiration from rainfed cropland is substantially greater than in the year 2000, ranging from 1,870 to 2,040km^3/year, while irrigation abstraction increases up to 194 to 330km^3/year.

The sum of the model experiments indicates that human appropriation of freshwater for the cultivation of crops in Africa has a strong influence on the continental hydrological cycle which, according to the calculated scenarios, is likely to further increase in the coming decades. Current green water fluxes from African cropland area are significant and add up to about one-half of the current continental runoff (4,500 km^3/year). Although the blue water fluxes of irrigation water withdrawals make up over 80% of current total African withdrawals, they are overshadowed by moisture fluxes from rainfed cropland; the water evaporated and transpired annually from Africa's rainfed cropland (green water) is 6.6 times greater than the volume of water used in liquid form to irrigate crops (crop-related part of blue water).

Furthermore, these model experiments suggest that the magnitude of green water flux will substantially increase over the coming years. Under cropland expansion until 2050, green water fluxes increase by 72% to 88%. This is proportionately greater than the expansion of rainfed cropland area (62 to 69%) and can be explained by the additional effect of warmer future temperatures stimulating the plants' evapotranspirative processes. These additional irrigation water withdrawals for newly converted land, changing climate and changes in efficiencies will compete with water demands of other sectors, e.g. the domestic and manufacturing sectors, which have to be fulfilled by the same water resource.

For both scenarios, the land-use simulations show that substantial areas of natural biomes are converted to cropland with consequences both for the land and water-side. On the one hand the loss of natural biomes has negative impacts on biodiversity leading to a trade-off between crop production and other ecosystem services. On the other hand also the impacts on the hydrological cycle become obvious. Especially the replacement of forests and tropical woodlands which, due to their greater leaf area and denser biomass tend to have higher evapotranspiration per unit area than cropland, leads to overall lower green-water fluxes under cropland than before. This development, accompanied by the withdrawals and consumption of irrigation water induces large changes of local and regional water cycles with potential effects on river discharge and even micro-climatic conditions.

These findings point out the significant role of water appropriated for rainfed crop production in the continental water cycle in contrast to the sum of water appropriated for irrigation. Further, the results underline that it is worthwhile to not only improve the irrigation water use efficiency, but also the efficiency of water used by rainfed crops, given its magnitude. In principle, this could allow the same amount of food to be produced with a reduced amount of water, leaving more water to maintain freshwater ecosystems and natural flows, and satisfying anthropogenic water uses.

On the other hand, these results, once again, underline the important role that evapotranspiration plays in the hydrological system, and that it is very important to enhance its representation in global models in order to improve the quality of model simulations. Based on these results, Chapters 5 and 6 will analyse the semi-physical approach to modelling potential evapotranspiration processes as currently implemented in the WaterGAP model. The results are summarized in the following section 8.3.

8.3 How can the representation of evapotranspiration in global models be improved for semi-arid to arid environments? How can improvements of evapotranspiration processes be implemented in global models?

In order to answer this research question, four different potential evapotranspiration equations were analysed with regards to their applicability on a global basis in Chapter 5. One radiation-based method (Priestley Taylor), two combination equations (Kimberly Penman and Penman Monteith) and one temperature-based method (Hargreaves) were chosen for comparison. The radiation-based equation according to Priestley Taylor was found to be most appropriate for global applications due to its overall low input requirements at comparably good performance. The performance was assessed 1) by comparison with Class A pan evaporation time series and 2) by carrying out hydrological simulations with the WaterGAP model under use of the different equations and comparing calculated river flows to measured stream gauge data for selected river basins.

The Priestley-Taylor equation contains an empirical α-coefficient, which accounts for the aerodynamic component of the evaporation process. Initially, it was introduced at the value of 1.26 by Priestley and Taylor, but has since been adapted to site-specific conditions in many small-scale studies. A global application of the Priestley Taylor equation was, up to now, limited to its most common value of $\alpha = 1.26$, or when differentiating arid and humid areas, to the use with two α-values (1.26 for humid conditions and 1.74 in arid environments).

Based on the fact that the Priestley Taylor equation was found to be most appropriate for application in a global model in Chapter 5, it was regionalized in Chapter 6 by parameterization of its α-coefficient using pan evaporation measurements supplemented by α-values from existing small-scale studies to enable a seamless application over all climate zones. As a result, 12 α-classes are now differentiated, as opposed to previously two. As part of this study, a different approach to assigning albedo values was implemented, because albedo directly influences potential evapotranspiration. In contrast to relying on a parameterization based on land cover classes, albedo is now calculated as a function of the LAI (leaf area index) development in combination with a background albedo based on soil type. For this purpose, the LAI function was also improved to better represent vegetation phenology.

The best agreement between measured and simulated potential evapotranspiration values was achieved in cooler climates. In warmer and drier climates, measured pan evaporation values were characterized by greater variability. This led to a lower mod-

elling efficiency because the α-value was derived as a longterm mean over time and all stations per climate class, but the fit was judged by time series comparison. The author concludes a) general problems in the observation of pan values in dry zones and b) suggests a subdivision of these classes in order to reduce the spread, which would require a higher density in pan measuring stations.

Still, the ambition of enhancing stream flow simulations in semi-arid to arid environments was crowned by success. Although the absolute value of the model efficiency is lower in dry climate classes than in humid classes due to the above-described problems, model simulations of river flow showed an increased efficiency in all climates when carried out with the new regionalised Priestly Taylor equation, as tested against independent stream gauge data.

The present regionalization of the Priestley Taylor coefficient for the calculation of potential evapotranspiration was designed to consider the deviation from equilibrium conditions in different climate zones. It provides a more realistic estimation of potential evapotranspiration, based on pan evaporation measurements, supplemented by knowledge gained form existing local studies. It is intended for use in large-scale studies rather than in point studies where the appropriate α-value should be determined for site-specific conditions. Nonetheless, the regionalized α-coefficients provide the basis for a more realistic assessment of potential evapotranspiration on the global scale, which could also be of interest to other large-scale hydrologic or climate modellers.

8.4 What is a systematic method for characterizing the sensitivity of river basin hydrology to climate change?

Nowadays, examining climate change and its effects has a history of almost three decades. Impact analysis has hereby mostly followed the conventional way of a cause-effect analysis. Based on a consistent set of socio-economic drivers, emission paths for various greenhouse gases are developed, which are then used to simulate future climates that constitute the basis for impact analyses. This type of scenario analysis only provides insight into the consequences of concrete action along rigid pathways. The new trend towards ensemble climate modelling systems and multi-model simulations for generating future climate projections, as well as the urge to address climate change from a large-scale perspective calls for a systematic approach in analyzing possible climate change impacts.

In chapter 7, a new method was developed that enables a systematic, consistent and objective climate change sensitivity and vulnerability assessment of an optional number of river basins. In this analysis, the response of water availability to climate change was computed for 18 European catchments. Multiple model simulations for each combination of temperature (T) perturbations in the range [-1°C to +6°C] and precipitation (P) perturbations in the range [-40% to +100%] were carried out. The discrete data points of water availability, one for each combination of perturbed T and P parameters, were then interpolated to a continuous surface in 3d space.

The sensitivity of river basins was assessed by analysing the volumes under the surfaces and the shifts in monthly flow regimes, thus considering both changes in annual flows as well as monthly flows. A strong climate sensitivity was hereby found for the Nordic basins due to their snow-dominated flow regime: temperature increases directly affect the onset of high discharges due to snowmelt, and therefore the stability of the flow regime. Southern European basins are less sensitive based on the fact that the flow regime is relatively steady, and evapotranspiration acts as buffer. Evapotranspiration makes up a major component in the water balance and increasing precipitation can be counterbalanced by increasing evaporation, especially under rising temperatures.

In the following vulnerability assessment, societal thresholds for high flow, low flow and water stress were defined based on intensive literature studies for each basin. These thresholds were imposed onto the response surfaces as isolines, connecting all those points of the surface where water availability is equal to the threshold value. Thus, all combinations of T and P that lead to a violation of the threshold can be identified. For an assessment of the water availability situation in the year 2100, climate

change results from six regional climate models (RCM) under the IPCC A1B scenario where used to identify the corresponding water availability value at the intersection of given (RCM) T and P changes. The vulnerability of river basins was then assessed under consideration of the number of RCM simulations, under which the thresholds are violated. When ranking the basins according to their vulnerability, quite an opposite ranking than for the sensitivity was found. Southern European basins together with some central European basins were highest in the ranking based on a higher water stress level they might be facing in the future due to unfavourable climate changes. The most vulnerable were the Vistula and Tiber basins, caused by a violation of both the low flow indicator and water stress indicator under all RCM simulations.

The application of this method, besides the sensitivity and vulnerability classification of river basins to climate change, additionally offered the opportunity to test and analyse model specific behaviour, because the response surface method can also be considered a sensitivity analysis of the model itself. Valuable information on the model-internal process of disaggregating monthly precipitation to daily values was revealed. Explicitly, the perturbation of precipitation was carried out 1) by increasing the intensity of precipitation but maintaining the number of rain days per month at the reference value, and 2) by increasing the number of rain days at constant precipitation intensity to test the impact of these two approaches on simulations of water availability. Obviously the second approach is confined by the number of days per months. Once all days in a month are assigned rain days, the intensity of precipitation will increase. An important result was that distributing the delta changes of precipitation by increasing intensity at constant number of rain days (approach 1) led to stronger responses in water availability. This is explained by the fact that the capacity of various storages, i.e. of canopy and soils, is excessed earlier, if additional water is received on an already wet day. Any additional water then cannot be buffered and is converted into direct runoff. The response of water availability to precipitation perturbation therefore appears more realistic if it is reached by increasing the number of rain days. In this case, the water is then diverted into another compartment of the hydrological cycle, e.g. to groundwater recharge, surface runoff or evapotranspiration.

Overall, this method offers a consistent way of judgment of a basin's current conditions, and future conditions affected by global change. It is flexible enough to include new indicators, different thresholds or additional climate change frequencies. It provides an immediate visual comparison of the relative impact of unit changes in temperature and precipitation and enables the direct identification of hot spots, which might require further detailed analysis.

8.5 Summary of major findings

Chapter 3 analysed, for the first time, the combined effect of climate change and changes in anthropogenic water uses on the return frequency of the 100 year drought for the whole Mediterranean region. Since hydrological modelling in sub-humid and semi-arid regions is difficult due to the often erratic nature of flows, the statistical significance of changes was further evaluated. In general, a strong dependency of the drought return frequency on climate conditions was found, while the impact of anthropogenic water use on the return frequency was weaker.

Chapter 4 examined, for the first time, the effect of climate change, land use change and technological change, both separately and combined, on human appropriation of fresh water for agricultural purposes in Africa. Hereby, a holistic approach was chosen, considering both blue and green water fluxes. The study revealed the significance of green water fluxes from African agricultural land, which are 6.6 times greater than blue water fluxes for irrigation. It further underlined the high potential of technological change, by which, theoretically, the same amount of food could be produced while using less water, thus 'freeing' more water to satisfy anthropogenic or ecosystem requirements.

Chapter 5 studied the global applicability of four different potential evapotranspiration (PET) equations and found the Priestley Taylor equation most suited due to its low input requirements and good agreement with Class A pan time series.

Chapter 6 regionalized the Priestley Taylor equation, resulting in a differentiation of 12 different classes in comparison to previously two. The improved representation of the PET process led to 1) improved simulation of PET time series with the WaterGAP model and 2) to improved simulations of river flow with the WaterGAP model in all climate classes, as tested against measured gauge data.

Chapter 7 developed a new method to systematically and objectively compare the sensitivity and vulnerability to climate change of an arbitrary number of river basins. Since at the same time, the method constitutes a sensitivity analysis of the model itself, it was further used to examine the model-internal process of downscaling monthly precipitation to daily values. A clear recommendation is made concerning future climate change studies with the WaterGAP model: delta changes of precipitation should be distributed by first increasing the number of rain days before increasing the rainfall intensity in order to trigger more realistic responses of simulated water availability.

8.6 Outlook on further research

Considering the fact that in global models, major hydrological processes are simplified by conceptual formulations due to persistent limitations in both global input data sets and large scale process descriptions, they offer much room for improvement as more and more data becomes available. The results in this thesis, especially Chapters 4-6, underline the relevance of the process of evapotranspiration for modelling water cycle components.

Further research is therefore justified that analyses the processes involved in e.g. calculating actual evapotranspiration from potential evapotranspiration. To date, this is a strongly model-specific process, involving the calculation of inflow in and outflow from various water storages. A comparison between two different models that rely on different physically-based process descriptions and different input data in Chapter 5 revealed that it is worthwhile to examine these storage balances in more detail in order to improve stream flow simulations.

This includes first of all soil moisture functions, as soil moisture plays an important role in the interaction of the land surface and atmosphere, particularly in the partitioning of the various water and energy fluxes. For example, water storage capacities of soils should be modified to depend on soil type rather than on land cover. Further, interflow should be included in the WaterGAP model, as this has improved modelling quality of most hydrological models to date. Further research could focus on restructuring WaterGAP by including a new data-based soil-module. As part of this, a new calibration factor could be included considering interflow recession. Thus, not only the magnitude of runoff could be calibrated, but also its phase. This would lead to more process-based modelling of water flows. Secondly, canopy water storages for different vegetation types could be enhanced given their importance for interception. Thirdly, surface water storage in the form of wetlands and lakes are essential in the calculation of surface water flows and residence times. Therefore, their representation should also be improved on a global scale.

Chapter 4 analysed the interaction between land cover changes and changes in evapotranspiration, as well as in runoff. It was shown that the conversion from natural land to agricultural area 1) decreases evapotranspiration, due to e.g. less denser biomass of vegetation on managed land in comparison to natural vegetation and 2) can lead to increased surface runoff because less water is retained per area land. Given the strong connection between land use and the hydrological system, further research could examine past land cover changes in order to improve the agreement between simulated and measured historical stream flows. On the other hand, a sequential cou-

pling of the LandSHIFT model with the WaterGAP model appears promising in order to include feedbacks in both modelling processes. For the allocation of new agricultural areas, as carried out by LandSHIFT, the information of water availability in each time step would be an important pre-requisite. Vice-versa, for a more realistic approach to simulating runoff, land cover is an important dynamic parameter.

LIST OF FIGURES

LIST OF TABLES

BIBLIOGRAPHY

Alcamo, J. M. 2008. *Environmental Futures, 2. The Practice of Environmental Scenario Analysis*. Developments in Integrated Environmental Assessment. Elsevier B.V., New York, USA.

Alcamo, J. M., P. Döll, T. Henrichs, F. Kaspar, B. Lehner, T. Rösch, and S. Siebert. 2003a. Development and testing of the WaterGAP 2 global model of water use and availability. *Hydrological Sciences* **48**:317-337.

Alcamo, J. M., P. Döll, T. Henrichs, F. Kaspar, B. Lehner, T. Rösch, and S. Siebert. 2003b. Global estimates of water withdrawals and availability under current and future "business-as-usual" conditions. *Hydrological Sciences* **48**:339-348.

Alcamo, J. M., M. Flörke, and M. Märker. 2007. Future long-term changes in global water resources driven by socio-economic and climatic changes. *Hydrological Sciences Journal-Journal Des Sciences Hydrologiques* **52**:247-275.

Alcamo, J. M., and T. Henrichs. 2002. Critical regions: A model-based estimation of world water resources sensitive to global changes. *Aquatic Sciences - Research Across Boundaries* **64**:352-362.

Alcamo, J. M., R. Leemans, and E. Kreileman. 1998. *Global Change Scenarios of the 21st Century. Results of the IMAGE 2.1 Model*. Pergamon, Oxford.

Alcamo, J. M., and R. Schaldach. 2006. LandShift: Global Modelling to Assess Land Use Change. Pages 223-230 *in* K. Tochtermann, and A. Scharl, editors. *EnviroInfo 2006. Managing Environmental Knowledge. Proceedings of the 20th International Conference Informatics for Environmental Protection.* Shaker, Graz, Austria.

Alcamo, J. M., D. van Vuuren, C. Ringler, W. Cramer, T. Masui, J. Alder, and K. Schulze. 2005. Changes in Nature's Balance Sheet: Model-based Estimates of Future Worldwide Ecosystem Services. *Ecology & Society* **10**:27.

Allen, R. G., M.E. Jensen, J.L. Wright, and R. D. Burman. 1989. Operational Estimates of Reference Evapotranspiration. *Agronomy Journal* **81**:650-662.

Allen, R. G., L. S. Pereira, D. Raes, and M. Smith. 1998. *Crop evapotranspiration - Guidelines for computing crop water requirements.* FAO, Rome.

Arnell, N. W. 1998. Climate Change and Water Resources in Britain. *Climatic Change* **39**:83-110.

Arnell, N. W. 1999a. The effect of climate change on hydrological regimes in Europe: a continental perspective. *Global Environmental Change* **9**:5-23.

Arnell, N. W. 1999b. A simple water balance model for the simulation of streamflow over a large geographic domain. *Journal of Hydrology* **217**:314-335.

Arnell, N. W. 2000. Thresholds and Response to Climate Change Forcing: The Water Sector. *Climatic Change* **46**:305-316.

Arnell, N. W. 2003. Effects of IPCC SRES emissions scenarios on river runoff: a global perpective. *Hydrology and Earth System Sciences* **7**:619-641.

Arnell, N. W., and C. Liu. 2001. Hydrology and water resources. *Climate Change 2001, Impacts, Adaptation, and Vulnerability. Intergovernmental Panel on Climate Change*. Cambridge University Press, Cambridge, UK.

Arora, K., and V. P. Singh. 1989. A comparative evaluation of the estimators of the log Pearson type (LP) 3 distribution. *Journal of Hydrology* **105**:19-37.

ASCE. 1996. *Hydrology Handbook.* ASCE Manuals and Reports on Engineering Practice ASCE, New York.

Avila, A., C. Neal, and J. Terradas. 1996. Climate change implications for streamflow and stream-water chemistry in a Mediterranean catchment. *Journal of Hydrology* **177**:99-116.

Barbier, E. B. 1997. The economic determinants of land degradation in developing countries. *Phil. Trans. R. Soc. Lond. B.* **352**:891-899.

Batjes, N. H. 1996. Development of a world data set of soil water retention properties using pedotransfer rules. *Geoderma* **71**:31-52.

Bergström, S. 1995. The HBV model. Pages 443-476 *in* V. P. Singh, editor. *Computer models of watershed hydrology*. Water Resources Publications, Highlands Ranch.

Bergström, S., B. Carlsson, M. Gardelin, G. Lindstrom, A. Pettersson, and M. Rummukainen. 2001. Climate change impacts on runoff in Sweden-Assessments by global climate models, dynamical downscaling and hydrological modelling. *Climate Research* **16**:101-112.

Bloemen, G. W. 1978. A high-accuracy recording pan-evaporimeter and some of its possibilities. *Journal of Hydrology* **39**:159-173.

Bobee, B. 1975. The log-Pearson type 3 distribution and its applications in hydrology. *Water Resources Research* **14**:365-369.

Bobee, B., and F. Ashkar. 1991. *The Gamma Family and Derived Distributions Applied in Hydrology*, Fort Collins, CO.

Bobee, B., and R. Robitaille. 1977. The use of the Pearson type 3 distribution and log Pearson type 3 distribution revisited. *Water Resources Research* **13**:427-443.

Böhm, U., M. Kücken, W. Ahrens, A. Block, D. Hauffe, K. Keuler, B. Rockel, and A. Will. 2006. Clm - the climate version of lm: Brief description and long-term applications. *COSMO Newsletter 6*.

Bouwman, A. F., T. Kram, and K. Klein Goldewijk. 2006. *Integrated Modelling of Global Environmental Change: An Overview of Image 2.4.* Netherlands Environmental Assessment Agency, Bilthoven, NL.

Bower, D., D. M. Hannah, and G. R. McGregor. 2004. Techniques for assessing the climatic sensitivity of river flow regimes. *Hydrological Processes* **18**:2515-2543.

Box, G. E. P., and N. R. Draper. 1959. A Basis for the Selection of a Response Surface Design. *Journal of the American Statistical Association* **54**:622-654.

Box, G. E. P., and K. B. Wilson. 1951. On the experimental attainment of optimum conditions (with discussion). *Journal of the Royal Statistical Society* **B13**:1-45.

Brown, J., O.J. Ferrians Jr., J. A. Heginbottom, and E. S. Melnikov. 1998. revised February 2001. *Circum-Arctic map of permafrost and ground-ice conditions*. Boulder, CO: National Snow and Ice Data Center/World Data Center for Glaciology. [online] http://nsidc.org/data/ggd318.html.

Bruckner, T., G. Petschel-Held, F. L. Tóth, H. M. Füssel, C. Helm, M. Leimbach, and H. J. Schellnhuber. 1999. Climate change decision-support and the tolerable windows approach. *Environmental Modeling and Assessment* **4**:217-234.

De Bruin, H. A. R., and J. Q. Keijman. 1979. The Priestley-Taylor Evaporation Model Applied to a Large, Shallow Lake in the Netherlands. *Journal of Applied Meteorology* **18**:898-903.

Brutsaert, W. 1982. *Evaporation into the atmosphere. Theory, History, and Applications.* Kluwer Academic Publisher, Dordrecht, Boston, London.

Burman, R., and L. O. Pochop. 1994. *Evaporation, Evapotranspiration and climatic data.* Elsevier Science B.V., Amsterdam.

Carpenter, S., P. Pingali, E. Bennett, and M. Zurek. 2005. *Scenarios of the Millenium Ecosystem Assessment*. Island Press, Oxfort, UK.

Castellvi, F., C. O. Stockle, P. J. Perez, and M. Ibañez. 2001. Comparison of methods for applying the Priestley-Taylor equation at a regional scale. *Hydrological Processes* **15**:1609-1620.

Chang, T. J., and J. R. Stenson. 1990. Is it realistic to define a 100-year drought for water management? *Journal of the American Water Resources Association* **26**:823-829.

CIESIN. 2004. *Global Rural-Urban Mapping Project (GRUMP), Alpha Version: Population Density Grids*. Socioeconomic Data and Applications Center (SEDAC), Columbia University. [online] http://beta.sedac.ciesin.columbia.edu/gpw/

CIESIN. 2005. *Gridded Population of the World Version 3 (GPWv3): Population Grids*. [online] http://sedac.ciesin.columbia.edu/gpw.

Clausen, B., and B. J. F. Biggs. 2000. Flow variables for ecological studies in temperate streams: groupings based on covariance. *Journal of Hydrology* **237**:184-197.

Collins, M. 2007. Ensembles and probabilities: a new era in the prediction of climate change. *Phil. Trans. R. Soc. A* **365**:1957–1970.

Cornell, J. A. 1987. *Response surfaces: designs and analyses.* Marcel Dekker, Inc.

Davies, J. A., and C. D. Allen. 1973. Equilibrium, Potential and Actual Evaporation from Cropped Surfaces in Southern Ontario. *Journal of Applied Meteorology* **12**:649-657.

Döll, P., K. Berkhoff, H. Bormann, N. Fohrer, D. Gerten, S. Hagemann, and M. Krol. 2008. Advances and visions in large-scale hydrological modelling: findings from the 11th Workshop on Large-Scale Hydrological Modelling. *Adv. Geosci.* **18**:51-61.

Döll, P., F. Kaspar, and B. Lehner. 2003. A global hydrological model for deriving water availability indicators: model tuning and validation. *Journal of Hydrology* **270**:105-134.

Döll, P., and B. Lehner. 2002. Validation of a new global 30-min drainage direction map. *Journal of Hydrology* **258**:214-231.

Döll, P., and S. Siebert. 2000. A digital global map of irrigated areas. *Irrigation and Drainage* **49**:55-66.

Döll, P., and S. Siebert. 2002. Global modeling of irrigation water requirements. *Water Resources Research* **38**:10.

Doorenbos, J., and W. O. Pruitt. 1977. *Crop water requirements.* FAO, Rome.

Douglas, E. M., K. Sebastian, C. J. Vörösmarty, S. Wood, and K. M. Chomitz. 2005. The role of tropical forests in supporting biodiversity and hydrological integrity: a synoptic overview *in* The World Bank, editor. *Policy Research Working Paper Series 3635*, Washington, D.C.

Droogers, P., and R. G. Allen. 2002. Estimating Reference Evapotranspiration Under Inaccurate Data Conditions. *Irrigation and Drainage Systems* **16**:33-45.

DVWK. 1996. *Ermittlung der Verdunstung von Land- und Wasserflächen (evaporation from land and water areas, in German)*. DVWK-Merkblatt. ATV-DVWK Deutsche Vereinigung für Wasserwirtschaft, Abwasser und Abfall e.V., Bonn, Germany.

Easterling, D. R., and T. C. Peterson. 1995. A new method for detecting undocumented discontinuities in climatological time series. *International Journal of Climatology* **15**:369-377.

Eastman, J. R., W. Jin, P. Kyem, and J. Toledano. 1995. Raster procedures for multiobjective land-use planning. *Photogrammetric Engineering and Remote Sensing* **61**:539-547.

Eaton, A. K., W. R. Rouse, P. M. Lafleur, P. Marsh, and P. D. Blanken. 2001. Surface Energy Balance of the Western and Central Canadian Subarctic: Variations in the Energy Balance among Five Major Terrain Types. *Journal of Climate* **14**:3692-3703.

Eichinger, W. E., M. B. Parlange, and H. Stricker. 1996. On the concept of equilibrium evaporation and the value of the Priestley-Taylor coefficient. *Water Resources Research* **32**:161-164.

Engstrom, R. N., A. S. Hope, D. A. Stow, G. L. Vourlitis, and W. C. Oechel. 2002. Priestley-Taylor alpha coefficient: Variability and relationship to NDVI in arctic tundra landscapes. *Journal of the American Water Resources Association* **38**:1647-1659.

Estrela, T., M. Menéndez, M. Dimas, C. Marcuello, G. Rees, G. Cole, K. Weber, J. Grath, J. Leonard, N. B. Ovesen, J. Fehér, and V. Consult. 2001. *Sustainable water use in Europe —Part 3: Extreme hydrological events: floods and droughts.* Environmental issue report European Envrionment Agency (EEA), editor. OPOCE, Copenhagen, DK.

Falkenmark, M. 1995. Land-water linkages: A synopsis *in* T. H. Mather, editor. *Land and water integration and river basin management. Proceedings of an FAO informal workshop*, Rome, Italy.

Falkenmark, M., and M. Lannerstad. 2005. Consumptive water use to feed humanity - curing a blind spot. *Hydrology and Earth System Sciences* **9**:15-28.

Falkenmark, M., and J. Rockström. 2006. The new blue and green water paradigm: Breaking new ground for water resources planning and management. *Journal of Water Resources Planning and Management-Asce* **132**:129-132.

Falkenmark, M., and C. Widstrand. 1992. Population and water resources: a delicate balance. *Population Bulletin* **47**:2-35.

FAO. 1995. Digital Soil Map of the World and Derived Soil Properties. FAO, Rome.

FAO. 1997. Irrigation potential in Africa: A basin approach. *Land and Water Bulletin 4*, Rome, Italy.

FAO. 2003a. *AQUASTAT online database*. Rome, Italy. [online] http://www.fao.org/nr/water/aquastat/dbases/index.stm.

FAO. 2003b. Digital Soil Map of the World and Derived Soil Properties. FAO, Rome.

FAO. 2008. *FAO Statistical Database*. [online] http://faostat.fao.org/.

Fekete, B., C. J. Vörösmarty, and W. Grabs. 1999. *Global composite runoff fields of observed river discharge and simulated water balances.* Report No. 22. Global Runoff Data Centre, Koblenz, Germany.

Fleig, A. K., L. M. Tallaksen, H. Hisdal, and S. Demuth. 2006. A global evaluation of streamflow drought characteristics. *Hydrology and Earth System Sciences* **10**:535-552.

Flörke, M., and J. Alcamo. 2007. Assessment of global scale water stress indicators. Pages 200-203 *in* J. Lozán, H. Graßl, P. Hupfer, L. Menzel, and C. D. Schönwiese, editors. *Global change: Enough water for all?* Wissenschaftliche Auswertungen und GEO-Verlag, Hamburg.

Folland, C. K., T. R. Karl, and K. Y. Vinnikov. 1990. Observed climate variations and change. Pages 195-238 *in* J. T. Houghton, Jenkins, G.J. and Ephraums, J.J.,, editor. *Climate Change, the IPCC Scientific Assessment*. Cambridge University Press, Cambridge, UK.

Fowler, A. 1999. Potential climate change impacts on water resources in the Auckland Region (New Zealand). *Climate Research* **11**:221-245.

Füssel, H.-M., and J. G. van Minnen. 2001. Climate impact response functions for terrestrial ecosystems. *Integrated Assessment* **2**:183–197.

Füssel, H. M., F. L. Toth, J. G. van Minnen, and F. Kaspar. 2003. Climate Impact Response Functions as Impact Tools in the Tolerable Windows Approach. *Climatic Change* **56**:91-117.

Geiger, R. 1961. Klima der Erde / Climate of the earth (Köppen / Geiger). *Wandkarte / Wall map 1:16 Mill.* Klett Verlag, Gotha.

Gerten, D., H. Hoff, A. Bondeau, W. Lucht, P. Smith, and S. Zaehle. 2005. Contemporary "green" water flows: Simulations with a dynamic global vegetation and water balance model. *Physics and Chemistry of the Earth* **30**:334-338.

Gerten, D., S. Schaphoff, U. Haberlandt, W. Lucht, and S. Sitch. 2004. Terrestrial vegetation and water balance - hydrological evaluation of a dynamic global vegetation model. *Journal of Hydrology* **286**:249-270.

Gibson, C. A., J. L. Meyer, N. L. Poff, L. E. Hay, and A. Georgakakos. 2005. Flow regime alterations under changing climate in two river basins: implications for freshwater ecosystems. *River Research and Applications* **21**:849-864.

Gleick, P. H. 1993. *Water in crisis: a guide to the world's fresh water resources.* Oxford University Press, New York.

Gottschalk, L., L. M. Tallaksen, and G. Perzyna. 1997. Derivation of low flow distribution functions using recession curves. *Journal of Hydrology* **194**:239-262.

GRDC. 2004. *Long Term Mean Monthly Discharges and Annual Characteristics of Selected GRDC Stations.* The Global Runoff Data Centre, Koblenz, Germany.

Groffman, P., J. Baron, T. Blett, A. Gold, I. Goodman, L. Gunderson, B. Levinson, M. Palmer, H. Paerl, G. Peterson, N. Poff, D. Rejeski, J. Reynolds, M. Turner, K. Weathers, and J. Wiens. 2006. Ecological Thresholds: The Key to Successful Environmental Management or an Important Concept with No Practical Application? *Ecosystems* **9**:1-13.

Guha-Sapir, D., D. Hargitt, and P. Hoyois. 2004. *Thirty years of natural disasters 1974-2003: the numbers.* Presses universitaires de Louvain, Louvain-la-Neuve.

Hagemann, S., and L. D. Gates. 2003. Improving a subgrid runoff parameterization scheme for climate models by the use of high resolution data derived from satellite observations. *Climate Dynamics* **21**:349-359.

Hargreaves, G. H., and R. G. Allen. 2003. History and Evaluation of Hargreaves Evapotranspiration Equation. *Journal of Irrigation and Drainage Engineering* **129**:53-63.

Hargreaves, G. L., G. H. Hargreaves, and J. P. Riley. 1985. Agricultural Benefits for Senegal River Basin. *Journal of Irrigation and Drainage Engineering* **111**:113-124.

Harmel, R. D., and P. K. Smith. 2007. Consideration of measurement uncertainty in the evaluation of goodness-of-fit in hydrologic and water quality modeling. *Journal of Hydrology* **337**:326-336.

Heistermann, M., C. Müller, and K. Ronneberger. 2006. Land insight? Achievements, deficits and potentials of continental to global scale land-use modeling. *Agriculture Ecosystems & Environment* **114**:141-158.

Henrichs, T., B. Lehner, and J. Alcamo. 2002. An Integrated Analysis of Changes in Water Stress in Europe. *Integrated Assessment* **3**:15-29(15).

Hess, T. M. 1998. Trends in reference evapo-transpiration in the North East Arid Zone of Nigeria, 1961-91. *Journal of Arid Environments* **38**:99-115.

Hill, W. J., and W. G. Hunter. 1966. A review of response surface methodology : a literature survey. *Technometrics* **8**:571-590.

Hisdal, H., and L. M. Tallaksen. 2000. Drought event definition. *ARIDE Tech. Report no. 6.* University of Oslo, Oslo, Norway.

Houghton, R. A. 1999. The annual net flux of carbon to the atmosphere from changes in land use 1850-1990. *Tellus B* **51**:298-313.

Hübener, H., M. Schmidt, M. Sogalla, and M. Kerschgens. 2005. Simulating evapotranspiration in a semi-arid environment. *Theoretical and Applied Climatology* **80**:153-167.

Hughes, B., and E. Hillebrand. 2006. *Exploring and Shaping International Futures.* Paradigm Publishers, Boulder, CO.

IACWD. 1982. *Interagency Advisory Committee on Water Data: Guidelines for Determining Flood Flow Frequency: Bulletin 17B.* , Reston, VA.

IEA. 1998. *Institution of Engineers: Australian rainfall and runoff - a guide to flood estimation*, Barton, Australia.

IPCC. 2000. *Special Report on Emission Scenarios*. Cambridge University Press, Cambridge.

IPCC. 2001a. *Climate Change 2001: Impacts, Adaptation, and Vulnerability. Contribution of Working Group II to the Third Assessment Report of the Intergovernmental Panel on Climate Change.* IPCC Third Assessment Report. J. J. McCarthy, O. F. Canziani, N. A. Leary, D. J. Dokken, and K. S. White, editors. Cambridge University Press, Cambridge, United Kingdom and New York, NY, USA.

IPCC. 2001b. *Climate Change 2001: Synthesis Report. A Contribution of Working Groups I, II, and III to the Third Assessment Report of the Intergovernmental Panel on Climate Change.* IPCC Third Assessment Report. R. T. Watson, and the Core Writing Team, editors. Cambridge University Press, Cambridge, UK, and New York, USA.

IPCC. 2001c. *Climate Change 2001: The Scientific Basis. Contribution of Working Group I to the Third Assessment Report of the*
Intergovernmental Panel on Climate Change. IPCC Third Assessment Report. J. T. Houghton, Y. Ding, D. J. Griggs, M. Noguer, P. J. van der Linden, X. Dai, K. Maskell, and C. A. Johnson, editors. Cambridge University Press, Cambridge, United Kingdom and New York, NY, USA.

IPCC. 2007. *Climate Change 2007: The Physical Science Basis. Contribution of Working Group I to the Fourth Assessment Report of the Intergovernmental Panel on Climate Change*. S. Solomon, D. Qin, M. Manning, Z. Chen, M. Marquis, K. B. Averyt, M. Tignor, and H. L. Miller, editors. Cambridge University Press, Cambridge, UK and New York, USA.

Jacob, D. 2001. A note to the simulation of the annual and inter-annual variability of the water budget over the Baltic Sea drainage basin. *Meteorology and Atmospheric Physics* **77**:61-73

Jacob, D., B. J. J. M. v. d. Hurk, U. Andræ, G. Elgered, C. Fortelius, L. P. Graham, S. D. Jackson, U. Karstens, C. Köpken, R. Lindau, R. Podzun, B. Rockel, F. Rubel, B. H. Sass, R. N. B. Smith, and X. Yang. 2001. A Comprehensive Model Intercomparison Study Investigating the Water Budget during the BALTEX-PIDCAP Period. *Meteorology and Atmospheric Physics* **77**:19-43.

Jensen, M. E., R. D. Burman, and R. G. Allen. 1990. *Evapotranspiration and irrigation water requirements*, New York.

Jewitt, G. 2006. Integrating blue and green water flows for water resources management and planning. *Physics and Chemistry of the Earth* **31**:753-762.

Jones, P. D., and K. R. Briffa. 1992. Global surface air temperature variations during the twentieth century: Part 1, spatial, temporal and seasonal details. *The Holocene* **2**.

Jury, W. A., and C. B. Tanner. 1975. Advection Modification of the Priestley and Taylor Evapotranspiration Formula. *Agronomy Journal* **67**:840-842.

Kaspar, F. 2004. Entwicklung und Unsicherheitsanalyse eines globalen hydrologischen Modells. Page 139. Kassel University Press, Kassel, Germany.

Kishk, M. A. 1990. Conceptual issues in dealing with land degradation/conservation problems in developing countries. *GeoJournal* **20**:187-190.

Kite, G. W. 1977. *Frequency and Risk Analysis in Hydrology*, Fort Collins, CO.

Kjellström, E., L. Bärring, S. Gollvik, U. Hansson, C. Jones, P. Samuelsson, M., and A. U. Rummukainen, U. Willén, and K. Wyser. 2005. A 140-year simulation of European climate with the new version of the Rossby Centre regional atmospheric climate model (RCA3). Page 54 pp. *in* SMHI, editor. *SMHI Reports Meteorology and Climatology, 108*, SE-60176 Norrköping, Sweden.

Komatsu, H. 2005. Forest categorization according to dry-canopy evaporation rates in the growing season: comparison of the Priestley-Taylor coefficient values from various observation sites. *Hydrological Processes* **19**:3873-3896.

Köppen, W. 1918. Klassifikation der Klimate nach Temperatur, Niederschlag und Jahresablauf (Classification of climates ccording to temperature precipitation and annual cycle - in German). *Petermann Geografische Mitteilungen* **64**:193-203 and 243-248.

Kottek, M., J. Grieser, C. Beck, B. Rudolf, and F. Rubel. 2006. World Map of the Köppen-Geiger climate classification updated. *Meteorologische Zeitschrift* **15**:259-263.

Krasovskaia, I., N. W. Arnell, and L. Gottschalk. 1994. Flow regimes in northern and western Europe: development and application of the procedures for classifying flow regimes. Pages 179-184 *in* P. Seuna, A. Gustard, N. W. Arnell, and G. A. Cole, editors. *FRIEND: Flow Regimes from International Experimental and Network Data.* IAHS.

Krinner, W., C. Lallana, T. Estrela, S. Nixon, T. Zabel, L. Laffon, G. Rees, and G. Cole. 1999. *Sustainable water use in Europe - Part 1: Sectoral use of water.* Environmental assessment report No 1. European Environment Agency, editor, Copenhagen, DK.

Krol, M. S., and A. Bronstert. 2007. Regional integrated modelling of climate change impacts on natural resources and resource usage in semi-arid Northeast Brazil. *Environmental Modelling & Software* **22** 259-268.

Kundzewicz, Z. W. 2003. Water and Climate - The IPCC TAR perspective. *Nordic hydrology* **34**:387-398.

Kwadijk, J., and J. Rotmans. 1995. The impact of climate change on the river rhine: A scenario study. *Climatic Change* **30**:397-425.

Laaha, G., and G. Blöschl. 2008. A national low flow estimation procedure for Austria. *Hydrological Sciences–Journal–des Sciences Hydrologiques* **52**:625-644.

Lamb, H. H. 1972. *Climate: Present, Past and Future.* Methuen & Co Ltd., London.

Legates, D. R., and C. J. Willmott. 1990. Mean seasonal and spatial variability in gauge-corrected, global precipitation. *International Journal of Climatology* **10**:111-127.

Lehner, B., and P. Döll. 2004. Development and validation of a global database of lakes, reservoirs and wetlands. *Journal of Hydrology* **296**:1-22.

Lehner, B., P. Döll, J. M. Alcamo, T. Henrichs, and F. Kaspar. 2006. Estimating the impact of global change on flood and drought risks in Europe: A continental, integrated analysis. *Climatic Change* **75**:273-299.

Limbrick, K. J., P. G. Whitehead, D. Butterfield, and N. Reynard. 2000. Assessing the potential impacts of various climate change scenarios on the hydrological regime of the River Kennet at Theale, Berkshire, south-central England, UK: an application and evaluation of the new semi-distributed model, INCA. *The Science of The Total Environment* **251-252**:539-555.

Linacre, E. T. 1994. Estimating U.S. Class-A pan evaporation from few climate data. *Water International* **19**:5-14.

Lockwood, J. G. 1983. The influence of vegetation on the Earth's climate. *Progress in Physical Geography* **7**:81-89.

Lohmann, U., R. Sausen, L. Bengtsson, U. Cubasch, J. Perlwitz, and E. Roeckner. 1993. The Koeppen Climate Classification as a Diagnostic Tool for General Circulation Models. *Climate Research* **3**:177 - 193.

Loveland, T. R., B. C. Reed, J. F. Brown, D. O. Ohlen, Z. Zhu, L. Yang, and J. W. Merchant. 2000. Development of a global land cover characteristics database and IGBP DISCover from 1 km AVHRR data. *International Journal of Remote Sensing* **21**:1303 - 1330.

Ma, Z., and C. Fu. 2003. Interannual characteristics of the surface hydrological variables over the arid and semi-arid areas of northern China. *Global and Planetary Change* **37**:189-200.

Madsen, H., P. F. Rasmussen, and D. Rosbjerg. 1997. Comparison of annual maximum series and partial duration series methods for modeling extreme hydrologic events. *Water Resources Research* **33**:747-757.

Maidment. 1992. *Chapter 4: Evaporation.* Handbook of hydrology. McGraw-Hill, New York.

Mansell, M. G. 1997. The effect of Climate Change on Rainfall Trends and Flooding Risk in the West of Scotland. *Nordic Hydrology* **28**:37-50.

McGraw-Hill. 2003. *Dictionary of Environmental Science.* The McGraw-Hill Companies, USA.

McMahon, T. 1979. Hydrological characteristics of arid zones. Pages 105-123. *Symposium on the Hydrology of Areas of Low Precipitation*, Canberra.

McNaughton, K. G., and T. A. Black. 1973. A Study of Evapotranspiration from a Douglas Fir Forest Using the Energy Balance Approach. *Water Resources Research* **9**:1579-1590.

MEA. 2005. *Ecosystems and Human Well-Being Scenarios. Findings of the Scenarios Working Group, Millennium Ecosystem Assessment Series*. S. R. Carpenter, P. L. Pingali, E. M. Bennett, and M. B. Zurek, editors. Island Press, Washington, Covelo, London.

Meigh, J. R., A. A. McKenzie, and K. J. Sene. 1999. A Grid-Based Approach to Water Scarcity Estimates for Eastern and Southern Africa. *Water Resources Management* **13**:85-115.

Menzel, L. 1997. *Modellierung der Evapotranspiration im System Boden-Pflanze-Atmosphäre (simulation of evapotranspiration at the soil-vegetation-atmosphere interface; in German).* Zürcher Geographische Schriften No.67. Swiss Federal Institute of Technology (ETH), Zürich.

Menzel, L. 1999. *Flächenhafte Modellierung der Evapotranspiration mit TRAIN (areal modelling of evapotranspiration with TRAIN; in German).* Potsdam-Institute for Climate Impact Research.

Menzel, L., E. Teichert, and M. Weiss. 2007. Climate change impact on the water resources of the semi-arid Jordan region. Pages 320-325 *in* M. Heinonen, editor. *3rd International Conference on Climate and Water*, Helsinki.

Meyer, W. B., and B. L. Turner II. 1992. Human Population Growth and Global Land-Use/Cover Change. *Annual Review of Ecology and Systematics* **23**:39-61.

Middelkoop, H., K. Daamen, D. Gellens, W. Grabs, J. C. J. Kwadijk, H. Lang, B. W. A. H. Parmet, B. Schädler, J. Schulla, and K. Wilke. 2001. Impact of Climate Change on Hydrological Regimes and Water Resources Management in the Rhine Basin. *Climatic Change* **49**:105-128.

Mimikou, M., E. Baltas, E. Varanou, and K. Pantazis. 2000. Regional impacts of climate change on water resources quantity and quality indicators. *Journal of Hydrology* **234**:95-109.

Mimikou, M., Y. Kouvopoulos, G. Cavadias, and N. Vayianos. 1991. Regional hydrological effects of climate change. *Journal of Hydrology* **123**:119-146.

van Minnen, J. G., J. Alcamo, and W. Haupt. 2000. Deriving and Applying Response Surface Diagrams for Evaluating Climate Change Impacts on Crop Production. *Climatic Change* **46**:317-338.

Mitchell, T. D., and P. D. Jones. 2005. An improved method of constructing a database of monthly climate observations and associated high-resolution grids. *International Journal of Climatology* **25**:693-712.

Mitosek, H. T., W. G. Strupczewski, and V. P. Singh. 2006. Three procedures for selection of annual flood peak distribution. *Journal of Hydrology* **323**:57-73.

MM5. 2007. *MM5 Community Model Homepage*. [online] http://www.mmm.ucar.edu/mm5/ accessed: 06/2007.

Monk, W. A., P. J. Wood, D. M. Hannah, and D. A. Wilson. 2007. Selection of river flow indices for the assessment of hydroecological change. *River Research and Applications* **23**:113-122.

Monteith, J. L. 1965. Evaporation and environment. *Symp Soc Exp Biol.* **19**.

Monteith, J. L. 1981. Evaporation and surface temperature. *Quarterly Journal of the Royal Meteorological Society* **107**:1-27.

Morin, J., and Y. Benyamini. 1977. Rainfall Infiltration Into Bare Soils. *Water Resources Research* **13**:813-817.

Mukammal, E. I., and H. H. Neumann. 1977. Application of the Priestley-Taylor evaporation model to assess the influence of soil moisture on the evaporation from a large weighing lysimeter and class a pan. *Boundary-Layer Meteorology* **12**:243-256.

Myers, R. H. 1999. Response surface methodology—current status and future directions (including discussion). *Journal of Quality Technology* **31**:30-74.

Myers, R. H., A. I. Khuri, and W. H. Carter. 1989. Response Surface Methodology: 1966-1988. *Technometrics* **31**:137-157.

Nash, J. E., and J. V. Sutcliffe. 1970. River flow forecasting through conceptual models part I — A discussion of principles. *Journal of Hydrology* **10**:282-290.

New, M., M. Hulme, and P. D. Jones. 2000. Representing twentieth century space-time climate variability: Part II: Development of 1901-96 monthly grids of surface climate. *Journal of Climate* **13**:2217-2238.

New, M., Hulme, M. and Jones, P.D. 1999. Representing twentieth century space-time climate variability. Part 1: development of a 1961-90 mean monthly terrestrial climatology. . *Journal of Climate* **12**:829-856.

Nijssen, B., G. M. O'Donnell, D. P. Lettenmaier, D. Lohmann, and E. F. Wood. 2001. Predicting the discharge of global rivers. *Journal of Climate* **14**:3307-3323.

NIMA. 1997. *Vector Map Level 0 (VMAP0)*. National Imagery and Mapping Agency. [online] http://earth-info.nga.mil/publications/vmap0.html.

NSIDC. 2007. *National Snow and Ice Data Center: World glacier inventory*. [online] http://nsidc.org/data/g01130.html accessed: 23.10.2008.

O'Brien, K. L. 1996. Tropical deforestation and climate change. *Progress in Physical Geography* **20**:311-335.

Olden, J. D., and N. L. Poff. 2003. Redundancy and the choice of hydrologic indices for characterizing streamflow regimes. *River Research and Applications* **19**:101-121.

Palmer, W. 1965. *Meteorological drought.* Research Paper 45. US Weather Bureau, editor, Washington D.C., USA.

Pardé. 1933. *Fleuves et rivières.* Collins, Paris, F.

Parlange, M. B., and G. G. Katul. 1992. Estimation of the diurnal variation of potential evaporation from a wet bare soil surface. *J. of Hydrology* **132**:71-89.

Parson, E., V. Burkett, K. Fisher-Vanden, D. Keith, L. Mearns, H. Pitcher, C. Rosenzweig, and M. Webster. 2007. *Global Change Scenarios: Their Development and Use.* Sub-report 2.1B of Synthesis and Assessment Product 2.1 by the U.S. Climate Change Science Program and the Subcommittee on Global Change Research, Department of Energy, Office of Biological & Environmental Research. Washington, DC., USA.

Parton, W. J., M. Hartman, D. Ojima, and D. Schimel. 1998. DAYCENT and its land surface submodel: description and testing. *Global and Planetary Change* **19**:35-48.

Peel, M. C., B. L. Finlayson, and T. A. McMahon. 2007. Updated world map of the Köppen-Geiger climate classification. *Hydrol. Earth Syst. Sci.* **11**:1633-1644.

Penman, H. L. 1948. Natural evaporation from open water, bare soil and grass. Pages 120-146. *Proc. Roy. Soc. London*.

Penman, H. L. 1956. Evaporation: An Introductory Survey. Pages 9-29. *Proc. Inf. Meeting on Physics in Agric., Neth. J. Agric. Sci.*

Pilgrim, D. H., T. G. Chapman, and D. G. Doran. 1988. Problems of rainfall-runoff modelling in arid and semiarid regions. *Hydrological Sciences Journal/Journal des Sciences Hydrologiques* **33**:379-400.

PNUE/PAM/PLAN BLEU. 2004. L'eau des Méditerranéens : situation et perspectives. No. 158 de la Série des rapports techniques du PAM, PNUE/PAM. *MAP Technical Report Series*, Athens.

Poff, N. L., J. D. Allan, M. B. Bain, J. R. Karr, K. L. Prestegaard, B. D. Richter, R. E. Sparks, and J. C. Stromberg. 1997. The natural flow regime. *Bioscience* **47**:769-784.

Postel, S. 1997. *Last Oasis: Facing Water Scarcity.* W. W. Norton and Company, New York.

Postel, S. L., G. C. Daily, and P. R. Ehrlich. 1996. Human appropriation of renewable fresh water. *Science* **271**:785-788.

Priestley, C. H. B., and R. J. Taylor. 1972. On the assessment of surface heat flux and evaporation using large scale parameters. *Monthly Weather Review* **100**:81-92.

Rao, A. R., and K. Hamed. 2000. *Flood Frequency Analysis.* CRC Press, West Palm Beach, USA.

Rechid, D., T. Raddatz, and D. Jacob. 2008. Parameterization of snow-free land surface albedo as a function of vegetation phenology based on MODIS data and applied in climate modelling. *Theoretical and Applied Climatology*.

Richter, B. D., J. V. Baumgartner, J. Powell, and D. P. Braun. 1996. A Method for Assessing Hydrologic Alteration within Ecosystems. *Conservation Biology* **10**:1163-1174.

Rockström, J. 1999. On-farm green water estimates as a tool for increased food production in water scarce regions. *Physics and Chemistry of the Earth Part B-Hydrology Oceans and Atmosphere* **24**:375-383.

Rockström, J., M. Falkenmark, L. Karlberg, H. Hoff, S. Rost, and D. Gerten. 2009. Future water availability for global food production: The potential of green water for increasing resilience to global change. *Water Resources Research* **45**:W00A12.

Rockström, J., and L. Gordon. 2001. Assessment of green water flows to sustain major biomes of the world: Implications for future ecohydrological landscape management. *Physics and Chemistry of the Earth Part B-Hydrology Oceans and Atmosphere* **26**:843-851.

Rockström, J., L. Gordon, C. Folke, M. Falkenmark, and M. Engwall. 1999. Linkages among water vapor flows, food production, and terrestrial ecosystem services. *Conservation Ecology* **3**.

Rockström, J., M. Lannerstad, and M. Falkenmark. 2007. Assessing the water challenge of a new green revolution in developing countries. *PNAS Proceedings of the National Academy of Sciences of the United States of America* **104**:6253-6260.

Roderick, M. L., and G. D. Farquhar. 2004. Changes in Australian pan evaporation from 1970 to 2002. *International Journal of Climatology* **24**:1077-1090.

Roeckner, E., K. Arpe, L. Bengtsson, M. Christoph, M. Claussen, L. Dümenil, M. Esch, M. Giorgetta, U. Schlese, and U. Schulzweida. 1996. The atmospheric general circulation model ECHAM-4: model description and simulation of present-day climate. Page 90 *in* Max-Planck Institute for Meteorology, editor. *Report No.218*, Hamburg, Germany.

Rosegrant, M. W., S. Meijer, and S. A. Cline. 2002. *International Model for Policy Analysis of Agricultural Commodities and Trade (IMPACT): Model Description.* International Food Policy Research Institute, Washington, D.C.

Rothman, D., J. Agard, and J. Alcamo. 2007. Chapter 9: The Future Today. Pages 395-454 *in* UNEP (United Nations Environment Programme), editor. *Global Environmental Outlook-4*. EarthPrint Limited, Stevenage, Hertfordshire, UK.

Rouse, W. R., P. F. Mills, and R. B. Stewart. 1977. Evaporation in High Latitudes. *Water Resources Research* **13**:909-914.

Sagan, C., O. B. Toon, and J. B. Pollack. 1979. Anthropogenic Albedo Changes and the Earth's Climate. *Science* **206**:1363-1368.

Saunders, I. R., W. G. Bailey, and J. D. Bowers. 1997. Evaporation regimes and evaporation modelling in an alpine tundra environment. *Journal of Hydrology* **195**:99-113.

Scanlon, B. R., I. Jolly, M. Sophocleous, and L. Zhang. 2007. Global impacts of conversions from natural to agricultural ecosystems on water resources: Quantity versus quality. *Water Resources Research* **43**:W03437.

Schaldach, R., and J. Alcamo. 2006. Coupled simulation of regional land use change and soil carbon sequestration: A case study for the state of Hesse in Germany. *Environmental Modelling and Software* **21**:1430-1446.

Schaldach, R., J. Alcamo, and M. Heistermann. 2006. The multiplescale land use change model LandShift: a scenario analysis of land use change and environmental consequences in Africa *in* A. Voinov, Jakeman, A.J., Rizzoli, A.E., editor. *Proceedings of the iEMSs Third Biennial Meeting: "Summit on Environmental Modelling and Software".* International Environmental Modelling and Software Society, CD ROM, Burlington, USA.

Schaldach, R., J. Priess, and J. Alcamo. 2008. Simulating the impact of bio-fuel development on country-wide land-use change in India. *Biomass and Bioenergy, in press*.

Schneider, K., B. Ketzer, L. Breuer, K. B. Vach, C. Bernhofer, and H.-G. Frede. 2007. Evaluation of evapotranspiration methods for model validation in a semi-arid watershed in northern China. *Adv. Geosci.,* **11**:37-42.

Schuol, J., K. C. Abbaspour, H. Yang, R. Srinivasan, and A. J. B. Zehnder. 2008. Modeling blue and green water availability in Africa. *Water Resources Research* **44**:W07406.

Scurlock, J., G. Asner, and S. Gower. 2001. Worldwide historical estimates of Leaf Area Index 1932-2002. Tech. rep. ORNL Oak Ridge National Laboratory (US).

Sheffield, J., and E. Wood. 2008. Projected changes in drought occurrence under future global warming from multi-model, multi-scenario, IPCC AR4 simulations. *Climate Dynamics* **31**:79-105.

Shi, T., D. Guan, A. Wang, J. Wu, C. Jin, and S. Han. 2008. Comparison of three models to estimate evapotranspiration for a temperate mixed forest. *Hydrological Processes* **22**:3431-3443.

Shiklomanov, I. A. 1997. *Comprehensive Assessment of the Freshwater Resources and Water Availability in the World: Assessment of Water Resources and Water Availability in the World.* World Meteorological Organization, Geneva, Switzerland.

Shuttleworth, W. J., and I. R. Calder. 1979. Has the Priestley-Taylor Equation Any Relevance to Forest Evaporation? *Journal of Applied Meteorology* **18**:639-646.

Sitch, S., B. Smith, I. C. Prentice, A. Arneth, A. Bondeau, W. Cramer, J. O. Kaplan, S. Levis, W. Lucht, M. T. Sykes, K. Thonicke, and S. Venevsky. 2003. Evaluation of ecosystem dynamics, plant geography and terrestrial carbon cycling in the LPJ dynamic global vegetation model. *Global Change Biology* **9**:161-185.

Smakhtin, V. U. 2001. Low flow hydrology: a review. *Journal of Hydrology* **240**:147-186.

Solh, M., A. Amri, T. Ngaido, and J. Valkoun. 2003. Policy and education reform needs for conservation of dryland biodiversity. *Journal of Arid Environments* **54**:5-13.

Stahl, K. 2001. Hydrological Drought - a Study across Europe. Page 122. *Geowissenschaftliche Fakultät.* Albert-Ludwigs-Universität Freiburg i. Br., Freiburg.

Stahl, K., and S. Demuth. 1999. Linking streamflow drought to the occurrence of atmospheric circulation pattern. *Hydrological Sciences Journal / Journal des Sciences Hydrologiques* **44**:467-482.

Stedinger, J. R., R. M. Vogel, and E. Foufoula-Georgiou. 1993. Frequency analysis of extreme events. Pages 18.11-18.66 *in* D. R. Maidment, editor. *Handbook of Hydrology*. McGraw-Hill, New York, USA.

Stehfest, E., M. Heistermann, J. A. Priess, D. S. Ojima, and J. Alcamo. 2007. Simulation of global crop production with the ecosystem model DayCent. *Ecological Modelling* **209**:203-219.

Stewart, R., and W. Rouse. 1976. A Simple Method for Determining the Evaporation from Shallow Lakes and Ponds. *Water Resources Research* **12**:623-628.

Tallaksen, L. M., and H. A. J. van Lanen. 2004. *Hydrological Drought - processes and estimation methods for streamflow and groundwater.* Developments in Water Science. Elsevier B.V., Amsterdam, NL.

Tanskanen, A., and T. Manninen. 2007. Effective UV surface albedo of seasonally snow-covered lands. *Atmospheric Chemistry and Physics* **7**:2759-2764.

Tate, E. L., and S. N. Freeman. 2000. Three modelling approaches for seasonal streamflow droughts in southern Africa: the use of censored data. *Hydrological Sciences Journal / Journal des Sciences Hydrologiques* **45**:27-42.

The World Bank. 1992. *World Development Report 1992: Development and the Environment*. Oxford University Press, Inc., New York.

Tockner, K., and J. A. Stanford. 2002. Riverine flood plains: present state and future trends. *Environmental Conservation* **29**:308-330.

Toth, F. L., W. Cramer, and E. Hizsnyik. 2000. Climate Impact Response Functions: An Introduction. *Climatic Change* **46**:225-246.

UN. 2009. *World Population Prospects: The 2008 Revision, CD-ROM Edition*. United Nations Population Division. [online] http://www.un.org/esa/population/unpop.htm. accessed: 01.04.2009.

UNEP. 2002. *Global Environment Outlook 3: Past, present and future perspectives (GEO-3)*. Earthscan Publications Ltd, London.

UNEP. 2007a. *Global Environment Outlook: environment for development (GEO-4)* U. N. E. Programme, editor. Progress Press, Ltd., Valletta, Malta.

UNEP. 2007b. *Global Environment Outlook: environment for development (GEO-4)*. Progress Press, Ltd, Valetta, Malta.

UNICEF. 2000. *Drought disasters*. [online] http://www.unicef.org/drought/. accessed: accessed 31 January 2007.

USGS. 1998. *HYDRO1k: Elevation derivative database*. U.S. Geological Survey, EROS Data Center, Sioux Falls. [online] http://edc.usgs.gov/products/elevation/gtopo30/hydro/index.html.

USGS. 2006. *GTOPO30 Digital Elevation Model*. U.S. Geological Survey, EROS Data Centre. [online] http://edc.usgs.gov/products/elevation/gtopo30/gtopo30.html. accessed: 27.12.2006.

USGS. 2007. *Global Land Cover Characterization*. U.S. Geological Survey, EROS Data Center. [online] http://edcsns17.cr.usgs.gov/glcc/ accessed: 8. June 2007.

Verma, S. B., N. J. Rosenberg, and B. L. Blad. 1978. Turbulent Exchange Coefficients for Sensible Heat and Water Vapor under Advective Conditions. *Journal of Applied Meteorology* **17**:330-338.

Vicente-Serrano, S. M., J. C. González-Hidalgo, M. de Luis, and J. Raventós. 2004. Drought patterns in the Mediterranean area: the Valencia region (eastern Spain). *Climate Research* **26**:5-15.

Viswanadham, Y., V. Silva Filho, and R. Andre. 1991. The Priestley-Taylor parameter alpha for the Amazon forest. *Forest Ecology and Management* **38**:211-225.

Vörösmarty, C. J., B. M. Fekete, M. Meybeck, and R. B. Lammers. 2000. Geomorphometric attributes of the global system of rivers at 30-minute spatial resolution. *Journal of Hydrology* **237**:17-39.

WDPA Consortium. 2004. *Word Database on Protected Areas*. [online] http://www.unep-wcmc.org/wdpa/.

Weiß, M., and L. Menzel. 2008. A global comparison of four potential evapotranspiration equations and their relevance to stream flow modelling in semi-arid environments. *Adv. Geosci.* **18**:15-23.

Widén-Nilsson, E. 2007. Global-Scale Modelling of the Land-Surface Water Balance : Development and Analysis of WASMOD-M. Page 76. Acta Universitatis Upsaliensis, Uppsala.

Widén-Nilsson, E., L. Gong, S. Halldin, and C.-Y. Xu. 2009. Model performance and parameter behavior for varying time aggregations and evaluation criteria in the WASMOD-M global water balance model. *Water Resources Research* **in press**.

Widén-Nilsson, E., S. Halldin, and C.-y. Xu. 2007. Global water-balance modelling with WAS-MOD-M: Parameter estimation and regionalisation. *Journal of Hydrology* **340**:105-118.

Wilhite, D. A. 2000. *Drought Volume I - A Global Assessment.* Routledge, New York, USA.

WMO. 1975. Report of the CagM Working Group on the Assessment of Drought *in* World Meteorological Organization, editor. *Technical Note 138*, Geneva, Switzerland.

Woo, M. K., and A. Tarhule. 1994. Stream flow droughts of Northern Nigerian rivers. *Hydrological Sciences Journal / Journal des Sciences Hydrologiques* **35**:19-34.

Woodwell, G. M., J. E. Hobbie, R. A. Houghton, J. M. Melillo, B. Moore, B. J. Peterson, and G. R. Shaver. 1983. Global Deforestation: Contribution to Atmospheric Carbon Dioxide. *Science* **222**:1081-1086.

Wright, J. L. 1981. *Crop coefficients for estimates of daily crop evapotranspiration.* Irrigation Scheduling for Water and Energy Conservation in the 80's. American Society of Agricultural Engineers, editor.

Wright, J. L. 1982. New evapotranspiration crop coefficiennts. *J. Irrig. and Drain. Div., ASCE* **108**:57-74.